Validation of dynamic models of wind farms (Erao-3)

Executive summary, benchmark results and model improvements

J.T.G. Pierik (ECN) J. Morren (TUD)

ABSTRACT

This report gives an overview of the objectives and methods, as well as the results and conclusions of the project "Verificatie dynamische modellen van windparken (Erao-3)". Three validation exercises have been executed:

- the first validation compares models of different project partners with regard to a voltage dip in a hypothetical benchmark system;
- the second validates the Constant Speed Stall wind farm model using measurements on the Alsvik wind farm;
- the third validates the Variable Speed Pitch model using measurements on the JWT wind turbine.

The Constant Speed Stall and Variable Speed Pitch validations are reported separately [16, 17]. Model improvements are documented in chapters 3 and 4. Appendix B gives an overview of IEA Annex XXI. The conference and journal papers prepared or contributed to in the Erao-3 project are included in appendix C.

The three validation exercises showed different levels of success. The results of the first validation showed only minor deviations from the results of others and these could be explained by small differences between the models. In the second validation, detailed turbine data was available and the model predictions were quite accurate. In the third validation the similarity between measurements and simulations was limited. The unavailability of detailed data on the system used for this validation played an important role with regard to the accuracy. To increase confidence in the dynamic wind turbine and wind farm models, additional validation work is still required.

This report is a contribution to IEA Annex XXI: Dynamic models of Wind Farms for Power System studies.

Keywords: wind turbine models, wind farm models, model validation, wind farm dynamics, wind farm electrical systems

Acknowledgement

Erao-3 is a continuation of the Erao and Erao-2 projects, in which steady state (load flow), economic and dynamic models of offshore wind farms have been developed. This project has been supported by the Dutch Agency for Energy and Environment (SenterNovem) in the DEN Program of the Netherlands, executed by SenterNovem by order of the Ministry of Economic Affairs.

Novem project number: 2020-02-12-10-002

Project title: Verificatie dynamische modellen windparken (Erao-3)

Penvoerder: ECN Medeaanvrager: TUD

Period: 1 januari 2003 - 1 februari 2007

ECN project number: 7.4336

Validation of dynamic models of wind farms (Erao-3)						
•						

CONTENTS

1 Executive summary 7					
	1.1	Project summary	7		
		1.1.1 Problem definition	7		
		1.1.2 Objective	8		
		1.1.3 Method	8		
		1.1.4 Project results	10		
	1.2	Commercialisation of project results	14		
	1.3	Contribution to BSE-DEN programme objectives	15		
2	Con	nparison of ECN-TUD benchmark system model with Risoe benchmark system	models 17		
	2.1	Introduction	17		
	2.2	Benchmark system to be modelled	17		
	2.3	ECN-TUD benchmark system model	18		
	2.4	Comparison ECN-TUD and Risoe results	18		
	2.5	Discussion	23		
	2.6	Appendix: Benchmark system parameters	24		
3	Mod	lel improvement: Protection of Wind Turbines with Doubly-fed Induction Gen	erator 25		
	3.1	Introduction	25		
	3.2	Fault response and protection of DFIG	25		
	3.3	Modelling	26		
	3.4	Simulation results	29		
	3.5	Conclusion	31		
	3.6	Machine and controller parameters	32		
4	Mod	lel improvement: Inertial response control for variable speed wind turbines	33		
	4.1	Introduction	33		
	4.2	Wind turbine inertia	34		
	4.3	Controller implementation	35		
	4.4	Modelling	36		
	4.5	Case study description	38		
	4.6	Results and discussion	41		
	4.7	Conclusion	44		
5	Avai	ilability of Dutch measurements for model validation	46		
A	Req	uired turbine data and measurements for validation of windturbines dynamic	models 49		
В	IEA	Annex XXI co-operation	51		

ECN-E-07-006 5

C Conference contributions and journal papers related to the Erao-3 project

53

1 EXECUTIVE SUMMARY

This report is the first of a set of three reports that documents the results of the project "Verificatie dynamische modellen van windparken (Erao-3)". The other two reports are titled:

- Constant Speed Stall Wind Farm Dynamic Model Validation: Alsvik measurements and simulations [16];
- Variable Speed Pitch Wind Turbine Dynamic Model Validation: JWT measurements and simulations [17].

The first chapter of this report gives an overview of the project objectives and methods, as well as the project results and conclusions. Chapter 2 describes the results of the first validation exercise in which different models are compared with regard to a voltage dip in a hypothetical benchmark system. Model improvements are documented in chapters 3 and 4. Appendix B gives an overview of IEA Annex XXI. The conference and journal papers prepared or contributed to in the Erao-3 project are included in appendix C.

1.1 Project summary

1.1.1 Problem definition

In the Netherlands the first steps towards large scale implementation of offshore wind power have been taken. The first offshore wind farm of about 100 MW, located near the coast of Egmond in the province of North Holland has been built. Plans exist for a substancial amount of offshore wind energy in the Dutch section of the North Sea. These offshore wind farm will feed into the Dutch high voltage grid. The effects of large amounts of wind power on the grid are not that well known yet. Wind power can cause problems for the European grid, as is illustrated by the first of two recent incidents (see box).

On 30 december 2004 a critical condition developed in the high voltage grid of the Netherlands, caused by an excess of wind power in the north of Germany. The excess resulted in large power flows through the Netherlands, Belgium and France to the south of Germany. This had happened before but during this particular event, an n-1 safe condition was no longer guaranteed in the Dutch grid [24].

A second more serious incident occured on the evening of Saturday 4 november 2006 [14]. A high voltage line in the North of Germany was taken out of operation to let a cruise ship, built at the Meyerwerft in Papenburg, pass the high voltage line. At the same time, the load pattern in Germany changed, which resulted in an overload of part of the German high voltage grid, causing a number of automatic trips. This resulted in a separation of the European grid into three sections (islands). A power shortage occurred in one of the island grid, which caused consumer load tripping in the Netherlands, Belgium, France, Spain, Portugal and Italy. In total about 10 million people were affected by this power failure. A total black-out was prevented, but this event demonstrated the need for grid reinforcements as well as reseach on intelligent grid management.

Most European countries with plans for a considerable amount of wind power have started research activities on the integration of wind power in the high voltage grid. In 2005 an IEA Annex has been started to gather information on wind power integration practices and research in a number of countries [10]. In the Netherlands, research started in 2003 to quantify the effect of 6000 MW offshore wind power on the high voltage grid [9, 1, 11]. Only the steady state behaviour has been considered so far, resulting in suggestions for grid reinforcement. This investigation needs to be complemented with studies on the dynamic interaction of wind power and the electrical grid. These studies range from power balance studies to transient event

ECN-E-07-006 7

studies and innovative grid control concepts, for instance using (dynamic) grid state estimation. Dynamic models of wind turbines and farms are needed in these studies.

The Erao projects, which started in 1999, intend to develop building blocks and knowledge needed in wind farm and grid studies. In the Erao and Erao-2 projects, steady state and dynamic models of wind turbines and wind farms have been developed by ECN and TUD-EPS [15, 18, 19]. These models have a number of applications. The dynamic models can be used to investigate and improve the dynamic behaviour of the electrical system of a wind farm, for instance by optimizing the control. A second level of application is the interaction between wind farms and the high voltage grid, locally as well as on a national level. The type of dynamic models needed will depend on the application. Generally individual wind farm studies require more detailed models than national grid studies.

Major steps have been taken in the development of the dynamic models of wind turbines and farms, but the development is not complete without a thorough validation. The basis for all models, simple as well as complex, are turbine models which include the dynamic properties necessary for controller design. These models have to be validated by comparing measurements and simulations for a specific wind turbine or wind farm. After validation, the models can be used in wind farm and local grid studies and as well as for the development of more simple, reduced order or aggregate models, especially useful in studies of national grids.

1.1.2 Objective

The main objectives of the Erao-3 project are:

- to validate the constant speed turbine model and the variable speed turbine model developed in the Erao-2 project;
- to improve the Erao-2 models.

The project also intends to find measurements of wind turbines and wind farms in the Netherlands suitable for model validation. It is not the intention to perform measurements in the Erao-3 project itself.

1.1.3 Method

Before any validation is executed it is relevant to know which operating conditions should be predicted by a dynamic model and to which level of detail. The operating conditions, that appear to be important from a grid operator's point of view, are:

- wind farm power variations caused by wind speed changes (balancing demand and supply);
- wind farm responce to grid faults, especially voltage dips (fault ride through);
- power quality aspects of wind turbines and wind farms (active and reactive power variation, flicker, harmonics);
- voltage regulation by wind farm reactive power control (requires a PCC with an inductive character)
- power curtailment and active power balance support by wind farm power control.

For the turbine manufacturer important operating conditions are:

- dynamic response of the turbine during different normal operation modes, i.e. the design of wind turbine controllers (pitch control, electric torque and reactive power control);
- dynamic response of the electrical system of the wind farm as a whole (control of the interface between wind farm and grid, especially in the case of DC connection to shore).

To validate dynamic models of wind turbines and wind farms, two sets of data are required:

- measurements of mechanical and electrical variables with a sufficiently high sample rate to include the relevant dynamic behaviour;
- turbine parameters, mechanical as well as electrical, including the controller design (if present).

When the project started, it was clear that this information can not be found easily.

In 2002-2003 nine research institutes joined the new IEA Annex XXI: *Dynamic models of Wind Farms for Power System studies*. The overall objective of the IEA Annex 21 is to develop and validate models of wind turbines and wind farms and to gather measurement data for validation purposes [23]. The emphasis is on models suitable for evaluating power system dynamics and transient stability. The Annex comprises the following main tasks:

- Establishment of an international forum for exchanging knowledge and experience within the field of wind farm modelling for power system studies;
- Development, description and validation of wind farm models. The wind farm models
 are developed by the individual participants of the Annex, while the description and
 validation will be coordinated by the Annex as to give the state of the art and to pinpoint
 key issues for further development;
- Set-up and operation of a common database for benchmark testing of wind turbine and wind farm models as an aid for securing good quality models.

For The Netherlands, ECN and TUD participated in this Annex. The participation was part of the Erao-3 project. Within the Annex three validation exercises were chosen:

- a "benchmark" exercise based on a hypothetical system chosen by Risoe;
- the validation of a constant speed stall wind farm model using measurements of the Alsvik wind farm;
- the validation of a variable speed pitch wind turbine model using measurements of the JWT wind turbine.

The benchmark exercise is described in this report (chapter 2), the constant speed stall and variable speed pitch validation cases are documented in separate reports [16, 17]. The IEA Annex XXI members agreed to perform the validations and report the results.

When wind turbine measurements and model simulations are compared, a number of complicating factors are encountered:

- the wind speed averaged over the turbine rotor plane (rotor effective wind speed) is not known. The measured single point wind speed is significantly different from the rotor effective wind speed. Therefore, comparing time histories of measurements and simulations can not give much information about the accuracy of the model. A work around for this problem is to compare measurement and simulation in the frequency domain, i.e. by means of power spectra. This requires measurements with a sufficiently high sample rate.
- the voltage measured at the generator terminals is often used as an input signal for the simulation. The correlation with the rotor effective wind speed is lost however since the instantaneous effective wind speed in the simulation is different from the measurement, although it is a statistically correct representation. For a constant speed turbine, where the correlation between wind speed and voltage is high, this leads to errors in the simulated power spectral desity. This effect should be quantified if the voltage is used as an input [16];
- the availability and accuracy of the turbine parameters is often a problem. Turbine manufacturers are not always willing to supply the required data and even if they do, the parameters of the measured turbine may be different, due to turbine modifications or different control settings.

When a model validation is evaluated, these complicating factors should be taken into account. Within the IEA Annex XXI different types of models are used by different participants [22]. This can not only lead to different results but also to different pre-treatment of the measurements, for instance conversion to RMS values or positive sequence values. Different types of models used in the Annex are:

- RMS phasor models (PSSE);
- instantaneous phasor models (Simulink, DigSilent, SimPowerSys, SimPow);
- abc models with or without power electronic switches (SimPowerSys, PSCAD).

The Erao-2 electrical system models are based on space phasor theory [8], which calculates instantaneous values under symmetrical conditions. This is fundamentally different from the phasor-type RMS models and abc models with or without PE switches. Space phasor models are primarily developed for design of the converter controller and evaluation of electrical transients under balanced conditions. This suggests the use of the instantaneous positive sequence voltage values as input. The Erao-2 electrical models do not include the switching of power electronic converters, the IGBT converters are treated as controlled voltage sources. Therefore, the frequency components in the range of the switching frequency (1 kHz) and higher are not represented correctly in systems with a converter and should be disregarded.

1.1.4 Project results

This section summarizes the results of the Erao-3 project for the four main topics: the benchmark exercise, the validation of the Constant Speed Stall model and the Variable Speed Pitch model (Alsvik wind farm and JWT turbine measurements) and the model improvements.

1. Benchmark exercise

In the benchmark exercise a short circuit is modelled in a hypothetical wind turbine grid connection. The wind turbine is modelled by an induction machine and capacitor bank. The grid connection consists of two transformers and a cable. The short circuit occurs at the low voltage side of the high voltage transfomer. The short circuit is modelled by a change in shunt resistance.

The results of the Risoe and ECN/TUD models have been compared. The most important deviations are the difference in oscillation frequency and damping of the oscillations. The oscillation frequency in the Risoe benchmark simulations is higher and the Risoe damping is lower. The deviations are probably caused by small differences between the Risoe and the ECN/TUD models. The most important modelling difference is that the ECN/TUD transformer model does not include the magnetizing inductance and the iron losses. Another difference in the simulation results is that the currents after dip clearance are somewhat higher for the ECN/TUD simulations then in the Risoe results. The torque and rotational speed are practically equal, except for some high-frequency oscillations. This is not so strange, because exactly the same mechanical model has been used. In general, the ECN/TUD simulation results are similar to the Risoe simulation results.

2. Validation of the constant speed wind farm model for the Alsvik wind farm

The most direct method of validation of dynamic models of wind turbines and wind farms is comparing measurements and simulation results. This validation process is hindered by a number of problems:

- the time series of the rotor effective wind speed during the measurement is not known, which makes comparing time series of measured and simulated variables difficult;
- voltage and wind speed measurements are not independent and this will result in errors when the voltage is used as an input to determine the frequency response by simulation.

For the first problem a work around is found by comparing the frequency response of measurements and simulations. Frequency domain representations are an excellent way to obtain the properties of dynamic models. The second problem requires the quantification of the coherence of voltage and wind speed. It was shown that the measured voltage is acceptable as an input for the Alsvik validation.

Three measurement sets have been used for the validation of the constant speed stall (CSS) wind farm model. In the first set, mainly mechanical parameters have been recorded. The voltage was not measured and a grid model was used to generate the voltage at the point of common coupling of the wind farm. The results with this measurement set are not that good. There are significant differences between the measured and the calculated Auto Power Spectral Density (APSD) of the electric power, reactive power and mechanical torque. Some oscillations are missing and the level of oscillation above 1 Hz is underestimated. These discrepancies can be caused by several factors:

- inaccurate mechanical parameters, for instance the stiffness and damping of the tower are not well known;
- incomplete modeling of the turbine rotor: only a simple steady state representation of the rotor is used, blade lead-lag and flap oscillations are absent in the simulation;
- an insufficient level of detail of the models of the electrical components of the wind farm (no saturation, simplified transformer and cable representations);

 an inadequate representation of the grid (a single synchonous generator, no grid load changes).

Especially the effect of the simplified rotor model and the grid model may be important. The wind farm independent variation of the grid voltage is not present in the grid model. The voltage in the simulation is much less variable than in the measurement. Including electric load changes in the grid or using the measured voltage as an input will give a better result.

The second measurement set included measurements of the instantaneous phase voltages and currents and is used to investigate the effect of the grid voltage variation on the simulation results. First, the Alsvik farm was simulated with the same grid model as in set 1 and these results are better than for set 1. Predicting the mechanical variables seems to be more difficult than predicting the electrical variables. When the measured voltage is used as input, the results are significantly better, especially for turbine 3. The only difference between measurement and simulation is a broad peak in the spectra of current and power around 8 Hz. The reactive power spectrum is practically identical. It would have been useful to use the measured voltage as input in set 1 as well as to see to what extent this improves the result for the mechanical variables, but unfortunately this voltage is not available.

The third measurement available for validation is a voltage dip. For this type of short measurement of about 3 seconds, the exact value of the rotor effective wind is not that important and time series of measurement and simulation are compared. To simulate the dip, the measured voltage is the main model input and has to be converted to the dq-reference frame. Since the frequency is not exactly known, two assumptions have been examinded: constant voltage phasor angle and constant voltage phasor rotational frequency. The second option gives the best result. Frequencies are estimated with reasonable accuracy, the damping (electrical or mechanical) is different.

Summarizing, the validation of the model for the Alsvik wind farm showed that:

- frequency response results for the electrical variables are good if the measured voltage is used as input instead of using a grid model;
- frequency response results on mechanical parameters are less good, which may partly be
 caused by variation of the grid voltage, which could not be included because it was not
 measured;
- the voltage dip result was quite good, with some mismatch in the damping.

3. Validation of the variable speed wind turbine model for the JWT wind turbine

It was not possible to obtain a set of measurements for a variable speed wind turbine or farm that satisfied all requirements for a validation. The IEA Annex XXI working group decided that the JWT turbine presented the best choice, even though detailed turbine data is missing. For the time being, a better option was not available. The lack of turbine parameters for the JWT turbine limits the scope of this model validation, however. The validation covered three cases of normal operation and a voltage dip.

For normal operation the power spectral density of the active and reactive power at the measurement locations (grid side converter and total) have been compared. From a general perspective, the APSDs of measurements and simulations were similar but the details were often different. This is not surprising since detailed knowledge on the JWT turbine parameters and control was missing. From the results for normal operation the following observation can be made:

- The spectra for the active powers showed a better match than for the reactive powers. The power control follows the wind power and if the wind input and the power control are modelled correctly, this will result in a good representation of the active power, unless the voltage spectrum in the measurement is different from that in the simulation, which is not the case since the measured voltage was input for the simulations.
- The differences between the spectra of the measured and simulated reactive powers can be explaineded by differences in the reactive power controller design, which consists of two separate designs, one for the stator reactive power via the rotor current and one for the grid side converter reactive power via the converter current. Since the details of the JWT turbine reactive power controllers were not known, a TUD-ECN design was used. A different design and setting can easily lead to the observed differences in behaviour.
- Peaks occurring at specific frequencies in the measurement were not reproduced in the simulations. This is no surprise, since the validation was limited by the missing turbine data. As mentioned before, this is the major drawback of this validation.

Form the comparison of the voltage dip measurements and simulations a similar conclusion can be drawn. The oscillation frequency in measurement and simulation was similar, but the oscillation was more extreme in the simulation and the damping was less. The differences between simulation and measurement are attributed to differences in parameter values. From a general perspective, measurements and simulation results for the voltage dip are not that far apart, however.

Due to the limitations in the JWT turbine measurements and data, detailed conclusions on the accuracy of the VSP-DFIG model can not be drawn. Nevertheless, the validation results showed that, even if most of the turbine parameters are not known, the dynamic simulation produces results which are not that different from the measurements. This is a useful conclusion, since detailed information on commercial turbines is often missing. On the other hand, the validation did not lead to suggestions for model improvement, since the model could only be validated in a global way.

It is recommended to execute additional validation exercises when a suitable set of VSP turbine measurements and turbine data is available.

4. Model improvements

The following model improvements have been implemented:

- the DC link model was improved: the voltage dip and short circuit calculation dynamic accuracy was improved;
- effect of high frequency noise in the measured voltage on the feedback control;
- DFIG controller operating on rotating voltage phasors;
- a fault ride through capability was implemented for the turbine with DFIG;
- inertial response control for variable speed turbines was implemented.

The improvement of the DC link model comprises the signals used in the control loops and is relatively small. The second and third improvement are described in the VSP model validation report [17]. The final two improvements are documented in chapter 3 and chapter 4.

Project conclusions and recommendations

- 1. The results for the Benchmark exercise were good. There were small differences which could be explained by differences between the models.
- 2. For the constant speed wind farm model it was shown that the measured voltage is acceptable as an input for the Alsvik validation.
- 3. The results for the first Alsvik measurement set, mainly mechanical measurements, are not that good. There are significant differences between the measured and the calculated APSDs of the electric power, reactive power and mechanical torque. Some oscillations are missing and the level of oscillation above 1 Hz is underestimated. A possible explanation is given. However, this did not lead to model improvements.
- 4. The results for the second Alsvik measurement set are much better. Predicting the mechanical variables seems to be more difficult than predicting the electrical variables. When the measured voltage is used as input, the results are significantly better.
- 5. The third Alsvik measurement is a voltage dip. The prediction of the transient response to the voltage dip was quite good, with some mismatch in the damping.
- 6. The lack of turbine parameters for the JWT turbine limited the scope of the variable speed turbine model validation.
- 7. From a general perspective, the APSDs of measurements and simulations for the JWT turbine were similar but the details were often different. This is not surprising since detailed knowledge on the JWT turbine parameters and control was missing.
- 8. For the voltage dip measurements and simulations for the JWT turbine the oscillation frequency in measurement and simulation was similar, but the oscillation was more extreme in the simulation and the damping was less. The differences between simulation and measurement are attributed to differences in parameter values.
- The JWT validation exercise did not lead to suggestions for model improvement. Still some improvements were made which impove and extend the control in the variable speed turbine model.
- 10. No Dutch wind farm or wind turbine measurements suitable for dynamic model validation could be contributed to Annex XXI.

It is recommended to:

- execute additional validation exercise(s) for the variable speed turbine model.
- extend the database with suitable variable speed turbine and wind farm measurements.

1.2 Commercialisation of project results

Electric power companies are developing an interest in tools to investigate electrical system configurations. Recently, Vattenfall expressed their interest in the steady state and economic model library, called EeFarm, which was developed with support of Novem and the Ministry of Economic Affairs in the Erao-1 project. The discussions on a possible transfer of the model showed that there still are steps to be taken towards a user friendly second version of the EeFarm model library. Similar considerations hold with respect to the dynamic model library of Erao-2 and Erao-3. Although the dynamic model library is better structured due to the chosen

computer language (Simulink), the library needs to be restructured and fine tuned. Until now the main focus has been on the development of new models and validation of existing models and not yet on the development of a well structured library using the full (library) capabilities of Simulink. First steps towards this goal have been taken in the fall of 2006 but this is still far from completed.

1.3 Contribution to BSE-DEN programme objectives

In the project proposal an estimate of the contribution of the Erao-3 project to the BSE-DEN programme objectives has been given. The point of departure of the calculation has been that the demands of grid operators with respect to the dynamic impact of wind power on the grid will increase and that validated dynamic models of wind farm are needed to meet this demand. These criteria still hold. The assumption of increasing demands on dynamic behaviour of wind farms proved to be correct, as can be seen from the requirements imposed on wind power implementation by for instance the Irish grid operator (demands specification of the detailed dynamic behavior of a wind farm, for instance during a frequency dip) or E.On Netz (demands voltage dip ride through capability). The model validation results of the Erao-3 project contribute to these requirements by developing validated dynamic models that can be used to study for instance frequency and voltage dip behavior and secondly by indicating accuracy limitations under specific model and turbine data conditions.

The project proposal estimated an amount of prevented primary energy of 8.8 PJ in 2020, by assuming a delay in the installed offshore wind power, due to a lack of validated dynamic models. The increasing demands by grid operators on the dynamic behavior of wind farms has materialised. Therefore, the only reason to adjust this estimate could be an only partial fulfilment of the project objectives. The project objectives are to validate two types of wind farm, constant speed and variable speed. Both objectives have been realised, the validation of the variable speed case was not optimal however, due to the lack of turbine data for the chosen turbine measurements (a better combination of measurements and turbine data was not available). For this drawback, a reduction on the originally estimated prevented primary energy appears to be logical. Although the effect is difficult to estimate, a reduction by 20% is assumed, which results in a energy benefit of 7 PJ in 2020.

Innovation

The recently published EWEA report on Large Scale Integration of Wind Energy in the European Power Supply [6] concludes that the major issues of wind power integration are changed approaches in operation of the power system, connection requirements for wind power plans to maintain a stable and reliable supply, extension and modification of the grid infrastructure, influence of wind power on system adequacy and the security of supply [6]. The same report concludes that dynamic studies provide the basis for improved connection practices. The dynamic models of wind turbines and wind farms, necessary for these studies, are not readily available and the existing models have not been validated. This project is a step towards a validated library of dynamic models of wind turbines and wind farms. Secondly, a database of measurements has been compiled by IEA Annex XXI, of which this project was part. The database is available for future validation exercises.

Bottlenecks solved

Validated dynamic models of wind turbines and wind farms are essential for the realisation

of a significant amount of offshore wind power in the power system of Europe. The project contributed to the validation of two categories of wind farm models: constant speed stall and variable speed pitch. Prior to the start of Annex XXI no suitable measurements for the validation of dynamic models for power system studies were available. The Annex made a start by compiling a measurement database.

Cost of renewable energy

The project proposal indicated the following costs that can be reduced by dynamic simulations of wind farms and power system studies:

- dynamic simulations of wind farms increase reliability, prevent over dimensioning of components and reduce investment costs;
- dynamic simulations of wind farms quantify the effect of the wind farms on the grid
 and meet the request of grid operators with regard to knowledge of wind farm dynamic
 behaviour, during normal operation as well as during faults;
- dynamic simulations of power systems which include large amounts of wind power enable alternative grid and wind farm control strategies and increase confidence in stable and reliable operation.

Without validated tools to perform these calculations, potential problems caused by the interaction of large amounts of wind power and the grid may not be noticed and eventually cause unnecessary problems.

2 COMPARISON OF ECN-TUD BENCHMARK SYSTEM MODEL WITH RISOE BENCHMARK SYSTEM MODELS

2.1 Introduction

The IEA Annex XXI participants decided to perform a comparison of models of the Annex participants (benchmark), based on a hypothetical electrical system described in the appendix of the report Risoe-R-1331 'Simulation and verification of transient events in large wind power installations' by Soerensen et al. [21]. In this chapter, similation results from the ECN-TUD model will be compared to the results from the Risoe models. This chapter starts with a short description of the benchmark system and the model of ECN and TUD. Next, the simulation results are compared. This chapter ends with a discussion of the results.

2.2 Benchmark system to be modelled

The benchmark system to be modelled is shown in figure 1. It contains a constant speed wind turbine with an induction generator that is connected to the 50kV grid via a 960/10.5kV transformer, a 10kV cable, a 10kV/50kV transformer and a 50kV grid. Actually, the Risoe models do not completely model the constant speed turbine, it is represented by the aerodynamic torque, the rotor mass, the shaft and the gear box ratio. A capacitor bank is connected to the rotor terminals. The capacitor bank is delta-connected. The induction generator in the Risoe benchmark models is a T-equivalent circuit. The mechanical system is modelled by a 2-mass model. The induction generator and capacitor bank are connected to a 10kV/50kV transformer. This transformer is connected to the grid transformer by a cable. The 50kV grid in the Risoe benchmark models is a Thévenin equivalent circuit, both transformers are modelled by a T-equivalent and the cable is modelled by a π -equivalent. A detailed description of the Risoe benchmark models and the used parameters can be found in the Risoe report [21]. The main parameters are also listed in section 2.6.

In the benchmark simulation, a short-circuit is applied at the low-voltage side of the 10kV/50kV transformer. The short-circuit is a balanced 3-phase short circuit. The Risoe simulations use DigSilent Powerfactory and EMTDC.

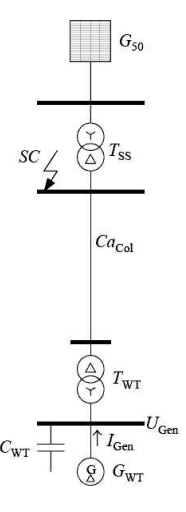


Figure 1: Benchmark benchmark system to be modelled

ECN-E-07-006

2.3 ECN-TUD benchmark system model

The ECN-TUD benchmark system model uses Simulink and the electrical components are modelled in a dq-reference frame. For the dq-models all signals are constant in steady-state situations. This will result in a significant increase in simulations speed. The models are described in the report 'Electrical and control aspects of offshore wind farms II (Erao II) - Vol. 1: Dynamic models of wind farms', ECN-C-04-050 [18]. The same parameters as in the Risoe-report have been used, see section 2.6.

2.4 Comparison ECN-TUD and Risoe results

In this section the simulation results obtained from the ECN-TUD models are compared to the Risoe benchmark simulation results. The case that has been modelled is a balanced three-phase short-circuit at the low-voltage side of the 10kV/50kV transformer. The dip is cleared after 100 ms. Figure 2 shows the ECN-TUD benchmark system model and the location of the short circuit. The response of the grid to the voltage dip is not an aspect of investigation and is not correctly represented. If the voltage dip is large enough, this will not affect the result. Figure 3 shows the short circuit model. A shunt resistance to ground is inserted at the short circuit location.

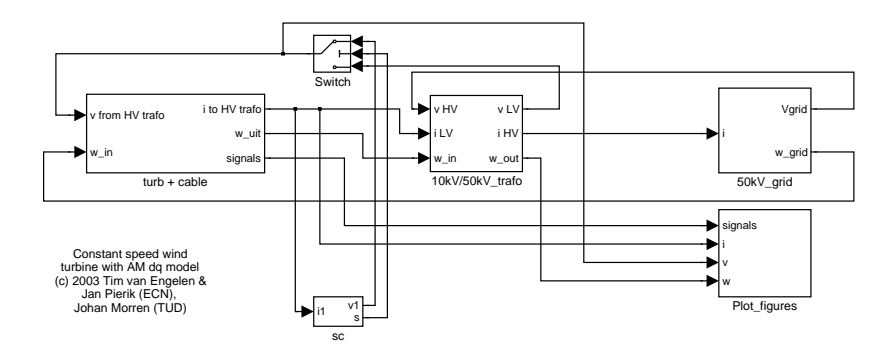


Figure 2: ECN-TUD benchmark system model

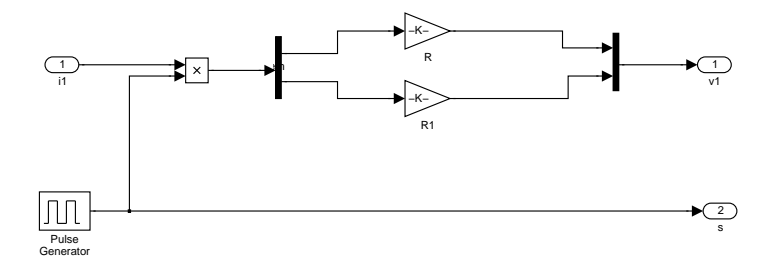


Figure 3: Short circuit model in ECN-TUD benchmark system model

The voltage at the terminals of the wind turbine during the voltage dip is shown in figure 4. The voltage dip start at t=0 s for the benchmark simulations while it starts at t=1s for the ECN-TUD simulations. A detailed view of the same voltages during the start of the voltage dip is shown in figure 5. A detailed view of the terminal voltage just after dip clearance is shown in figure 6.

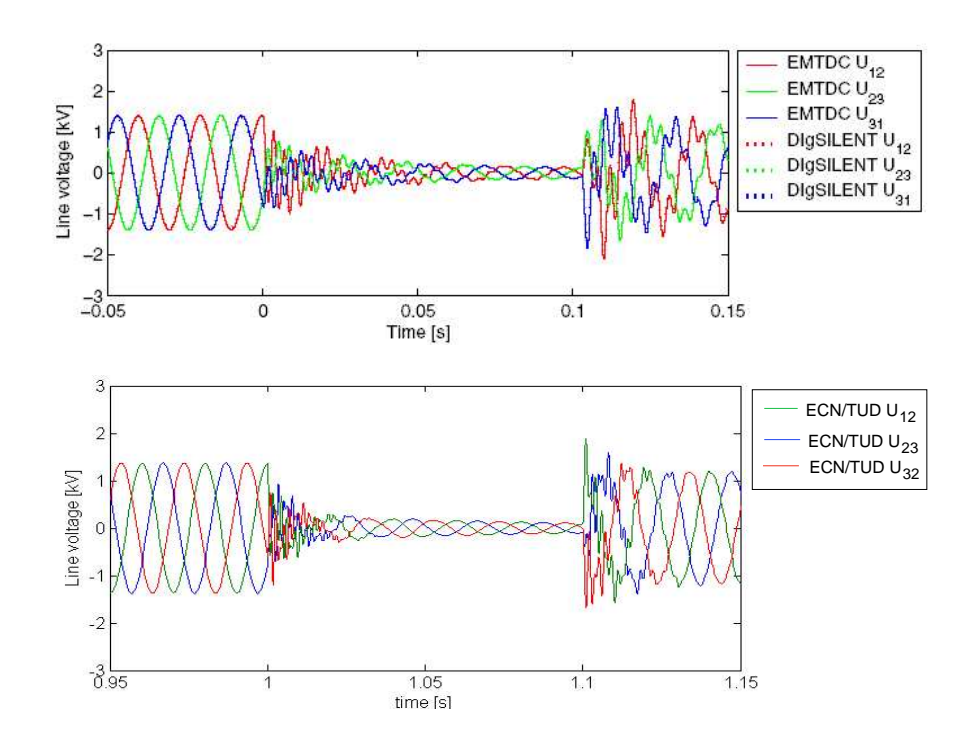


Figure 4: Voltage at turbine terminals in the Risoe (top) and ECN-TUD models (bottom)

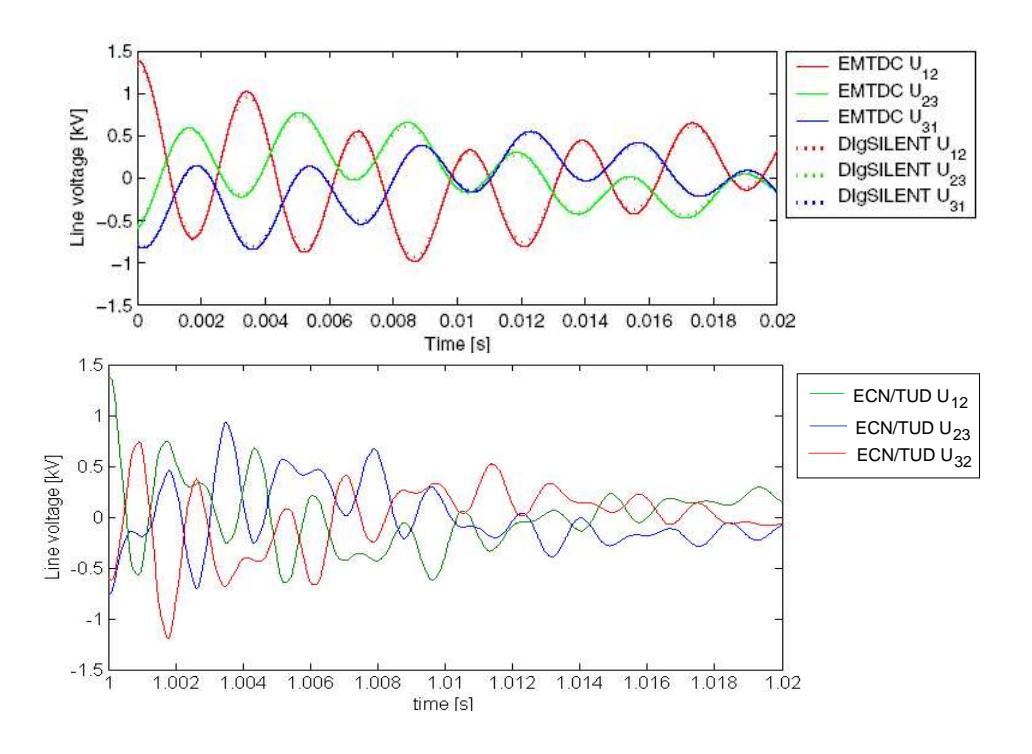


Figure 5: Detailed view of voltage at turbine terminals during start of dip in the Risoe (top) and ECN-TUD models (bottom)

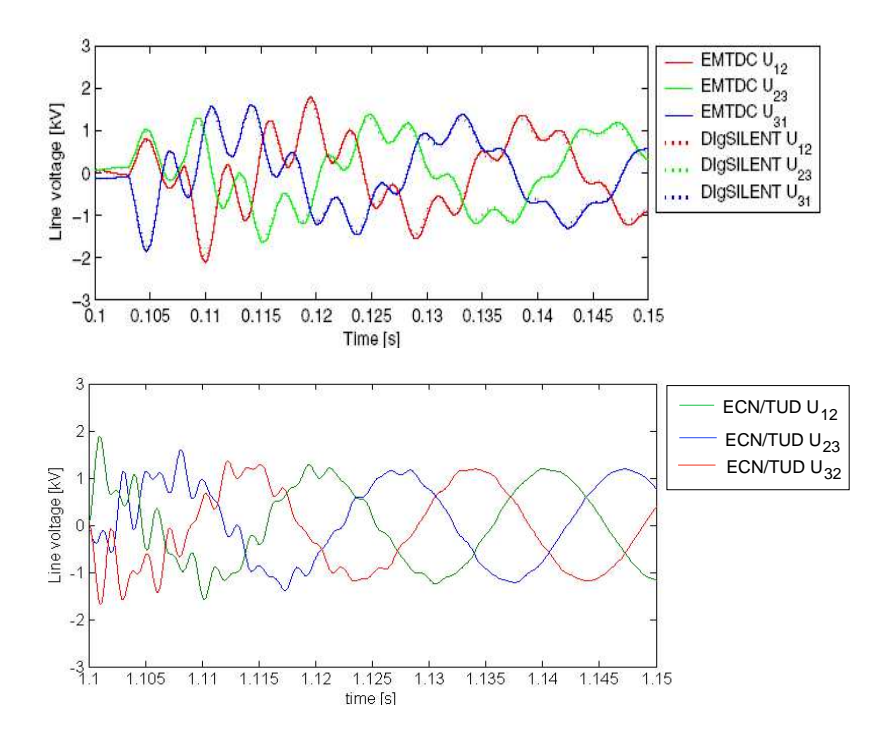


Figure 6: Detailed view of voltage at turbine terminals after dip clearance in the Risoe (top) and ECN-TUD models (bottom)

The stator currents of the turbine are shown in figure 7. The electrical torque of the generator is shown in figure 8. In order to see the long term fluctuations in the torque, it has been plotted again in figure 9. The rotational speed of the turbine is shown in figure 10.

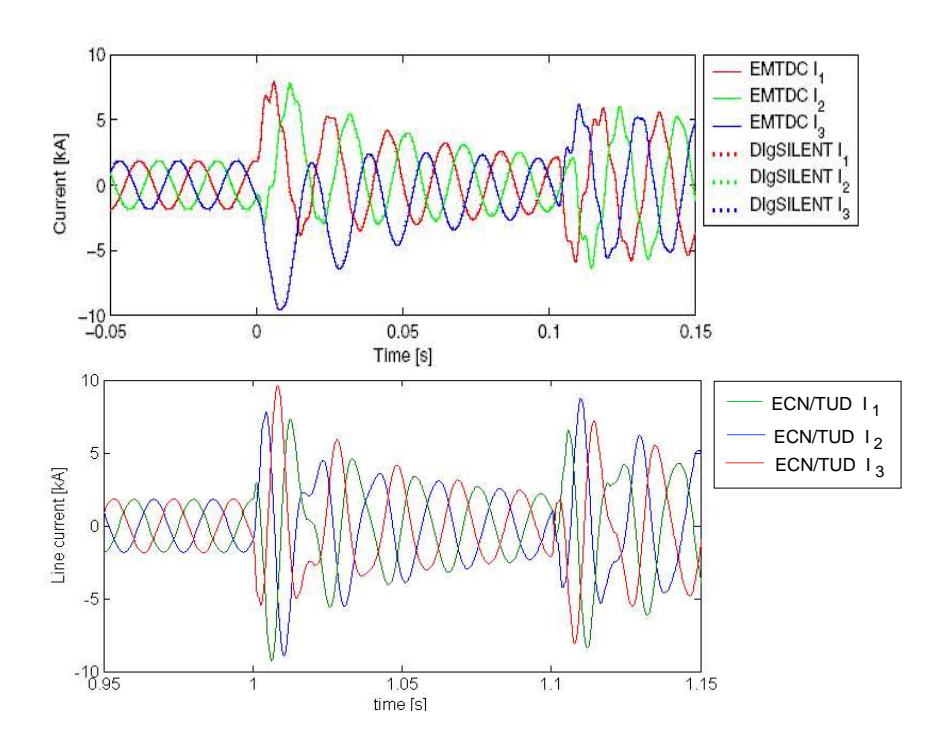


Figure 7: Stator current before, during and after dip in the Risoe (top) and ECN-TUD models (bottom)

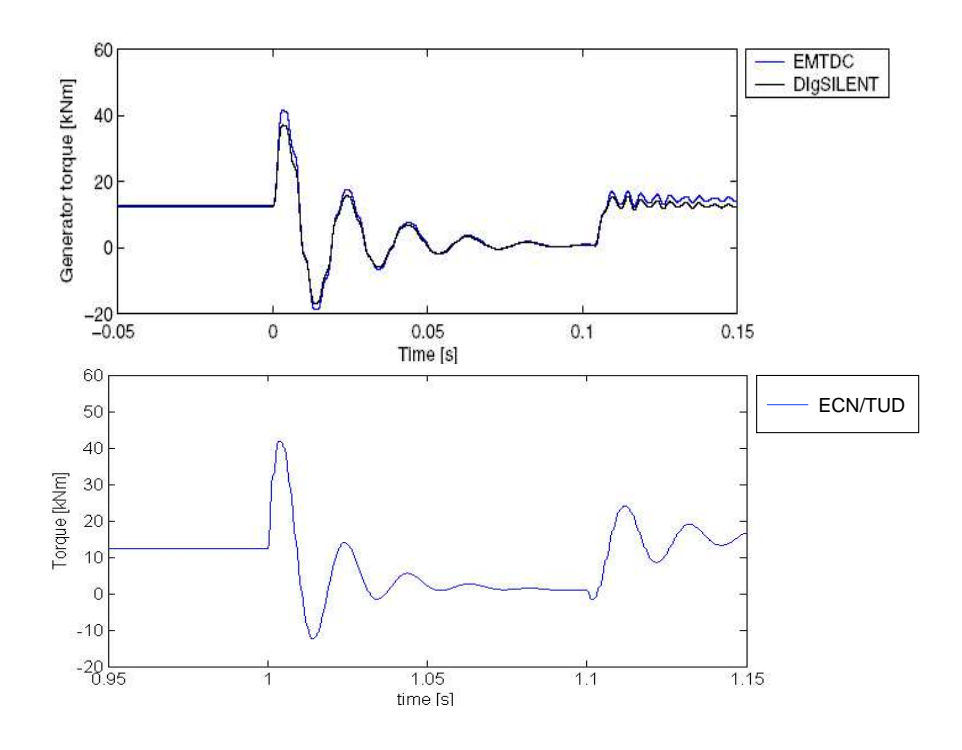


Figure 8: Generator torque during dip in the Risoe (top) and ECN-TUD models (bottom)

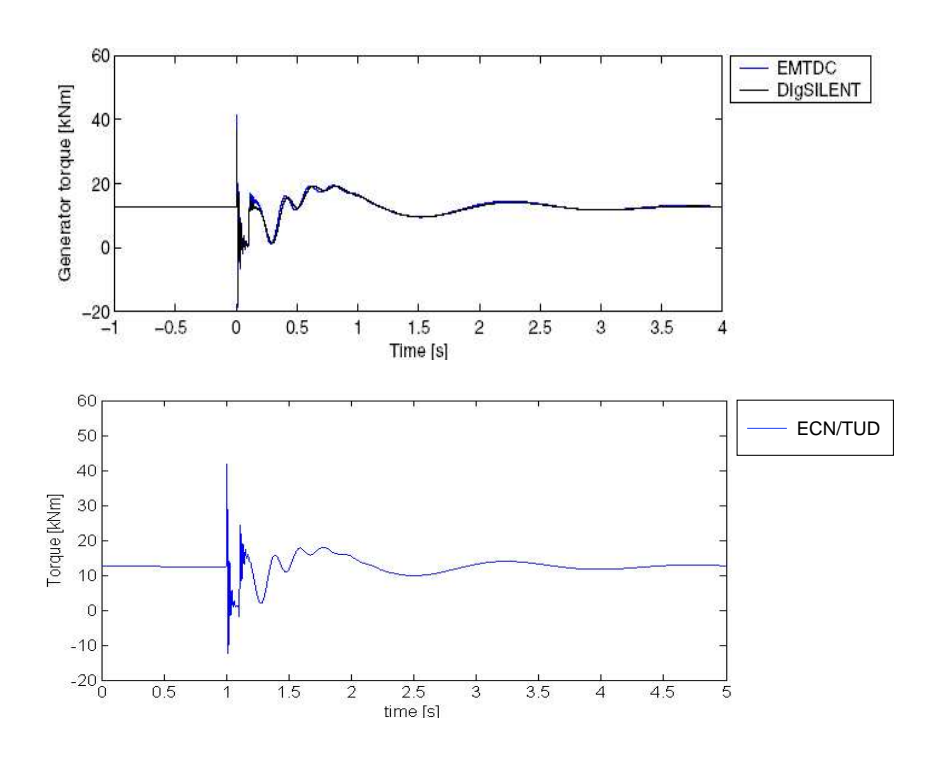


Figure 9: Generator torque for longer period in the Risoe (top) and ECN-TUD models (bottom)

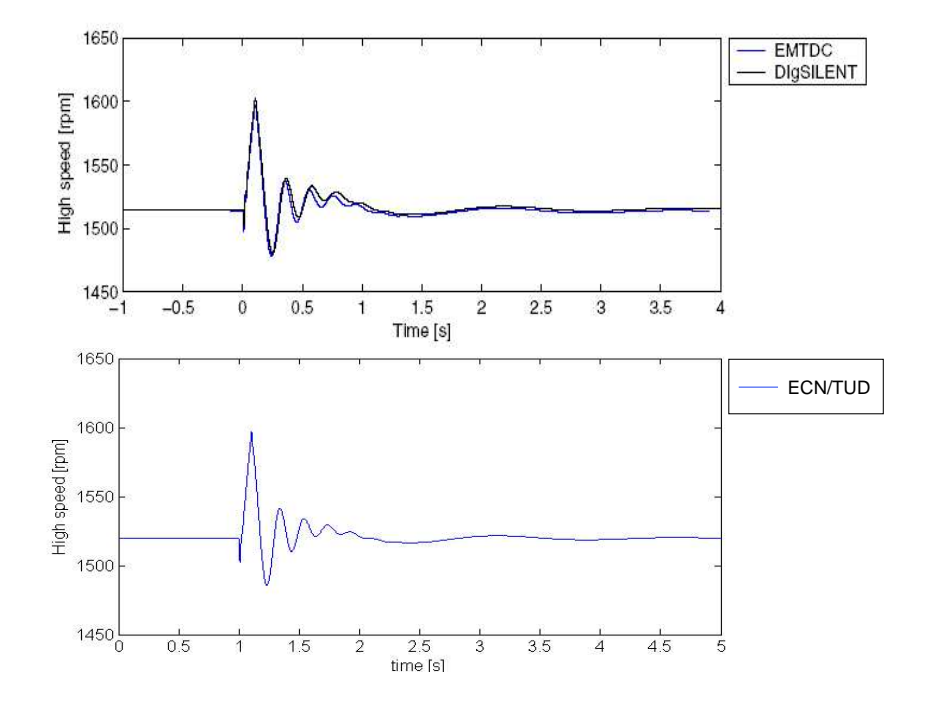


Figure 10: Generator rotational speed in the Risoe (top) and ECN-TUD models (bottom)

2.5 Discussion

In this section the differences between the Risoe and ECN-TUD simulation results will be discussed. The most important deviations are the difference in oscillation frequency and damping of the oscillations. The oscillation frequency in the Risoe benchmark simulations is higher and the Risoe damping is lower. These deviations are probably caused by small differences between the Risoe and the ECN-TUD models. The most important difference in the models is that the ECN-TUD transformer model does not include the magnetizing inductance and the iron losses. Another difference between the Risoe and ECN-TUD simulation results is that the currents after dip clearance are somewhat higher for the ECN-TUD simulations then for the Risoe benchmark results. The torque and rotational speed are practically equal, except for some high-frequency oscillations. This is not so strange, because exactly the same mechanical model has been used. In total, the ECN-TUD results are similar to the Risoe results and give no reason for model adaptations or improvements.

2.6 Appendix: Benchmark system parameters

	58 μF	1	C_1	50 kV	U_{Th}
	568 Ω	0.7	R	2.1156Ω	R_{Th}
	473 Ω	0.4	X	$8.2998~\Omega$	X_{Th}
	58 μF	1	C_2	1. $50kV$ grid (G_{50}) data	
cable (Ca _{Col}) da	10 kV collection	3. Wind farm			
	2 MVA	S_n		16 MVA	$S_{\rm n}$
	10.5 kV	$U_{\mathfrak{p}}$		50 kV	$U_{\mathfrak{p}}$
	$0.96~\mathrm{kV}$	U_{s}		$10.5~\mathrm{kV}$	$U_{\rm s}$
	$0.2756~\Omega$	R_{p}		$0.4052~\Omega$	$R_{\rm p}$
	$1.654~\Omega$	X_{p}		$7.655~\Omega$	X_{p}
	6890Ω	X_{m}		$19530~\Omega$	$X_{\rm m}$
	$0.2756~\Omega$	$R_{\rm s}'$		$0.4052~\Omega$	$R_{\rm s}'$
	1.654 Ω	X_{s}'		7.655 Ω	X_{s}'
ner (1 _{WT1}) data).96 kV transform	4. 10/6	data	2. 50/10 kV transformer (T _{Gr})	
$6 \cdot 10^6 \text{ kg m}^2$	4.176	$I_{ m WTR}$		2.3 MVA	S_n
93.22 kg m^2		$I_{ m gen}$		0.96 kV	$U_{\rm n}$
10 ⁷ Nm / rad	8.949 · 1	$k_{ m ms}$		1500 rpm	N_0
80		f		$0.004~\Omega$	$R_{\rm s}$
l system data	6. Mechanical			$0.05~\Omega$	$X_{\rm s}$
				$1.6~\Omega$	$X_{\rm m}$
				$0.004~\Omega$	$R_{\rm r}'$

5. Induction generator data

 0.05Ω

Figure 11: Benchmark system parameters

3 MODEL IMPROVEMENT: PROTECTION OF WIND TUR-BINES WITH DOUBLY-FED INDUCTION GENERATOR

3.1 Introduction

Most new wind turbines that are installed nowadays are variable speed turbines with a doubly-fed induction generator (DFIG). This turbine has a power electronic converter between the rotor windings and the grid. A major drawback of wind turbines with a DFIG, is their operation during grid faults. Faults in the power system, even far away from the location of the turbine, can cause a voltage dip at the connection point of the wind turbine. The dip in the grid voltage will result in an increase of the current in the stator windings of the DFIG. Because of the magnetic coupling between stator and rotor this current will also flow in the rotor circuit and the power electronic converter. This can lead to destruction of the converter. It is possible to try to limit the current by current control on the rotor side of the converter, however this will lead to high voltages at the converter terminals, which might also lead to destruction of the converter.

The method which is proposed limits the high current in the rotor and provides a by-pass for it via a set of resistors that are connected to the rotor windings. With these resistors it is possible to survive grid faults without disconnection of the turbine from the grid. Because generator and converter stay connected, synchronism of operation remains during and after the fault and normal operation can be continued immediately after the fault has been cleared. A control strategy has been developed that takes care of the transition back to normal operation. Without this transition control, large transients would occur. When the dip duration is longer than a few hundred milliseconds, the short-circuit resistors can be disconnected and the system can resume normal operation at reduced grid voltage. It can even supply reactive power to the grid during the fault.

3.2 Fault response and protection of DFIG

This section analyses the response of a DFIG to a dip in the voltage at its terminals. The stator voltage equation of the induction machine can be written in different ways. For ease of explanation it is written as a space-vector in a stationary reference frame:

$$\vec{v}_s = R_s \vec{i}_s + \frac{d}{dt} \vec{\Psi}_s \tag{1}$$

In normal operation the space-vectors rotate at a synchronous speed with respect to the reference frame. Ignoring the stator resistance the derivative of the stator flux is directly proportional to the grid voltage. When the voltage drops to zero (in case of a fault at the generator terminals) the stator flux space-vector will stop rotating. This will produce a dc-component in the stator flux. The dc-component in the rotor flux of the machine is fixed to the rotor and will continue rotating. This will thus add an alternating component to the dc-component of the stator flux. The maximum value that the currents reach depends mainly on the dip depth and the stator and rotor leakage inductance. How fast the dc-component will decay is mainly determined by the transient time constants of the stator and rotor.

The voltage dip will cause large (oscillating) currents in the rotor circuit of the DFIG, to which the converter is connected. A high rotor voltage will be needed to control the rotor current. When this required voltage exceeds the maximum voltage of the converter, it is not possible any longer to control the current as desired. This implies that a voltage dip can cause high

ECN-E-07-006 25

induced voltages or currents in the rotor circuit that can destroy the converter. In order to avoid breakdown of the converter switches, there should be a by-pass for the rotor currents in case of a voltage dip. This can be done by connecting a set of resistors to the rotor winding via bi-directional thyristors, also called a crowbar, as is shown in figure 12. When the rotor currents become too high the thyristors are fired and the high currents do not flow through the converter but into the by-pass resistors. Meanwhile it is not necessary to disconnect the converter from the rotor or the grid. Because generator and converter stay connected, the synchronism of operation remains established during the fault.

When the fault in the grid is cleared, or the dc offset in voltage and current has decayed far enough, the resistors can be disconnected by stopping the gate signals of the thyristors and the generator can resume normal operation. A control strategy has been developed that takes care of the transition to normal operation. Without special control action large transients would occur. During the period that the resistors are connected to the rotor circuit the controller signals should be limited to a small band around the values they had at the moment that the fault occurred. The controllers will try to control the currents, the power, the rotational speed and so on to the reference values. This is not possible however as long as the by-pass resistors are connected to the rotor circuit. When the signals are not limited large overshoot in the signals will occur.

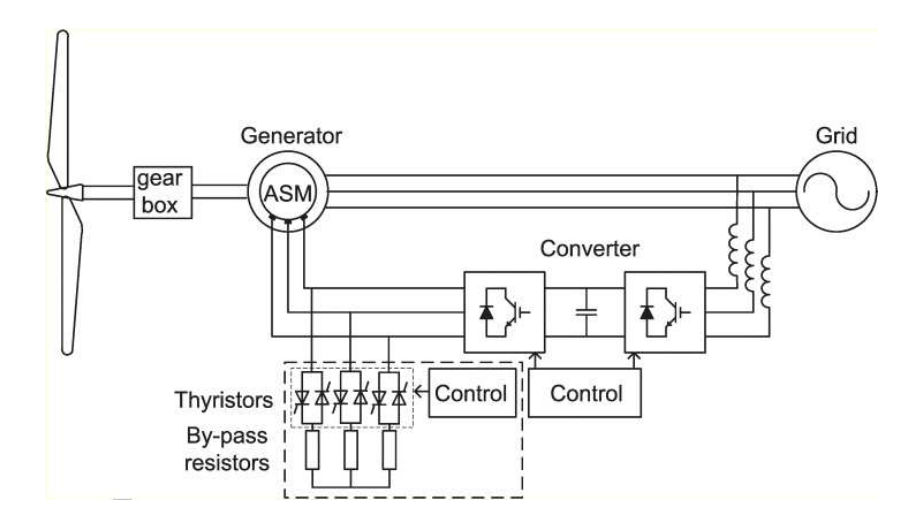


Figure 12: DFIG by-pass resistors in the rotor circuit

An important issue is the value of the by-pass resistance. On the one hand the resistance should be high, to limit the short-circuit current. On the other hand it should be low to avoid a too high voltage in the rotor circuit. A too high voltage can result in breakdown of the isolation material of the rotor and the converter. It is further possible that when the voltage becomes higher than the dc-link voltage, large currents will flow through the anti-parallel diodes of the converter, charging the dc-link to an unacceptable high voltage. The thermal time constant of the rotor will be high enough to handle the short-circuit currents for a short period and the by-pass resistors should be designed for it.

3.3 Modelling

The model of the DFIG and its control has been presented in the Erao-II already and will not be repeated here. Three sub-blocks of the Erao-II model have been changed to include the

crowbar protection. These will be explained here shortly. One block has been added to the 'Comp-DFIG-abc' block shown in figure 83 of the Erao-II report, which models the induction machine. The block that has been added models the crowbar resistances. Figure 13 shows how the 'protection' block is included in the model. The block itself is shown in figure 14. The output voltage of the block is equal to the input voltage, as long as the protection is not activated. The block 'mag(ir)' determines the magnitude of the rotor current. When this current becomes too high, the protection is activated, and the output voltage is obtained from the input current times the crowbar resistance. The two 'rate limiters' model the turn-on and turn-off time of the thyristors. When the protection is activated, there is a certain period in which it will not be de-activated, even if the rotor current drops below the threshold value. This is done to avoid that the protection turns on and off continuously, because of the oscillations in the rotor current. The time delay is obtained from the integrator and gain at the right side of the model.

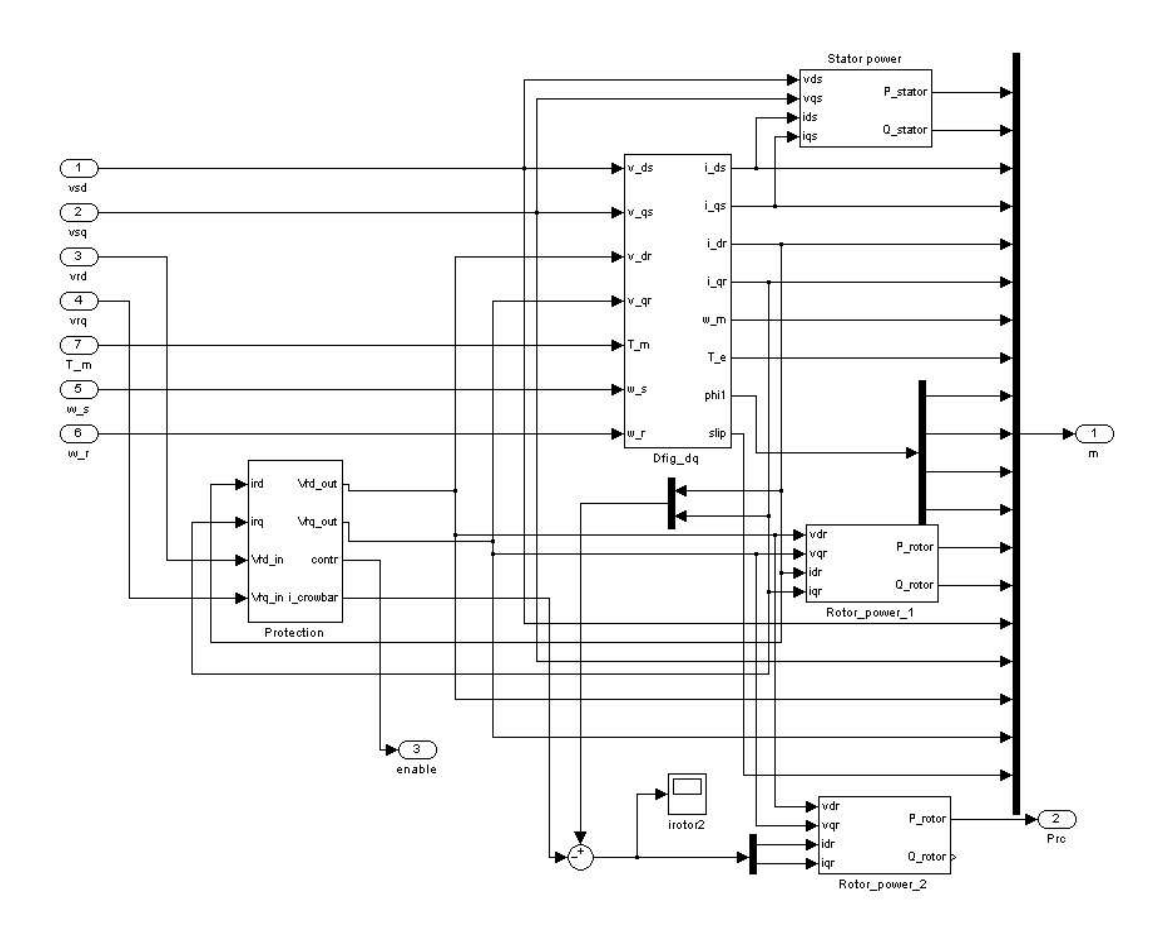


Figure 13: Induction machine model with protection block

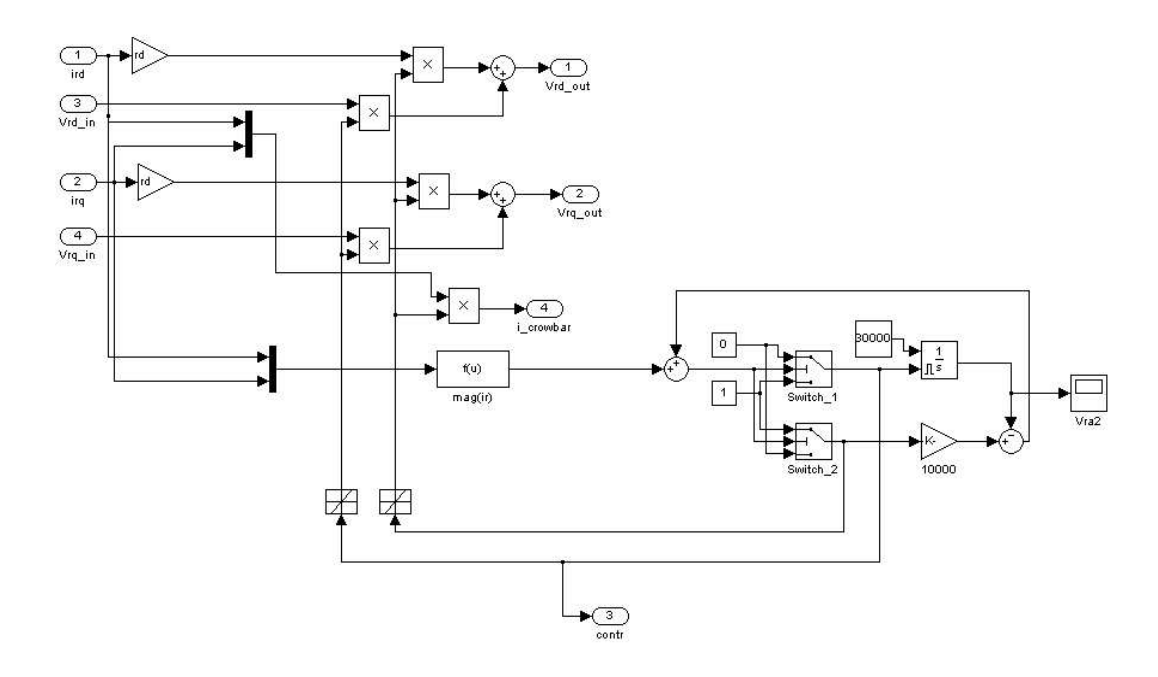


Figure 14: Protection block that models the crowbar resistances

During the period that the resistors are connected to the rotor circuit the controller signals are limited to avoid large oscillations at the moment that the protection circuit is disabled. The torque control block that was shown in Figure 78 of the Erao-II report is shown again in figure 15, but now with different blocks for the 'wm-controller' and the 'iq-controller', to limit the output of these controllers. The content of the 'wm-controller' block is shown in figure 16. The output of the PI-controller is limited and the difference between the output of the PI controller and the limited output is fed back, to avoid saturation of the controller. A similar block is used for the current controller. The reactive power control block has been changed in a similar way as the torque controller block.

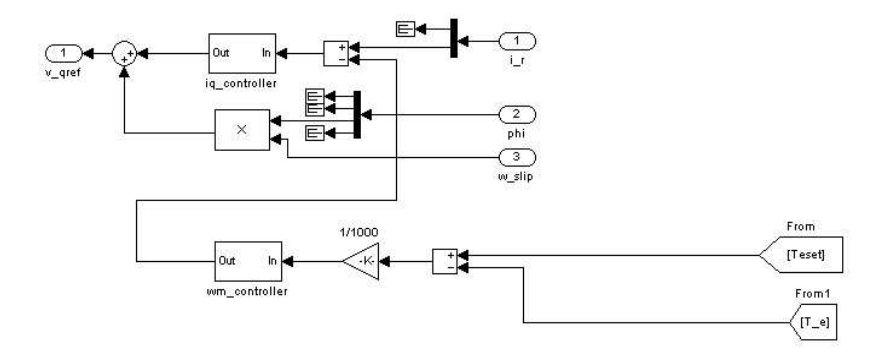


Figure 15: Torque controller block

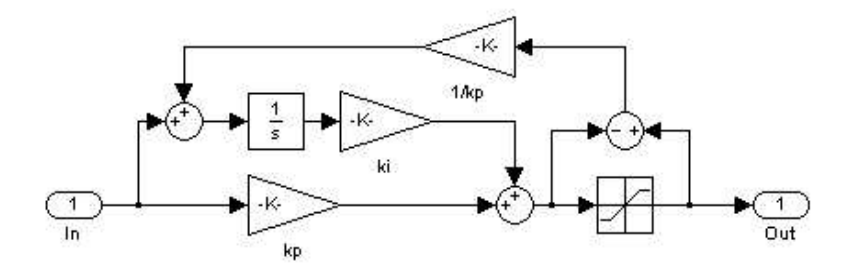


Figure 16: Torque controller block

3.4 Simulation results

In order to show the effectiveness of the protection scheme, simulation results will be presented. The wind turbine is connected to a 10kV distribution network, which is modelled as a Thévenin equivalent circuit with a short-circuit impedance of 50MVA and an X/R ratio of 0.75. Data of the 2.75MW DFIG is given in section 3.6. The by-pass thyristors are activated when the rotor current exceeds 1.1pu. All values refer to the stator with the nominal generator power and voltage as the base values. The maximum allowable rotor (line-line) voltage is 0.35pu. The value of the by-pass resistors is 0.1pu.

In the first case the behaviour of the DFIG during a voltage dip of 85% (15% remaining voltage) and 200ms is simulated. The stator voltage and current are shown in figure 17a and 17b and the rotor voltage and current are shown in figure 17c and 17d, respectively. A large peak in the stator and rotor current can be noticed. The rotor current is not flowing through the converter however, but in the by-pass resistors. The power that is consumed by the resistors is shown in figure 17e. The rotor voltage oscillates to 0.3pu. This is slightly below the maximum rotor voltage of 0.35pu. Due to the drop in stator power, the wind turbine will accelerate. Because of the large inertia of the wind turbine rotor the increase in rotational speed is limited however, as can be seen from figure 17f. When the dip lasts longer eventually the pitch controller can be used to reduce the aerodynamic power and to limit the increase in rotational speed.

After about 50ms the by-pass resistors are disconnected and the DFIG can resume normal operation (at a lower voltage). The clearance of the voltage dip results again in high oscillating currents and the by-pass resistors will be turned on again to protect the converter. After the current has decayed far enough the resistors are disconnected again and the turbine can resume normal operation.

By appropriate control the wind turbine can supply reactive power during the dip, as is demanded by some grid connection requirements for wind turbines. When the by-pass resistors are de-activated the turbine can resume normal operation and supply reactive power. This will be shown in an example. The same network and wind turbine as in the previous example are used. Now a 50% - 1s dip is applied. The stator voltage is shown in figure 18a and the active and reactive power supplied by the DFIG are shown in figure 18b and 18c respectively. It can be seen that 0.25pu reactive power is supplied, while the generator is still supplying ≈ 0.5 pu active power. When more reactive power has to be supplied, the active power should be reduced, or a higher current should be allowed. Figure 18d shows the rotor current. During the dip it is operating at 1pu. The rotor voltage is shown in figure 18e and the rotational speed is shown in figure 18f.

Large reactive power peaks can be noted at the occurrence and clearance of the fault. They are caused by the (de-)magnetizing of the machine. The large amount of reactive power that is absorbed immediately after fault clearance may cause voltage stability problems and in a further study it should be investigated how it can be limited.

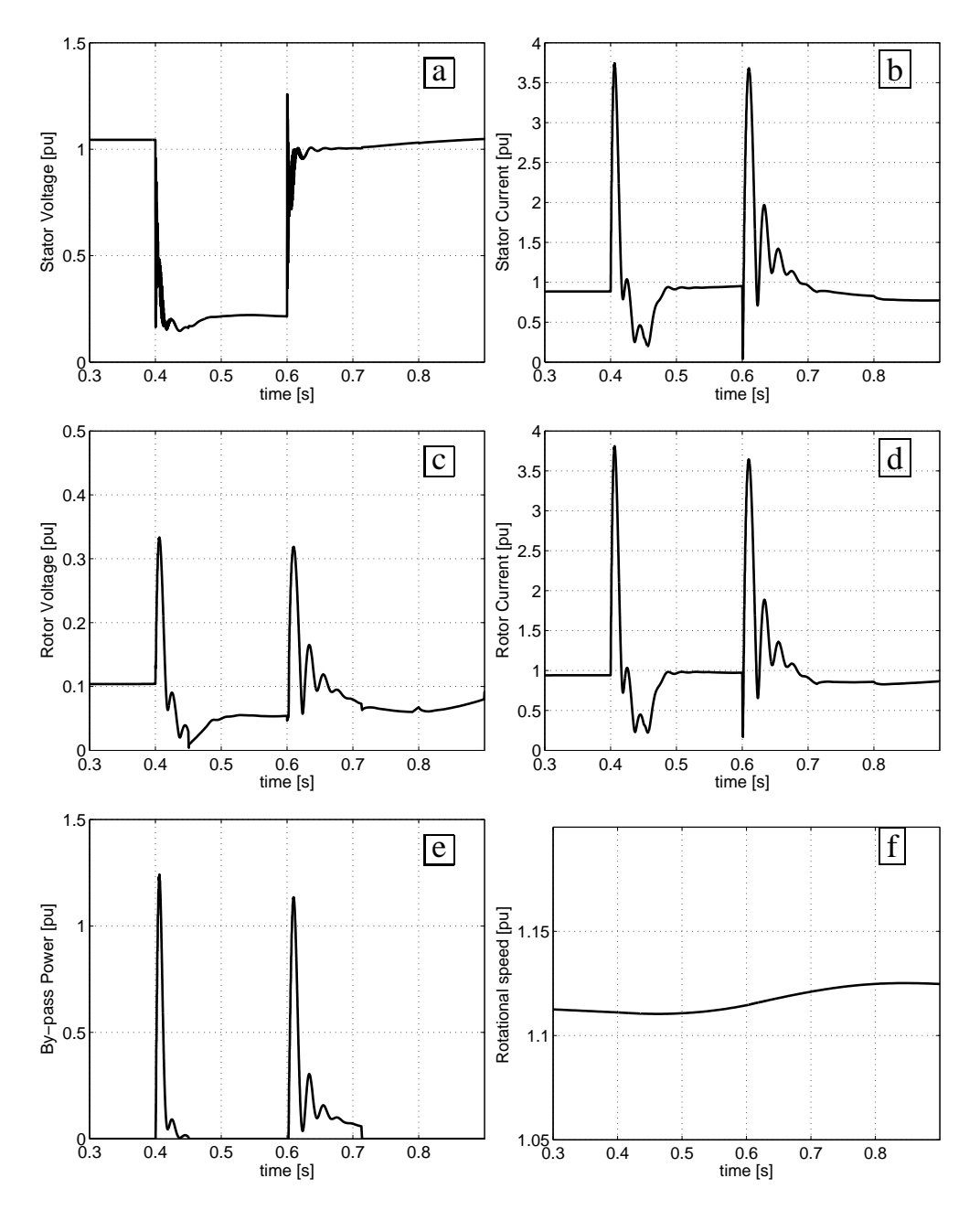


Figure 17: Voltage dip of 85%, 0.2 seconds applied to DFIG with protection: (a) stator voltage; (b) stator current; (c) rotor voltage; (d) rotor current; (e) power consumed in by-pass resistors; (f) rotational speed of generator

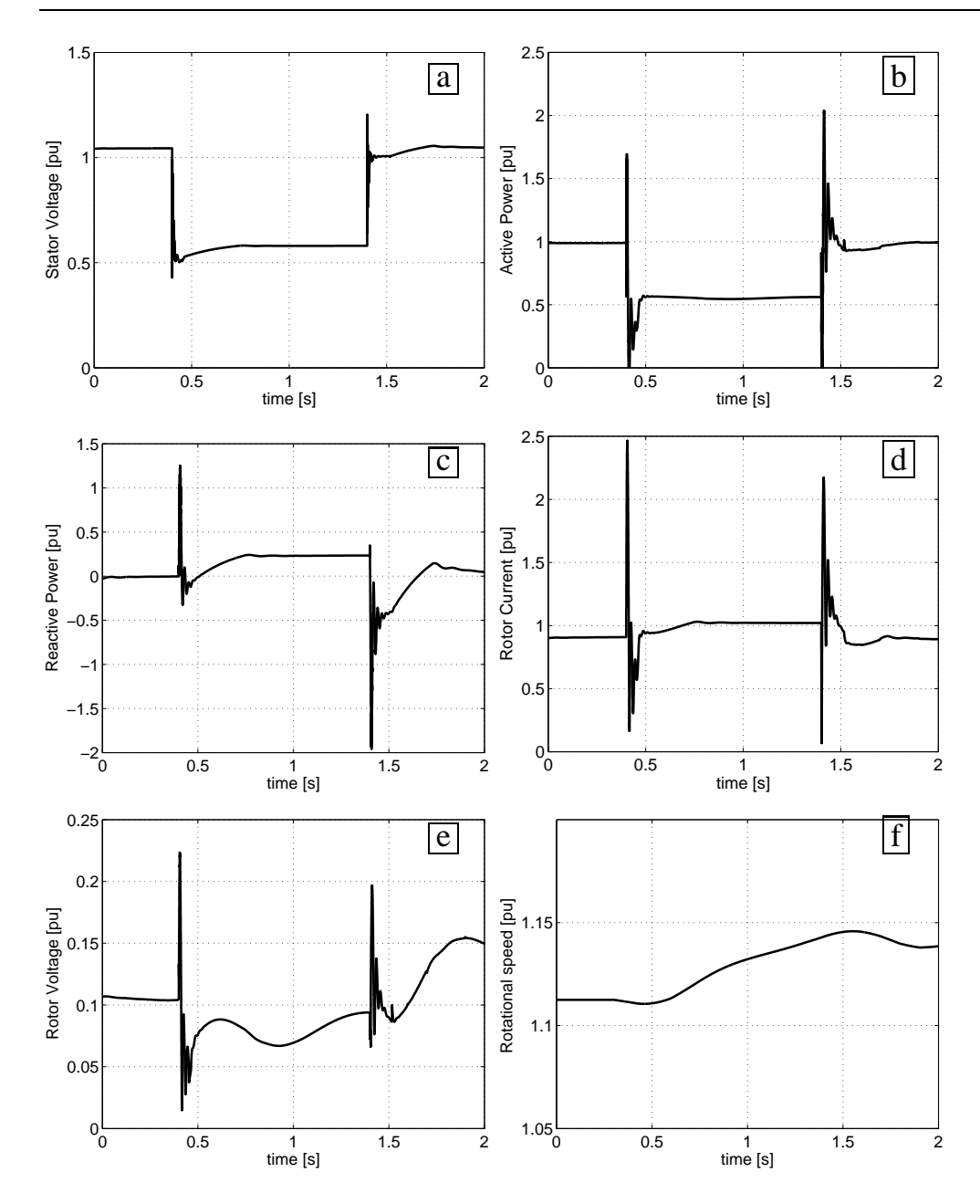


Figure 18: Voltage dip of 50%, 1 second applied to DFIG with protection: (a) stator voltage; (b) DFIG active power; (c) DFIG reactive power; (d) rotor current; (e) rotor voltage; (f) rotational speed

3.5 Conclusion

A method is demonstrated which keeps the generator connected to the grid in case of a grid failure so that it can resume power generation after clearance of the fault in the grid. The key is to limit the high currents in the converter by providing a by-pass in the rotor circuit via a set of resistors that are connected to the rotor windings without disconnecting the converter from the rotor or from the grid. The wind turbine can resume normal operation within a few hundred milliseconds after the fault has been cleared. For longer voltage dips, the generator can even

supply reactive power to the grid. Simulation results show the effectiveness of the proposed method.

3.6 Machine and controller parameters

The machine and controller parameters that have been used during the simulations are given below.

Machine parameters:				
Apparent power S_{nom}	2.5 MW			
Mutual inductance L_m	2.5 pu			
Stator leakage inductance L_s	0.11 pu			
Rotor leakage inductance L_r	0.07 pu			
Stator resistance R_s	0.0021 pu			
Rotor resistance R_r	0.0021 pu			
Pole number p	3			
Inertia J	240 kg m2			
By-pass resistor R_{bp}	0.86 pu			
Controller parameters:				
k_p	2			
k_i	32			
k_{ps}	25			
k_{is}	155			

4 MODEL IMPROVEMENT: INERTIAL RESPONSE CONTROL FOR VARIABLE SPEED WIND TURBINES

4.1 Introduction

In the AC grid as we know it today, the grid frequency is controlled by conventional power plants. The goal of frequency control is to keep the frequency within a small band around 50 (or 60) Hz and to maintain the power balance [12], [4]. The inertia of synchronous machines plays a significant role in maintaining the stability of the power system during a transient situation. Differences between the supplied and demanded power will immediately result in a change in the rotational speed of the synchronous generator, and correspondingly to a change in the grid frequency, according to the following equation:

$$J\omega_m \frac{d}{dt}\omega_m = P_{gen} - P_{load} \tag{2}$$

with J the total inertia of the system, ω_m the mechanical rotational speed of the generator and P_{qen} and P_{load} the total power supplied by all generators in the system and the power demanded by all loads in the system, respectively. The more rotational mass (the more inertia) the synchronous generators have, the less the rotor-speed of the generators will change during an imbalance of power. The relatively large amount of rotating mass in the present interconnected power systems tends to keep the system stable following a disturbance. With an increasing penetration level of variable speed wind turbines, assuming that they (at least partly) replace conventional generation, the stabilisation is becoming increasingly difficult because of the decreasing level of inertia that is connected to the grid, or that is 'seen' by the grid [20]. The inertia is reduced because the control of the variable speed wind turbines decouples the mechanical and electrical systems and a change in system frequency will not be experienced by the wind turbine rotor. This will be undesirable when there are a large number of wind turbines, especially in periods of low load and on small power systems [3]. The lower the inertia of a system, the more and faster the frequency will change after abrupt variations in generation or load. It has been noticed recently, that it is necessary to let variable speed wind turbines contribute to the system inertia [3],[13], [2]. It has been shown that supplementary control loops can be implemented, which let the turbines contribute to the inertia of the system.

Two different control strategies to give variable speed wind turbines an inertial response will be investigated in this chapter. With inertial response is meant that the wind turbine will increase its power supplied to the grid, during a drop in the grid frequency. The first control strategy has been proposed in [3]. Basically, it gives the wind turbine a response to frequency deviations that is equal to the inherent behaviour of a synchronous machine. The additional amount of power supplied is proportional to the derivative of the frequency. It will be called inertia control. The second control strategy implements on the wind turbine the primary frequency control that is used by conventional power plants. The amount of power supplied is proportional to the difference between the measured and the nominal frequency. It will be called droop control. The goal of this chapter is to investigate how both types of control can be implemented in a wind turbine and to compare the different solutions, to see which one gives the smallest frequency deviation.

The inertia of a wind turbine will be strongly dependent on the size and rated power of the turbine, which are steadily increasing throughout the years. The report starts with deriving scaling rules for the inertia of modern variable speed wind turbines. Based on these scaling rules the potential for short-term frequency control is considered. Next, two different control loops that can be used to implement inertial response will be discussed. After a short description of the

ECN-E-07-006 33

simulation setup, the implementation of the controllers will be discussed and their operation will be evaluated by time-domain simulations. The chapter concludes with a discussion of the results and a summary.

4.2 Wind turbine inertia

After a drop in network frequency conventional power plants will immediately release energy from their rotating mass. The energy stored in this rotating mass is given by:

$$E = 0.5J\omega_m^2 \tag{3}$$

with J the inertia of the machine and wm the rotational speed of the machine. In electrical power engineering often the so-called inertia constant H is used, which is defined as:

$$H = \frac{J\omega_m^2}{2S} \tag{4}$$

with S the nominal apparent power of the generator. The inertia constant has the dimension time and gives an indication of the time that the generator can provide nominal power by only using the energy stored in its rotating mass. Typical inertia constants for the generators of the large conventional power plants are in the range of 2 - 9 s, depending on the type of power plant in which they are used and on the nominal rotational speed [7]. The kinetic energy of a wind turbine consists of the kinetic energy of the rotating blades, the gearbox and the electrical generator. The inertia of the turbine blades will be much higher than that of the electrical generator. The latter will have a much higher rotational speed however, which will also result in a large amount of kinetic energy. The inertia J of a body can be expressed as:

$$J = \sum m_i r_i^2 \tag{5}$$

where r_i is the radial distance from the inertia axis to the representative particle of mass m_i and where the summation is taken over all particles of the body. To approximate the inertia of a wind turbine it can be assumed that the blade has its mass middle-point at about 1/3 of the radius. The total moment of inertia for a three-bladed turbine is then given by:

$$J = 3m_b(\frac{r}{3})^2 = \frac{1}{9}m_r r^2 \tag{6}$$

with m_b the mass of one blade and m_r the mass of the whole rotor including the three blades. For a typical 2MW wind turbine the total mass of the rotor is about 40 tons [5]. The rotor diameter for this turbine is about 75m. According to (6) this gives an inertia of 6.3 million kgm2. The wind turbine has a nominal rotational speed of 1.8 rad/s. Thus the amount of energy stored can be calculated from (3) and is about 10 MJ. The inertia of the electrical generator is about 200 kgm2 and with a nominal rotational speed of 104 rad/s, this gives an energy of about 2 MJ. So the total kinetic energy that is stored is 12 MJ and the inertia constant, with (4), is 6 s, which is more or less equal to the average of conventional power plants. The size of modern wind turbines is steadily increasing, in order to increase the rated output power of the turbine. With the size of the turbine, also the diameter and mass of the blades will increase, which means an increasing inertia. The rotational speeds tends to decrease however with increasing power, which will decrease the kinetic energy stored in the blades. From [5] some trends and developments in wind turbine manufacturing and design can be obtained. The approximate relation between rotor diameter and rated power of MW-class wind turbines is given by:

$$P_r = 195 \cdot d_r^{2.155} \tag{7}$$

and the approximate relation between rotor mass and diameter is given by:

$$m_r = 0.486 \cdot d_r^{2.6} \tag{8}$$

With P_r the rated power of the wind turbine in MW, d_r the diameter of the rotor in m, and m_r the rotor mass in kg. Combining these two equations gives the relation between rated power of the wind turbine and rotor mass as:

$$m_r = 14500 \cdot P_r^{1.2} \tag{9}$$

To give a trend for the energy stored in the rotating mass of a wind turbine, we need to know the rotational speed. The rotational speed of a turbine is directly coupled to the speed of the blade tips (tip speed) which is an important design parameter for wind turbines. Tip speeds for wind turbines are roughly between 70 and 90 m/s [5]. The total energy stored in the rotating mass can be obtained from (3) and (6) as:

$$E = \frac{1}{18}m_r r^2 \omega_m^2 \tag{10}$$

It should be noted that $r\omega_m$ is the tip speed. Assuming that this will be 80 m/s on average, the equation can, with (9), be written as:

$$E = 5.2 \cdot 10^6 P^{1.2} \tag{11}$$

One should be aware that this is just a rough estimation! The most important conclusion from this equation is that the energy stored in the rotating mass tends to increase slightly more than linear with the rated power of the turbine.

4.3 Controller implementation

The control of the doubly-fed induction generator has been described in the Erao-II report already. A speed controller generates a torque setpoint, which generates a setpoint for the current control of the generator. The electrical torque controller is used to extract maximum power from the wind. A change in rotor speed wm will result in a change in the torque setpoint. In order to create inertial response, an additional term will be added to this torque setpoint. The value for this additional torque term, which should improve the inertial response of a wind turbine, can be implemented in different ways. Two different control schemes will be described here. The first one is given in [3]. It is meant to mimic the inherent behaviour of the synchronous generators that are used in conventional power plants. It is based on the observation that by taking the derivative of the kinetic energy available at any speed wm, the power that can be extracted from a rotating mass can be obtained as [3]:

$$P = \frac{dE_k}{dt} = J\omega_m \frac{d\omega_m}{dt} \tag{12}$$

Substituting H for J, the following result is obtained:

$$\frac{P}{S} = 2H \cdot \frac{\omega_m}{\omega_s} \cdot \frac{d(\frac{\omega_m}{\omega_s})}{dt} \tag{13}$$

with ω_s the grid frequency. With \overline{P} and $\overline{\omega}$ the per-unit quantities of power and speed this can be written as:

$$\overline{P} = 2H \cdot \overline{\omega} \frac{d\overline{\omega}}{dt} \tag{14}$$

And the per-unit torque as:

$$\overline{T} = 2H \cdot \frac{d\overline{\omega}}{dt} \tag{15}$$

The controller is shown in figure 19. Noise on the speed measurement may cause large variations in the torque setpoint. In order to minimize the impact on mechanical drive train (the rotating mechanical system) loads, the rate of change of power injection was modified by adding a first order filter after the $\frac{d\omega}{dt}$ input [3]. The delay due to this filter not only reduces the rate of increase of the electromagnetic torque but also reduces the magnitude of the peak torque [3]. This type of control will be called 'inertia control'. The second type of controller that will be investigated can be considered as a proportional controller. The additional torque setpoint is based on the absolute deviation of the frequency from the nominal value:

$$T = k_p(\omega_0 - \omega_{meas}) \tag{16}$$

where k_p is the proportional constant, and ω_0 the nominal speed. This type of control is equal to the primary frequency control that is applied to the conventional synchronous generators. As this is called droop control, the control strategy according to (16) will also be called 'droop control'. The controller is shown in figure 20.

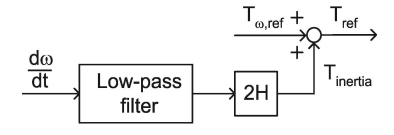


Figure 19: Inertia controller

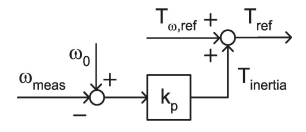


Figure 20: Droop controller

4.4 Modelling

This section describes the implementation of the proposed controllers in the wind turbine model of the variable speed wind turbine with doubly-fed induction generator. In the same way it can be implemented in the control of the permanent magnet generator. Figure 21 shows the implementation of the inertia control and figure 22 shows the implementation of the droop control. The 'Start' block in both implementations is used to active the controller after a few seconds. When the controllers are activated already when the simulation starts, oscillations occur.

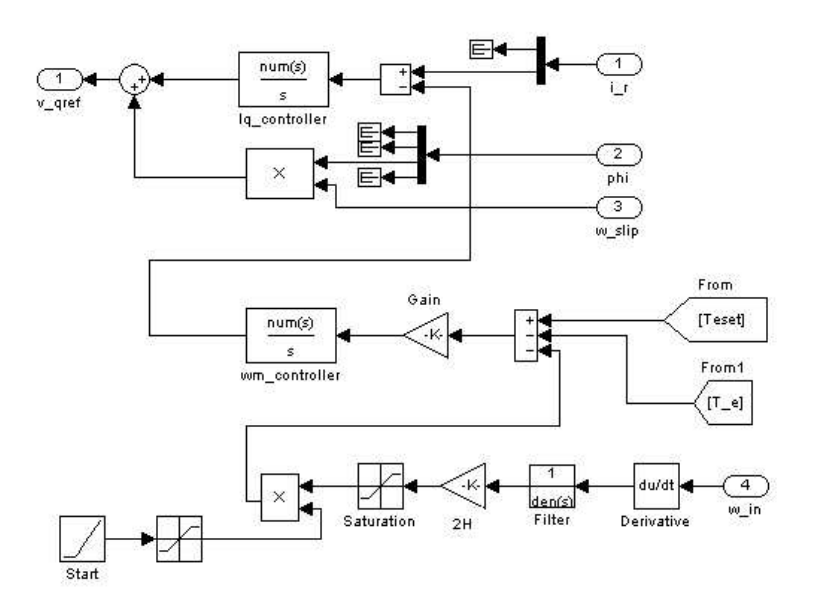


Figure 21: Torque controller block of DFIG with inertia control implementation

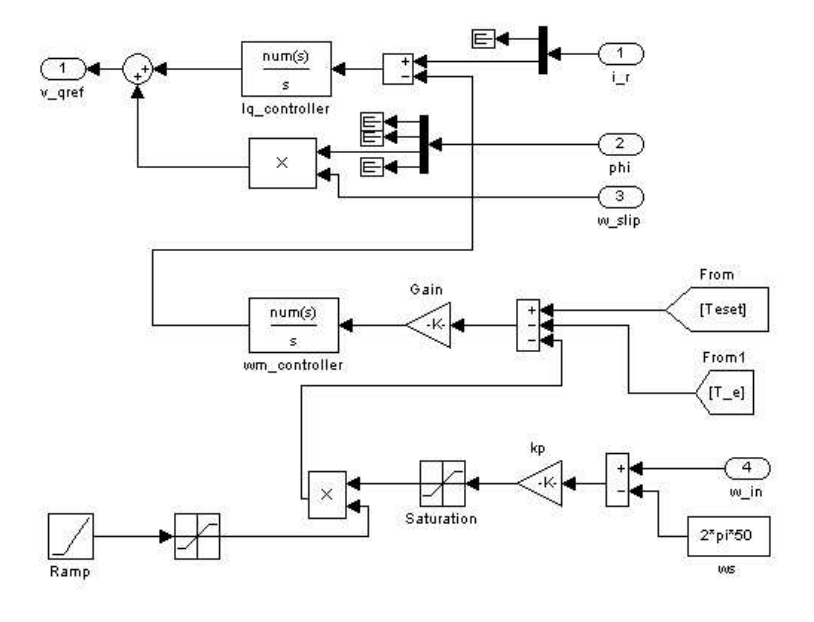


Figure 22: Torque controller block of DFIG with droop control implementation

4.5 Case study description

The goal of this chapter is to show that it is possible to implement 'inertial response' in wind turbines and to compare different ways of implementation. In order to achieve this goal, a case study has been defined. In the case study the system of figure 23 will be used. The grid is modelled by a 200MVA synchronous machine. The two loads are 10 and 90MW respectively. The nominal voltage of the grid is 13.8kV. To this grid a wind farm is connected, through a 34kV cable and a 34kV/13.8kV transformer. The wind farm is assumed to consist of 6 DFIG wind turbines of 2.75MW, so in total 15MW. Only one turbine is modelled. Its current is multiplied by six. An additional load of 10MW is connected to the grid. This changes the total load from 100MW to 110 MW.

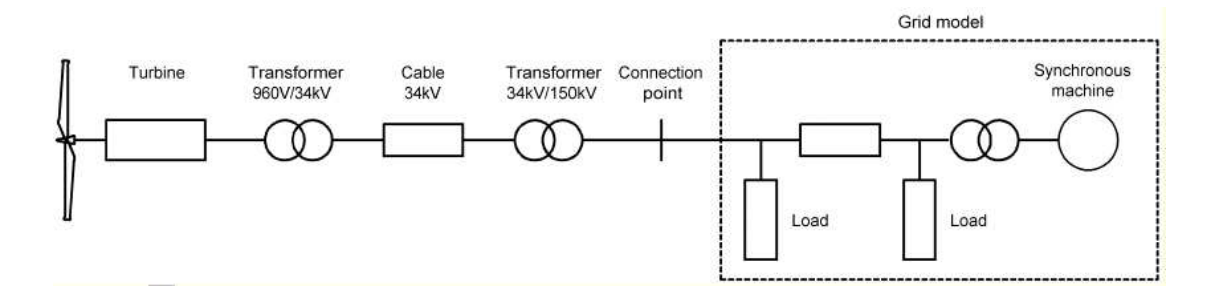


Figure 23: Simulation setup

The grid frequency in response to the connection of the additional 10MW load is shown for three cases in figure 24. The solid line gives the response without additional control implemented on the wind turbines. Due to the weak network that has been assumed, the grid frequency will drop rapidly to about 49.7Hz after which the speed controller of the synchronous machine (which represents the grid) brings it back to 50Hz. The overshoot is due to the (parameter value) of the integrating part of the PI controller that is used for the speed controller. When the wind turbines are modified with the inertia controller, the drop in frequency is less. This situation is presented by the dashed line in figure 24. The time that it takes to bring the frequency back to 50Hz increases while also the overshoot is larger. Only a small time window is shown. The oscillation will damp out slowly.

When the droop controller is implemented, also in figure 24, the frequency goes faster to 50Hz and without overshoot. The drop in frequency is even slightly less than in case of the inertia controller, although the differences are small. A value of 50~kNm/Hz has been used for the droop constant k_p . A higher value of the droop constant will result in a smaller frequency deviation, but will also imply that the wind turbine has to supply more power. Therefore the value should not be too large, as the turbine will not be able to supply this power from its kinetic energy.

During the drop in frequency, the controllers cause the power that the wind turbines supply to the grid to increase. The power (in p.u.) for the inertia control and the droop control is shown in figure 25. From these figures the interesting point can be noted that the increase in active power output is significantly lower for the droop control than for the inertia control, resulting in lower over-currents and lower electrical and mechanical stresses. The base values that have been used are given in table 1.

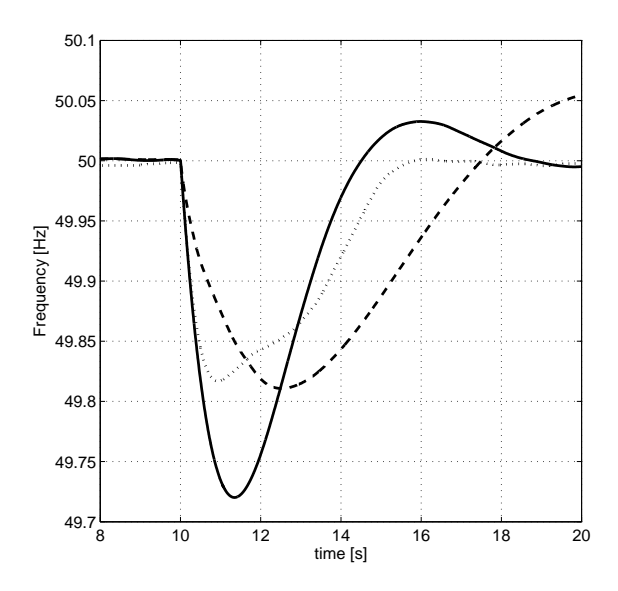


Figure 24: Grid frequency: without wind turbine contribution (solid line), with inertia control (dashed line) and with droop control (dotted line)

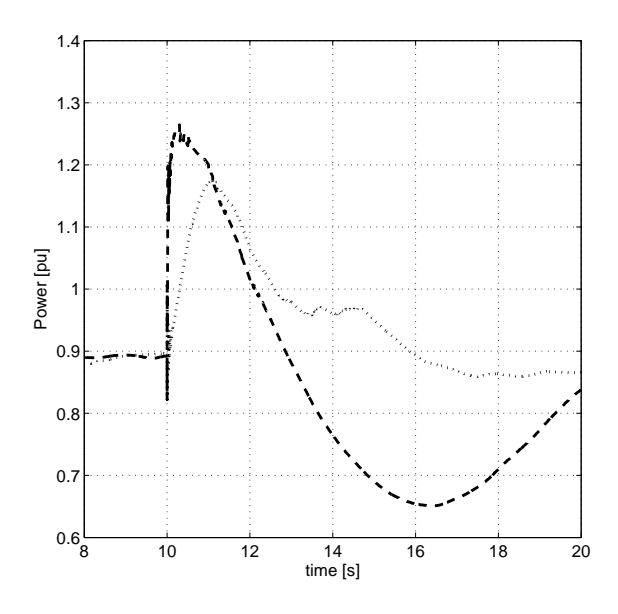


Figure 25: Wind turbine active power: with inertia control (dashed line) and with droop control (dotted line)

Table 1: Base values of the inertal response cases

Parameter	Nominal value	Parameter	Nominal value
Stator power	2.75 MW	Rotor power	750 kW
Stator voltage	960 V	Rotor voltage	690 V
Rotational speed	105 rad/s		

In case of the droop control also the rate of increase of the power (dP/dt) is much lower, and this is expected to give lower mechanical stress and torque pulsations in the drive train. It leads at least to much lower shaft torque excursions, as can be seen from figure 26.

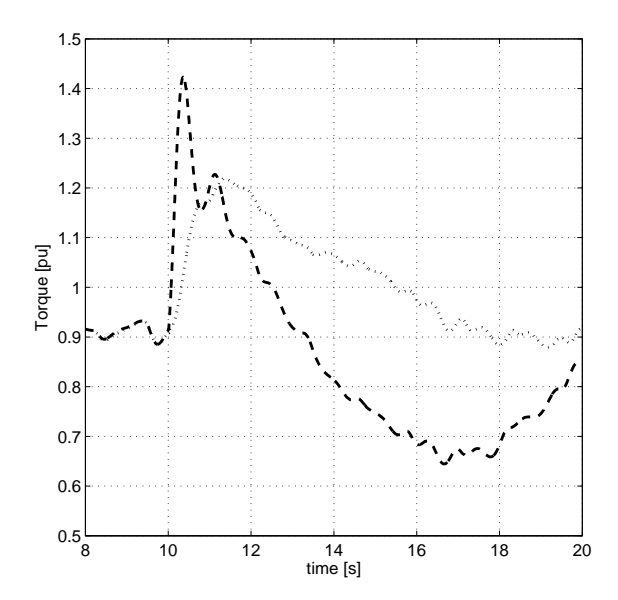


Figure 26: Wind turbine shaft torque: with inertia control (dashed line) and with droop control (dotted line)

The DFIG wind turbines have a power electronic converter connected to their rotor circuit. These power electronic converters can't withstand over-current for a long time. This might limit the amount of additional power that is supplied to the grid during frequency deviations, as the rotor current should be limited. The rotor converter current for both cases is shown in figure 27. It can be seen that it doesn't exceed the nominal value. The current might be dependent on the operating point however. For other operation points the current might be higher, but no large excursions above the nominal current have to be expected.

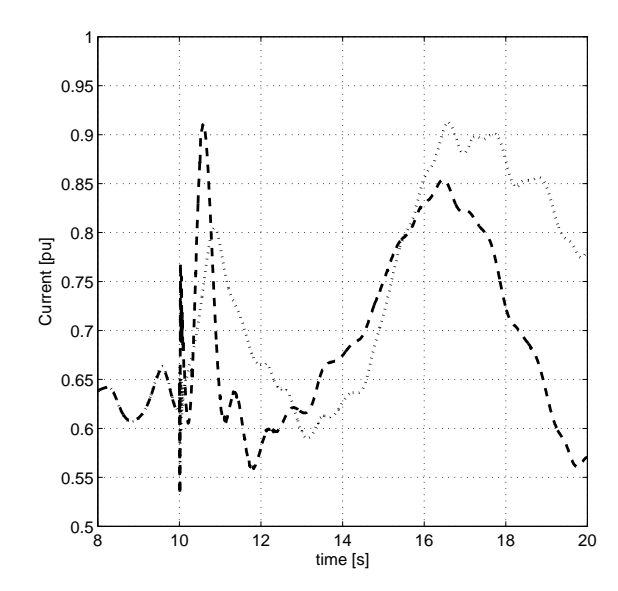


Figure 27: Wind turbine rotor converter current: with inertia control (dashed line) and with droop control (dotted line)

4.6 Results and discussion

Two different supplementary controllers that give a variable speed wind turbine with doubly-fed induction generator an 'inertial response' have been compared. With these controllers, the drop in frequency after a disturbance is shown to be smaller than without the controllers.

When comparing the two different implementations, the droop controller seems to be preferable above the inertia controller. The drop in frequency is slightly lower; there is no overshoot in the frequency response, the required power is smaller and mechanical and electrical stresses, on the mechanical system and power electronic converter, are lower. As the total amount of power supplied will be more or less the same, it can be assumed that the power supplied by the power plant will be larger. The active power supplied by the synchronous machine is shown in figure 28. With the inertia controller implemented, a short peak in synchronous machine power can be noted, but the supplied power immediately drops due to the high amount of power supplied by the wind turbine with inertia controller, figure 28. On the other hand, for the wind turbine with droop controller, the additional amount of power supplied by the synchronous machine is larger, meaning that the wind turbine has to supply less power.

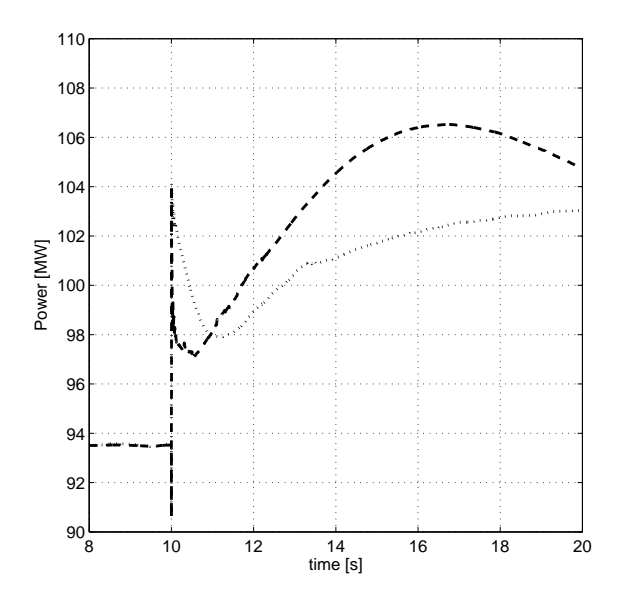


Figure 28: Synchronous generator active power: with inertia control (dashed line) and with droop control (dotted line)

The power sharing between the wind turbines and the synchronous generator will depend on how fast the controllers are acting. This can be seen from figure 29, where the stator power for both controller types is shown again, but now with a faster controller on the synchronous machine. Comparing the results to figure 25, it can be seen that the power for the inertial controller is more or less the same.

The additional power supplied in case of a droop controller is significantly lower however, when a faster controller on the synchronous machine is used. This implies that the synchronous machine will supply more power. It will also have significant influence on the frequency response. This can be seen from figure 30 where the frequency responses are shown. It can be seen that now the inertia controller results in a smaller frequency drop, although the differences are again small. It should be noted that the additional power supplied by the droop controller is also much smaller.

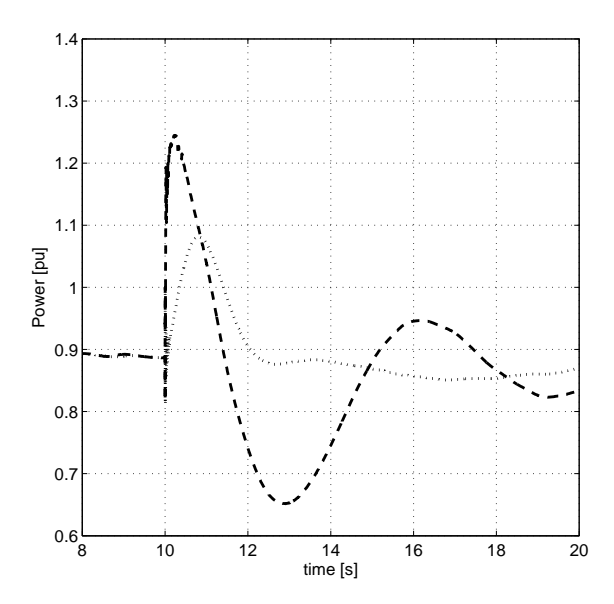


Figure 29: Wind turbine active power for a faster control on synchronous machine: with inertia control (dashed line) and with droop control (dotted line)

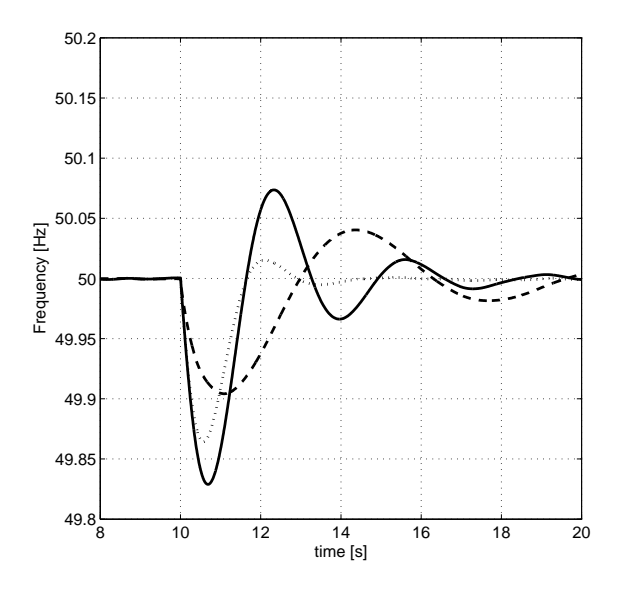


Figure 30: Grid frequency for a faster control on synchronous machine: without wind turbine contribution (solid) with inertia control (dashed line) and with droop control (dotted line)

So far only situations have been considered in which the wind turbine operated at almost full power. The question should be answered whether the proposed solutions also work for wind turbines operating at reduced power levels. To investigate this the simulations have been performed again for an average wind speed of 8 m/s. The turbine operates at about 30% of its rated power then. The resulting wind turbine output power and grid frequency waveforms are shown in figure 31 and figure 32 respectively. The frequency for the case with the inertia control damps out slowly. The speed controller of the synchronous machine has the same value as it had in the first simulation. The results of figure 31 and figure 32 are comparable to figure 25 and figure 26.

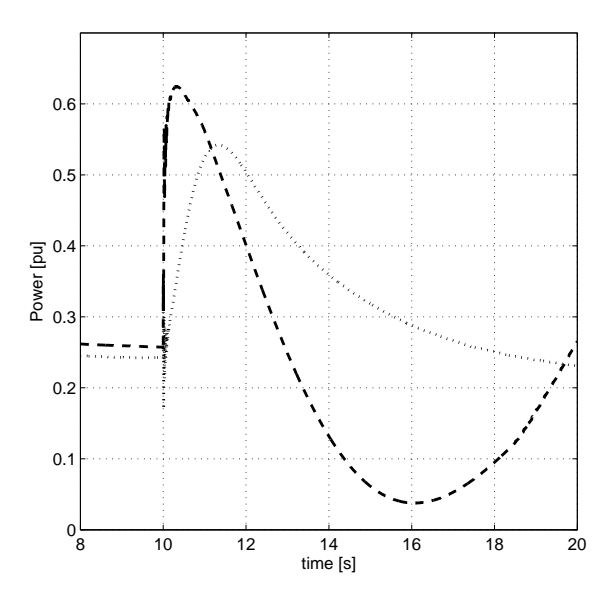


Figure 31: Wind turbine stator power with turbine operating at lower wind speed: with inertia control (dashed line) and with droop control (dotted line)

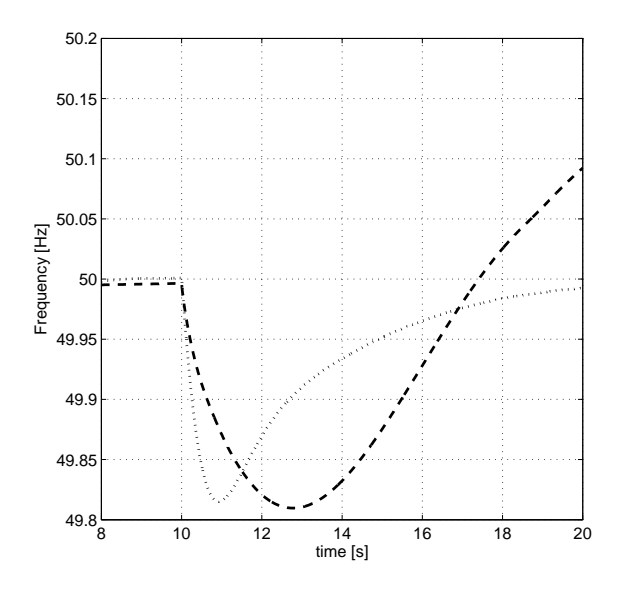


Figure 32: Grid frequency with turbine operating at lower wind speed: with inertia control (dashed line) and with droop control (dotted line)

4.7 Conclusion

Two different control loops that implement 'inertial response' in the control of variable speed wind turbines have been compared. It has been shown that both limit the drop in frequency after a disturbance. Which of the two controller types results in the smallest frequency drop depends on the speed of response of the synchronous generator controllers. For faster controllers the inertia controller seems to be slightly preferable. More in general, the droop controller has some important advantages over the inertia controller however. The amount of power that is required to limit the frequency drop is smaller and consequently the mechanical and electrical

stresses are lower. Also the rate of increase of power, dP/dt, is lower, which will further reduce the mechanical stresses, especially the shaft torque.

The inertia constant for the variable speed wind turbines that have been considered is in the same range as that of conventional power plants. Both have inertia constants in the range of about 2 - 6 s. That means that introduction of wind turbines doesn't decrease the inertia of the grid, as long as the correct controllers are implemented on the wind turbines.

5 AVAILABILITY OF DUTCH MEASUREMENTS FOR MODEL VALIDATION

An effort was made to acquire measurement data on one of the variable speed turbines installed in The Netherlands. The problem is that the requirements on measurements for the validation of a dynamic model are high:

- detailed information on the turbine design and parameters is required, especially regarding the controller design (pitch controller as well as the electrical controllers);
- the measurement should have a high sample rate and adequate anti-aliasing filtering;
- preferably simultaneous measurement of mechanical as well as electrical variables;
- the wind turbine should preferably be a representative, commercial turbine.

For the Erao-3 project the use of the following Dutch measurement data have been investigated:

- Kema measurement on the Proefwindcentrale;
- Measurements on turbines in the Multi Megawatt Testveld of ECN (MMW);
- Measurements of the data-aquisition system of the Dowec turbine;
- A short circuit measurement on a turbine at the Multi Megawatt Testveld.

The Proefwindcentrale turbine is not a representative, commercial turbine. The MMW have a low sample rate and do not include individual voltages and currents. The measurements on the Dowec turbine have a relatively low sample rate and are too short for the calculation of spectra. The short circuit measurement, which was planned in a different project, was not executed due to lack of cooperation from the turbine manufacturer. Therefore, no contribution of Dutch measurements to the IEA data basecould be made.

46 ECN-E-07-006

REFERENCES

- [1] R.A.C.T de Groot and C.P.J. Jansen. Aansluiting van 6000 MW offshore windvermogen op het Nederlandse elektriciteitsnet, Deel 1: Net op zee. Technical Report 40330050-TDC 03-37073B, Kema, 2003.
- [2] J. Ekanayake, L. Holdsworth, and N. Jenkins. *Control of DFIG wind turbines . Power Engineering Journal, Vol. 17, No. 1*, pages 28 32, 2003.
- [3] J. Ekanayake and N. Jenkins. Comparison of the Response of Doubly Fed and Fixed-Speed Induction Generator Wind Turbines to Changes in Network Frequency. IEEE Trans. Energy Conversion, Vol. 19, No. 4,, pages 800–802, 2004.
- [4] J. H. R. Enslin. Interconnection of Distributed Power to the Distribution Network. In IEEE Young Researcher Symposium Proceedings, 2004.
- [5] EWEA. Wind Energy The Facts, Vol. 1: Technology . Technical report, www.ewea.org , 2003.
- [6] EWEA. Large scale integration of wind energy in the European Power Supply: analysis, issues and recommendations . Technical Report EWEA publication, EWEA , 2006.
- [7] J.J. Grainger and W.D. Stevenson. *Power System Analysis*. McGraw-Hill, New York, 1994.
- [8] Kleinrath H. *Stromrichtergespeiste Drehfeldmachinen*. Springer Verlag, Wien, New York, 1980. p. 197.
- [9] S.A. Herman and Pierik. J.T.G. Locaties en opwekkosten 6000 mw offshore windenergie. Technical Report ECN-CX-03-086, ECN, 2003.
- [10] Hannele Holttinen, Peter Meibom, Cornel Ensslin, John McCann, Jan Pierik, John Olav Tande, Ana Estanqueiro, Hortensia Amaris, Lennart Söder, Goran Strbac, and Brian Parsons. Design and Operation of Power Systems with Large Amounts of Wind Power Production, IEA collaboration. In EWEC 2006, Athene, 2006.
- [11] C.P.J. Jansen and R.A.C.T de Groot. Aansluiting van 6000 MW offshore windvermogen op het Nederlandse elektriciteitsnet, Deel 2: Net op land. Technical Report 40330050-TDC 03-37074B, Kema, 2003.
- [12] N. Jenkins. *Impact of Dispersed Generation on Power Systems*. *Electra No. 199*, pages 6–13, 2001.
- [13] G. Lalor, J. Ritchie, S. Rourke, D. Flynn, and M.J. O'Malley. *Dynamic Frequency Control with Increasing Wind Generation*. In *Proc. 2004 IEEE PES General Meeting*, Denver, Co., 2004.
- [14] Eon Netz. Berich ueber den Stand der Untersuchungen zu Hergang und Ursachen der Stoerung des kontinentaleuropaeischen Stromnetzes am Samstag 4 November 2006 nach 22:10 Uhr. Technical Report –, Eon Netz , 2006.
- [15] J.T.G. Pierik, M.E.C. Damen, P. Bauer, and S.W.H. Electrical and control aspects of offshore wind farms, Phase 1: Steady state electrical design and economic modeling, Vol. 1: Project results. Technical Report ECN-CX-01-083, ECN Wind Energy, 2001.

ECN-E-07-006 47

- [16] J.T.G. Pierik and J. Morren. *Constant Speed Wind Farm Dynamic Model Validation; Alsvik measurements and simulations.* Technical Report ECN-E-07-007, *ECN*, 2007.
- [17] J.T.G. Pierik and J. Morren. *Variable Speed Wind Turbine Dynamic Model Validation; JWT measurements and simulations.* Technical Report ECN-E-07-008, *ECN*, 2007.
- [18] J.T.G. Pierik, J. Morren, E.J. Wiggelinkhuizen, S.H.W. de Haan, T.G. van Engelen, and J. Bozelie. *Electrical and Control Aspects of Offshore Wind Turbines II (Erao-2). Volume 1: Dynamic models of wind farms*. Technical Report ECN-C- -04-050, ECN, 2004. available at the web site of ECN (*www.ecn.nl*, use search option).
- [19] J.T.G. Pierik, J. Morren, E.J. Wiggelinkhuizen, S.H.W. de Haan, T.G. van Engelen, and J. Bozelie. *Electrical and Control Aspects of Offshore Wind Turbines II (Erao-2). Volume 2: Offshore wind farm case studies*. Technical Report ECN-C- -04-051, ECN, 2004. available at the web site of ECN (www.ecn.nl, use search option).
- [20] M. Reza, J. Morren, P. H. Schavemaker, W. L. Kling, and L. van der Sluis. Power Electronic Interfaced DG Units: Impact of control strategy on power system transient stability. In Proc. 3rd IEE Int. Conf. on Reliability in Transm. and Distr. Netw., 2005.
- [21] P Soerensen, A.D. Hansen, P. Christensen, M. Mieritz, J. Blech, B. Bak-Jensen, and H. Nielsen. Simulation and verification of transient events in large wind power installations. Technical Report Risoe-R-1331, Risoe, 2003.
- [22] J.O Tande, E. Muljadi, O. Carlson, J. Pierik, A. Estanqueiro, P. Sørensen, M. O'Malley, A. Mullane, O. Anaya-Lara, and B. Lemstrom. Dynamic models of wind farms for power system studies Ü status by IEA Wind R&D Annex 21. In European Wind Energy Conference and Exhibition 2004, London, 2004.
- [23] John O. Tande, Eduard Muljadi, Ola Carlson, Jan Pierik, Ana Estanqueiro, Poul Sørensen, Mark O-Malley, Alan Mullane, Olimpo Anaya-Lara, and Bettina Lemstrom. *Dynamic models of wind farms for power system studies: status by IEA Wind R&D Annex 21*. In Proceedings of the EWEC 2004, London, 2004.
- [24] Tennet. Tennet Jaarverslag 2005. Technical Report –, TenneT, 2005.

A REQUIRED TURBINE DATA AND MEASUREMENTS FOR VALIDATION OF WINDTURBINES DYNAMIC MODELS

For the validation of dynamic models of wind turbines the following data and measurements are required:

- turbine parameters, i.e. rotor data, drive train parameters, generator and converter data and finally the control parameters;
- statistical wind speed data: Weibull parameters;
- (estimated) turbulence level at the wind turbine location, position of the turbine in a wind farm;
- · measurements during normal operation at different wind speeds;
- measurement(s) of voltage dip(s) or short circuit(s).

The statistical wind speed parameters are used to generate statistically correct wind speed input files for the model validation. Since the measurements will be used to validate relatively high frequency behavior, the sample rate of the measurement needs to be sufficiently high. For validation of normal operation, spectral analysis has to be used, which requires filtering of the measurements before sampling. The measurement sets need not be very long, about 10 minutes. It is best to have a few measurements for each wind speed interval and cover the whole range of operation, i.e. divide the range in 5 intervals and perform 3 measurements per interval. Voltage dip and short circuit measurements can be shorter in length than normal operation measurements, about 1 minute, since these will be compared in the time domain and the dip itself is of limited length (for instance 50 ms). The turbine operating conditions during the dip or short circuit are not that important (the operating condition of the turbine will have little effect on the result).

Turbine parameters

Rotor	diameter, nr of blades, $C_P(V, \theta)$ tables, $C_T(V, \theta)$ tables, tower height,
	tower stiffness, tower damping, nacelle mass, rotor mass, rotor moment
	of inertia, structural data tower and blades ¹ , aerodynamic profile data
	blades ¹ , hydrodynamic profi le data tower ¹
Mechanical drive train	gear box ratio, drive train eigenfrequency, drive train stiffness, drive train
	damping
Generator ²	generator type, moment of inertia, nr of pole pairs, stator dq inductances,
	stator resistance, rotor dq inductances, rotor resistance, mutual induc-
	tances, field winding inductance, field winding resistance, field strength,
	saturation curve
Converter ²	converter type, switching frequency, single line diagram, DC link capaci-
	tor, DC link inductor, grid side harmonic fi lter parameters
Converter control	control diagrams, DC voltage setpoint, DC voltage control parameters, re-
	active power setpoint, reactive power control parameters, electromechani-
	cal control parameters
Pitch control	pitch control diagram, pitch control parameters
Power-speed control	power-speed control curve, including any hysteresis

¹as used in PHATAS

ECN-E-07-006 49

²the type of generator or converter determines which parameters are required

Measured variables and sample rates for normal operating conditions

Type	variable	sample rate [Hz]
Mechanical	rotor position	20
	rotational speed rotor	20
	blade pitch angles ³	20
	pitch angle setpoints ³	20
	blade pitch speeds ³	20
	blade pitch speed setpoints ³	20
	mechanical torque	2048
	blad root moments in lead lag	20
	tower top tilt-rotation and torsion	20
	rotor speed setpoint ⁴	20
Aerodynamic	wind speed	2
	wind direction	2
	yaw angle	2
Electrical ⁴	rotational speed generator	2048
	all stator phase voltages	2048
	all stator phase currents	2048
	all machine converter phase currents (rotor or stator)	2048
	all machine converter phase voltages (rotor or stator)	2048
	DC link current	2048
	DC link voltage	2048
	all grid converter phase currents	2048
	electrical torque setpoint	2048
3 11 1 1	reactive power setpoint(s)	2048

³all blades

The high sample rate is determined by the frequency range of the power spectral densities to be used for validation. The given values are typical, i.e. suitable for most purposes. The sample rate should preferably be 8 times higher than the highest frequency of interest. From the measured instantaneous phase voltages and currents the instantaneous active and reactive power at the different locations (stator, machine side converter and grid side converter) can be calculated. It is also possible to calculate the instantaneous dq0 or positive-negative-zero sequence values at these locations, if required.

Measured variables and sample rates for a short circuit or voltage dip

Type	variable	sample rate [Hz]
Electrical ⁵	rotational speed generator	2048
	all stator phase voltages	2048
	all stator phase currents	2048
	all machine converter phase currents (rotor or stator)	2048
	all machine converter phase voltages (rotor or stator)	2048
	DC link current	2048
	DC link voltage	2048
	all grid converter phase currents	2048
	electrical torque setpoint	2048
	reactive power setpoint(s)	2048

⁵ if a converter is not present, some measurements expire

⁴if a converter is not present, some measurements expire

B IEA ANNEX XXI CO-OPERATION

IEA Annex XXI *Dynamic Models for Power System Studies* started in 2003 and was completed in december 2006. The participants are:

Sintef (Norway), operating agent	John Tande
Risoe (Denmark)	Poul Soerensen
Chalmers (Sweden)	Ola Carlsson
VTT (Finland)	Bettina Lemstroem, Sanna Uski
UMIST (UK)	Olimpo Anaya-Lara
NREL (USA)	Eduard Muljadi
UCD (Ireland)	Mark O'Malley, Alan Mullane
Ineti (Portugal)	Ana Estanqueiro
ECN and TUD (Netherlands)	Jan Pierik, Johan Morren, Edwin Wiggelinkhuizen

The collaboration in IEA Annex XXI focussed on:

- making measurements and turbine parameters available for the model validations;
- documenting the models of the participants;
- discussing views about the validation method and model requirements for a given model application;
- comparing and discussing validation results.

At the end of 2006, the data base contained the following wind turbine and wind farm measurement sets:

Name	WT type	variables	measurement type	sample rate (Hz)	WT data
Alsvik	4 CSS	M, E	NO, VD	31.25, 62.5, 256	M, E
Azoren	5 CSS	Е	NO	40	M, E
Cart	1 VSP	M, E	NO, VD	?	M, E, C
JWT	1 VSP	Е	NO, VD	2048	NA
Olos	5 CSS	Е	NO	1	M, E
Smola	20 CSAS	Е	NO, VD	25	?
wt500	1 CSS	Е	NO	35	M, E
Riso benchmark	hypothetical	-	-	-	-
aaa	1 . 11 TIOD		1 ' 1 00 4 0		. 11

CSS = constant speed stall, VSP = variable speed pitch, CSAS = constant speed active stall

M = mechanical, E = electrical, C = control

NO = normal operation, VD = voltage dip, SC = short circuit

NA = not available

Riso benchmark is a hypothetical system for comparison of different models

The Alsvik set (constant speed turbines) and the JWT set (variable speed turbine) are the most suitable for a first validation exercise and were chosen by the Annex XXI participants for the joint validation effort.

The IEA Annex XXI organised meetings 7 meetings and a separate meeting to prepare the workshop at the Athens conference:

ECN-E-07-006 51

Venue	Year	ECN-TUD participation
Oslo	2002	y
Madrid conference	2003	y
NREL	2003	y
Chalmers	2004	y
Dublin	2004	y
Lissabon	2005	y
Amsterdam	2005	y
Athens conference	2006	n

Participants prepared a literature list with information on their models and model development.

The Annex prepared papers for the wind energy conferences in London (2004) and IEEE Trans PWRS, Special Section on Power System Performance Issues Associated with Wind Energy (2006). Participants prepared papers for the wind energy conference in Athens (2006).

C CONFERENCE CONTRIBUTIONS AND JOURNAL PAPERS RELATED TO THE ERAO-3 PROJECT

2006:

Benchmark Test of Dynamic Wind Generation Models for Power System Stability Studies

John Olav G Tande, Ian Norheim, Ola Carlson, Abram Perdana, Student Member IEEE, Jan Pierik, Johan Morren, Student Member IEEE, Ana Estanqueiro, Joao Lameira, Poul Sørensen, Member IEEE, Mark O'Malley, Senior Member IEEE, Alan Mullane, Member IEEE, Olimpo Anaya-Lara, Member IEEE, Bettina Lemström, Sanna Uski, Eduard Muljadi, Senior Member IEEE.

IEEE Trans PWRS, Special Section on Power System Performance Issues Associated with Wind Energy, 2006

• Development and validation of wind farm models for power system studies: Alsvik wind farm results.

Jan Pierik, Johan Morren, Tim van Engelen, Sjoerd de Haan, Jan Bozelie. EWEC 2006. Athene.

2005:

- Grid interaction of Offshore Wind Farms. Part 1. Models for Dynamic Simulation Johan Morren, Jan T.G. Pierik, Sjoerd W.H. de Haan, Jan Bozelie.
 Article Wind Energy 2005, 8: 265-278 (John Wiley & Sons Ltd.).
- Grid interaction of Offshore Wind Farms. Part 2. Case Study Simulations Johan Morren, Jan T.G. Pierik, Sjoerd W.H. de Haan, Jan Bozelie. Article Wind Energy 2005, 8: 279-293 (John Wiley & Sons Ltd.).

2004:

- Fast Dynamic Modelling of Direct-Drive Wind Turbines.
 J. Morren, J.T.G. Pierik, Sj. de Haan.
 PCIM 2004 Conference, Nuremberg.
- VOLTAGE DIP PROOF CONTROL OF DIRECT-DRIVE WIND TURBINES.
 J. Morren, J.T.G. Pierik, S.W.H. de Haan.
 UPEC 2004 Conference.
- Dynamic models of wind farms for power system studies. Status by IEA Wind R&D Annex 21

J.O Tande, E. Muljadi, O. Carlson, J. Pierik, A. Estanqueiro, P. Sørensen, M. O'Malley, A. Mullane, O. Anaya-Lara and B. Lemstrom.

European Wind Energy Conference and Exhibition 2004, London.

ECN-E-07-006 53

Benchmark Test of Dynamic Wind Generation Models for Power System Stability Studies

John Olav G Tande, Ian Norheim, Ola Carlson, Abram Perdana, Jan Pierik, Johan Morren, Ana Estanqueiro, Joao Lameira, Poul Sørensen, Mark O'Malley, Alan Mullane, Olimpo Anaya-Lara, Bettina Lemström, Sanna Uski, Eduard Muljadi.

IEEE Trans PWRS, Special Section on Power System Performance Issues
Associated with Wind Energy, 2006

Benchmark Test of Dynamic Wind Generation Models for Power System Stability Studies

John Olav G Tande, Ian Norheim, Ola Carlson, Abram Perdana, Student Member IEEE, Jan Pierik, Johan Morren, Student Member IEEE, Ana Estanqueiro, Joao Lameira, Poul Sørensen, Member IEEE, Mark O'Malley, Senior Member IEEE, Alan Mullane, Member IEEE, Olimpo Anaya-Lara, Member IEEE, Bettina Lemström, Sanna Uski, Eduard Muljadi, Senior Member IEEE

Abstract— This paper presents benchmark testing of dynamic wind generation models for power system stability studies. The paper gives the rationale for the proposed testing, a description of the test procedure and example benchmark test results. The example benchmark test results compare model performance with measurements of wind turbine response to voltage dips. The tests are performed for both a fixed-speed wind turbine with squirrel-cage induction generator and a variable-speed wind turbine with doubly-fed induction generator. The test data include three-phase measurements of instantaneous voltage and currents at the wind turbine terminals during a voltage dip. The benchmark test procedure includes transforming these measurements to fundamental positive sequence RMS phasors, and from that calculation of active and reactive power for comparison with simulation results. A total of ten simulation models are tested. The results give a clear indication of accuracy and usability of the models tested, and pin-point need both for model development and testing.

Index Terms— Measurements, Modelling, Power system, Wind energy

I. INTRODUCTION

DYNAMIC wind generation models for power system stability studies are at present not a standard feature of many software tools, but are being developed by research

Manuscript received August 30, 2006. This work was prepared as a joint effort of IEA Wind R&D Annex 21. The co-funding by national research programmes is acknowledged.

John Olav G Tande, SINTEF Energy Research, 7465 Trondheim, Norway, phone: +47 73 59 74 94, fax: +47 73 59 72 50, john.o.tande@sintef.no

Ian Norheim, SINTEF Energy Research, Norway, <u>ian.norheim@sintef.no</u> Ola Carlson, Chalmers University of Technology, Sweden,

Ola.Carlson@chalmers.se

Abram Perdana, Chalmers University of Technology, Sweden, abram.perdana@chalmers.se

Jan Pierik, ECN, Netherlands, Jan.Pierik@ecn.nl
Johan Morren, TU Delft, Netherlands, j.morren@ewi.tudelft
Ana Estanqueiro, INETI, Portugal, ana.estanqueiro@ineti.pt
João Lameira, INETI, Portugal, joao.lameira@ineti.pt
Poul Sørensen, Risø, Denmark, poul.e.soerensen@risoe.dk
Mark O'Malley, UCD, Ireland, mark.omalley@ucd.ie
Alan Mullane, UCD, Ireland, alan.mullane@ucd.ie
Olimpo Anaya-Lara, University of Strathclyde, UK,

olimpo.anaya-lara@eee.strath.ac.uk

Bettina Lemström, VTT, Finland, <u>bettina.lemstrom@vtt.fi</u> Sanna Uski, VTT, Finland, <u>sanna.uski@vtt.fi</u> Eduard Muljadi, NREL, USA, <u>eduard_muljadi@nrel.gov</u> institutes, universities and commercial entities. Accurate dynamic wind generation models are critical; hence model validation is a key issue and taken up by a working group (Annex 21) under the International Energy Agency (IEA) Wind R&D agreement. Annex 21 includes participants from nine countries, and has since start-up in 2002 developed a systematic approach for model benchmark testing. See [1] and [2] for a status on the Annex works; a final report is due by end 2006.

The rationale for the proposed benchmark testing is that currently dynamic wind generation models are being applied for assessing grid connection of large wind farms, but model accuracy are in many cases unknown. This at best leads to uncertainty in the market, and at worst to an erroneous design jeopardising power system stability. The challenge is twofold. Firstly, the technology in modern wind farms is fairly complex, and their dynamic behaviour may differ significantly depending on the wind turbine type and manufacturer specific technical solutions. Thus, it is not trivial to develop accurate wind generation models. Aspects of wind farm modelling are outlined further in Section II of this paper; for more detailed coverage see e.g. [3]-[5]. Secondly, model validation must be transparent and adequate for providing confidence. In this respect, this paper contributes by proposing the benchmark procedure as described in Section III.

The example test results presented in Section IV demonstrates the usability of the benchmark procedure. The tested wind generation models (ten in total) are all developed by the participants of Annex 21. The models vary in detail, from instantaneous type models to phasor type models, and also in format from being programmed from scratch, possibly in Matlab/Simulink to being part of commercial power system software tools like PSCAD/EMTDC, SIMPOW, PSS/E and DIgSILENT.

The description of the benchmark test procedure and presentation of test results provide for a significant technical contribution. The paper is the first to present a systematic comparison of wind generation models against measurements. The paper concludes (Section V) that results give a clear indication of accuracy and usability of the models tested, and pin-point the need for both model development and testing.

Symbols used in this paper are listed in the Appendix.

II. DYNAMIC WIND GENERATION MODELS

Accurate simulation of wind farms relies on detailed modelling of the applied wind turbine technology, e.g. the dynamic behaviour of a fixed-speed wind turbine may differ significantly from that of a variable-speed wind turbine. Fig. 1 shows the main wind turbine types, but there will also be manufacturer specific variations, in particular related to control system solutions. Aggregated models may be applied, i.e. letting one wind turbine model representing multiple turbines in a wind farm, but the impact of the spatial distribution and the internal wind farm grid must be reflected.

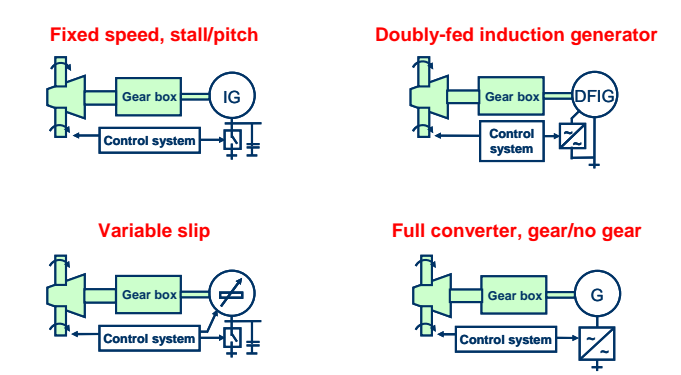


Fig. 1: Main types of wind turbine technologies.

Space limitations of this paper do not allow for a detailed presentation of all the various models developed by the participants of the Annex. Hence, in the following only the common building blocks of the models are presented, whereas example publications on models developed by the Annex participants are [3]-[23].

A. Wind turbine model building blocks

A detailed wind turbine model may include the following components:

- wind speed
- turbine aerodynamics
- mechanical drive-train
- generator
- capacitors or frequency converter
- control system
- other issues (relay protection, tower swings, etc)

A fair wind speed and turbine aerodynamic representation is required for simulating the aerodynamic torque fluctuations. One challenge in this relation is to include the effect of wind speed variations over the turbine area, i.e. an effect that may cause enhanced periodic power fluctuations from wind turbines. This can be done using wind field simulations and detailed blade profile data or by application of the following relation:

$$T_t = 0.5 \rho A u_t^3 C_p(\lambda, \beta) \omega_t^{-1}$$
(1)

Here, T_t is aerodynamic torque, ρ is the air density, A is the swept turbine area, u_t is the weighted average wind speed over the three rotating turbine blades, $C_p(\lambda, \beta)$ is the turbine aerodynamic efficiency as a function of tip-speed ratio (λ) and blade pitch angle (β) , and ω_t is the rotational speed of the turbine. The weighted average wind speed over the three rotating turbine blades, u_t , can be determined from wind field simulations or by filtering of a single point wind speed timeseries.

The mechanical drive train is commonly approximated by a two-mass model, i.e. the turbine and generator inertia with a shaft and an ideal gearbox between them. Applying pu values with reference to the generator the two-mass model is given by:

$$\frac{d\omega_t}{dt} = \frac{\omega_b}{2H_t} \left(T_t - d_m \left(\omega_t - \omega_g \right) - k\theta_t \right)$$
 (2)

$$\frac{d\omega_g}{dt} = \frac{\omega_b}{2H_g} \left(d_m \left(\omega_t - \omega_g \right) + k\theta_t - T_g \right)$$
 (3)

Here, $d\omega/dt$ is the time derivate of the turbine rotational speed, ω_b is the base angular frequency, H_t is the turbine inertia, d_m is the mutual damping, ω_g is the rotational speed of the generator, k is the shaft stiffness, θ_t is the shaft twist, $d\omega_g/dt$ is the time derivate of the generator rotational speed, and H_v is generator inertia.

The generator models applied may be of varying complexity. Third-order models are commonly used in tools for simulation of large power systems, whereas more detailed models may be used in tools for analyses of smaller systems. These detailed models may include stator dynamics (fifth-order model), and further particulars such as full three-phase description.

The capacitors applied for reactive compensation of fixedspeed wind turbines are commonly modelled as one or more shunt impedances.

In tools for simulation of large power systems the frequency converter is commonly described as an ideal component, i.e. neglecting losses and the switching dynamics. In more detailed studies these effects may be included, e.g. for assessment of harmonics.

The control system model for a fixed-speed wind turbine is commonly split into two independent blocks, i.e. one for the pitching of the blades and one for switching the capacitors. The control system of variable-speed wind turbines may be fairly complex, including speed control for optimising the production, but also producing a smooth output power, and further special regulation may be implemented for low-voltage ride-through and other off-normal grid situations.

Other issues such as relay protection and tower swings may be included in some models. The relevance of including such issues depends on the scope of the analysis.

B. Wind farm models

Wind farm models may be built to various level of detail ranging from a one-to-one modelling approach to full

aggregation. The one-to-one approach is more computer demanding and in many cases not practical, hence aggregated wind farm models are often applied in power system studies. The aggregation is however not trivial, i.e. considering that a wind farm may consist of hundreds of wind turbines distributed over a large area with different impedance of line feeder from one turbine with respect to the others, different wind speeds at each turbine and different voltage drops on each bus. Aggregated models must therefore be applied with care. Possibly a cluster-by-cluster aggregation may be a fair compromise between one-to-one modelling and full aggregation.

III. BENCHMARK TEST PROCEDURE

The benchmark test procedures suggested by IEA Wind R&D Annex 21 consider operation during normal conditions and wind turbine response to a voltage dip. In both cases the test data include three-phase measurements of instantaneous voltages and currents at the wind turbine or wind farm terminals. The benchmark test procedure includes transforming these measurements to RMS fundamental positive sequence values of voltage, active power and reactive power for comparison with simulation results. The benchmark test may include both validation against measurements and model-to-model comparisons.

A. Dynamic operation during normal conditions

This test is for validating model capability to simulate wind turbine or wind farm characteristic power fluctuations during normal grid conditions. The test is outlined below.

Input:

Wind speed time series (and optionally voltage time series)

Output:

- Time series plot of active power output, reactive power, and voltage (optionally)
- Power spectral density of active power output
- Short-term flicker emission
- Optionally plots of reactive power versus voltage and reactive power versus active power

B. Response to voltage dip

This test is for validating model capability to simulate wind turbine or wind farm response to a voltage dip. The test is outlined below.

Input:

 Voltage time series and constant aerodynamic torque (or optionally wind speed time series)

Output:

- Time series plot of active and reactive power output
- Time series of voltage at wind turbine terminals

C. Transformation of measurement data

Assuming a perfectly balanced three-phase system it

requires a minimum of data processing to transforming the measured instantaneous values of voltages $(u_a, u_b, \text{ and } u_c)$ and currents $(i_a, i_b, \text{ and } i_c)$ to RMS voltage (U), current (I), active power (P) and reactive power (Q):

$$U = \sqrt{u_a^2 + u_b^2 + u_c^2} \tag{4}$$

$$I = \sqrt{\frac{i_a^2 + i_b^2 + i_c^2}{3}} \tag{5}$$

$$P = u_a i_a + u_b i_b + u_c i_c \tag{6}$$

$$Q = -\frac{(u_b - u_c)i_a + (u_c - u_a)i_b + (u_a - u_b)i_c}{\sqrt{3}}$$
 (7)

The recommendation of the Annex is however *not* to use the above eqs. (4) - (7), but rather to calculate the fundamental positive sequence voltage and current phasors, and from these calculate the active and reactive power for comparison with simulation results. The fundamental voltage and current phasors are determined using the complex Fourier transformation (shown here for the voltage in phase *a* only):

$$U_{a1} = \frac{2}{T} \int_{t-T}^{T} u_a(t) e^{-j\omega_1 t} dt$$
 (8)

Here, U_{al} is the fundamental voltage phasor of phase a, T is the fundamental period time and ω_l is the fundamental frequency in radians. The positive sequence values are given by (shown here for voltage only):

$$U_{+} = (U_{a1} + U_{b1}e^{j2\pi/3} + U_{c1}e^{-j2\pi/3})/3$$
(9)

Here, U_+ is the fundamental positive sequence voltage phasor, U_{bl} is the fundamental voltage phasor of phase b and U_{cl} is the fundamental voltage phasor of phase c. Calculation of the active and reactive power is now straight forward:

$$S_{\perp} = \sqrt{3}U_{\perp}I_{\perp}^{*} = P_{\perp} + jQ_{\perp} \tag{10}$$

Here, S_+ is the complex apparent power, the subscript plussign ($_+$) indicates that the value is based on the fundamental positive sequence, and the superscript asterisk-sign (*) indicates the complex conjugate. Active and reactive power calculated according to eq. (10) is hereafter in this paper denoted positive sequence active and reactive power.

The reason for using the fundamental positive sequence values is twofold. Firstly, perfectly balanced conditions can not generally be assumed, and events of voltage dips are often unbalanced. Secondly, most power system simulator models are phasor-type models, meaning that the electrical variables (voltages and currents) are represented as positive sequence values. This is also discussed in [25]. The use and calculation of the positive sequence values are described in detail in [24].

IV. BENCHMARK TEST RESULTS

This section presents example benchmark test results of wind turbine response to voltage dips. Example of benchmark test of operation during normal operation is found in [1]. The voltage dip measurements are from a 180 kW fixed-speed, stall-controlled wind turbine and an 850 kW variable-speed, pitch controlled wind turbine. The data are part of the IEA Wind R&D Annex 21 measurement database described in [1]. The data in the database are for the use of the Annex partners only.

A. Fixed-speed wind turbine

This test considers a 180 kW fixed-speed wind turbine with squirrel-cage induction generator and stall control. The assumed wind turbine data are listed in the Appendix. Measurements of three-phase instantaneous voltages and currents at the wind turbine terminals are recorded with a sample rate of 256 Hz during a voltage dip. The sample rate should preferably be higher, say at least 1 kHz, so for the purpose of this paper, the data are numerically re-sampled to 1250 Hz. The measured instantaneous data are shown in Fig. 2.

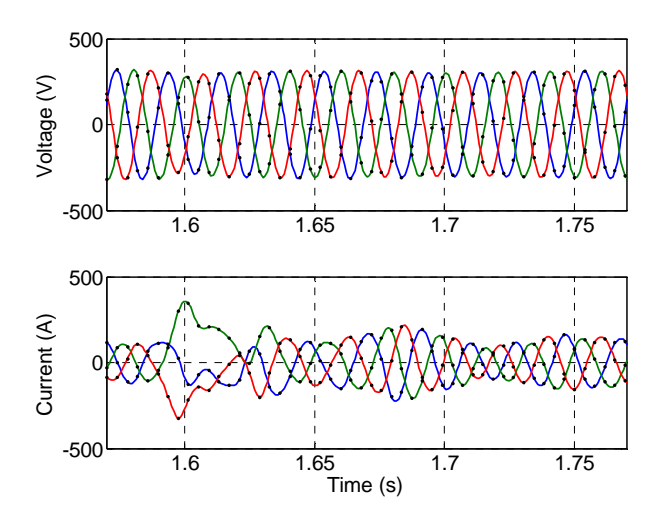


Fig. 2: Measured instantaneous three-phase voltages and currents at wind turbine terminals during a grid fault causing a voltage dip. The original data are indicated by dots.

Analysis of the measurement data reveals some unbalance just when the dip occurs, but apart from this, no significant difference is observed between positive sequence values and those calculated using eqs. (6)- (7), see Fig. 3.

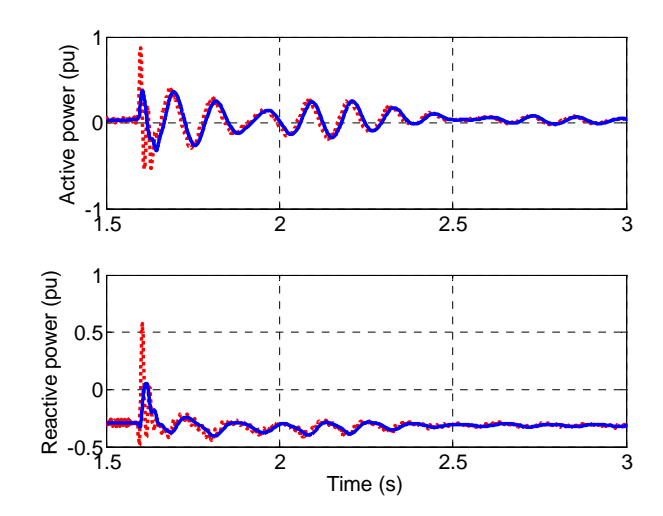


Fig. 3: Instantaneous (dotted line) and positive sequence (solid line) values of measured active and reactive power at wind turbine terminals during a voltage dip.

The measurements are compared with simulation results of models developed by the Annex partners:

- Model A is built in Matlab/Simulink with a third-order generator model and a two-mass model of the mechanical drive train.
- Model B is built in Matlab/Simulink using a fourth order machine model and two-mass shaft model.
- Model C is implemented in PSCAD/EMTDC by using the standard component library components. The generator is modeled by the Squirrel-cage Induction Machine component, the mechanical drive-train with the Torsional Shaft Model component (multi-mass) and the capacitor bank with Capacitor components.
- Model D is built in DIgSILENT using an RMS simulation which applies a standard third-order model of the induction generator, together with a user-built twomass model of the mechanical drive train.
- Model E is part of a wind farm simulation tool (InPark) programmed in Fortran. It applies a fifth-order model of the induction generator, the representation of the structural oscillations first mode, and a two-mass model of the mechanical drive train.
- Model F is part of a renewable energy power systems modular simulator (RPMSim). It applies a fifth-order model of the induction generator and a two-mass model of mechanical drive train.
- Model G is built in Matlab/Simulink with a fifth-order generator model and a two-mass spring and damper model of the mechanical drive train.
- Model H is built in PSS/E using a standard third-order model (CIMTR3) together with a user-built two-mass model of the mechanical drive train.

The models (A-G) apply the measured voltage dip as input, whereas H simulates a grid fault that approximates the dip, see Fig. 4.

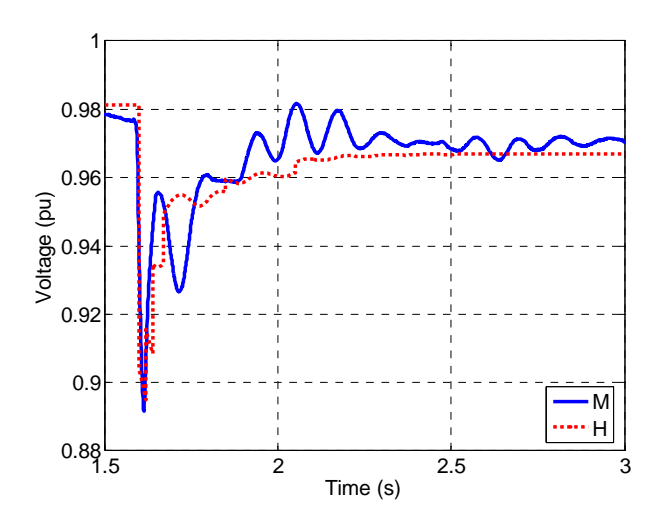


Fig. 4: Measured (M) and simulated (H) positive squence RMS values of voltage at wind turbine terminals.

Comparing the measured and simulated response in active and reactive power (Fig. 5 and Fig. 6), the models provide for varying results. This is in part due to differences in model type, but also due to variations in model input data. In particular it is noted that the wind turbine data as given in the Appendix are uncertain, and slightly different parameters have been applied in some models:

- The stated generator inertia seems very small ($H_g = 0.12$ s), and in models A-D and H a higher inertia was applied ($H_g = 0.24$ s) providing for fluctuations in active power with a frequency closely matching the measurements. The reasoning is that in a two mass representation, the generator inertia should be lumped with the inertia of the high speed shaft.
- The shunt capacitor is rated $Q_c = 60$ kvar, but it is not know if it was connected at the time of the voltage dip. Using $Q_c = 16$ kvar (models A-C and H) provides for a better match between simulations and measurements.
- The presence of the high frequency components shown in the simulation by model F is probably caused an underdamped mechanical ringing in the flexible shaft.
- Model G did not use the positive sequence RMS values of the voltage as an input but instead used the instantaneous values, since this model calculates instantaneous values. This explains the presence of the high frequency components in the result of model G.

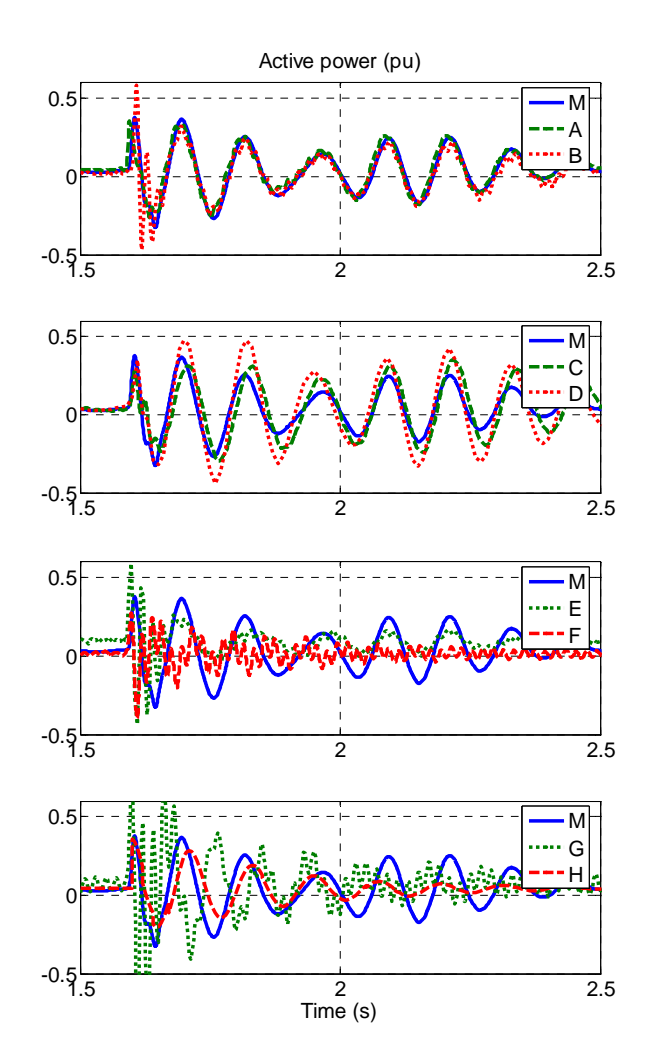


Fig. 5: Measured (M) and simulated (A-H) positive sequence active power at wind turbine terminals during a voltage dip.

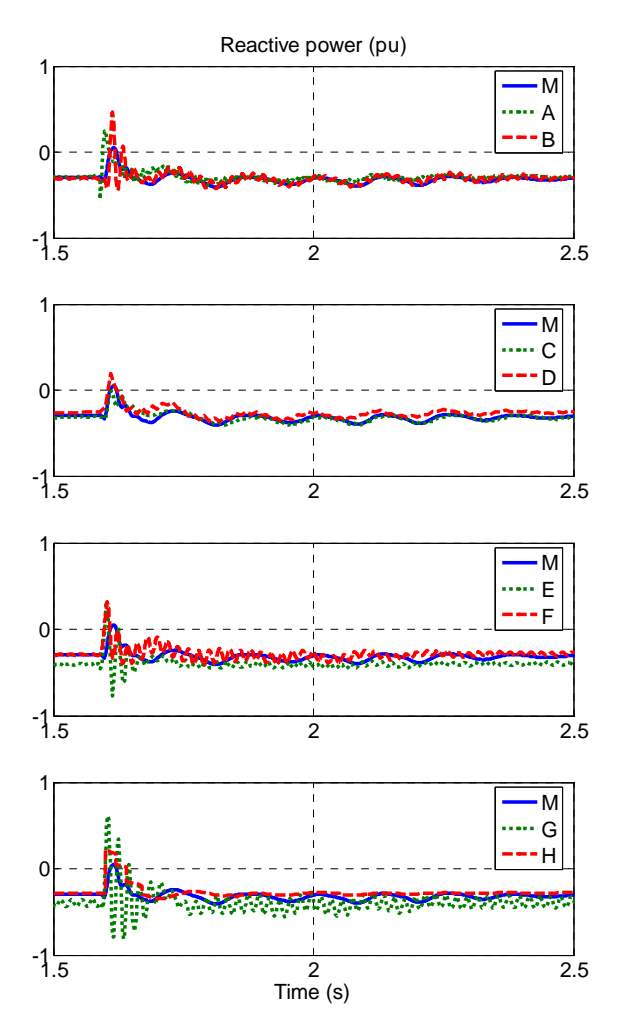


Fig. 6: Measured (M) and simulated (A-H) positive sequence reactive power at wind turbine terminals during a voltage dip.

B. Variable-speed wind turbine

This test considers an 850 kW variable-speed wind turbine with doubly fed induction generator and pitch control. The assumed wind turbine data are listed in the Appendix. Measurements of three-phase instantaneous voltages and currents at the wind turbine terminals are recorded with a sample rate of 2048 Hz during a voltage dip. The measured instantaneous data are shown in Fig. 7.

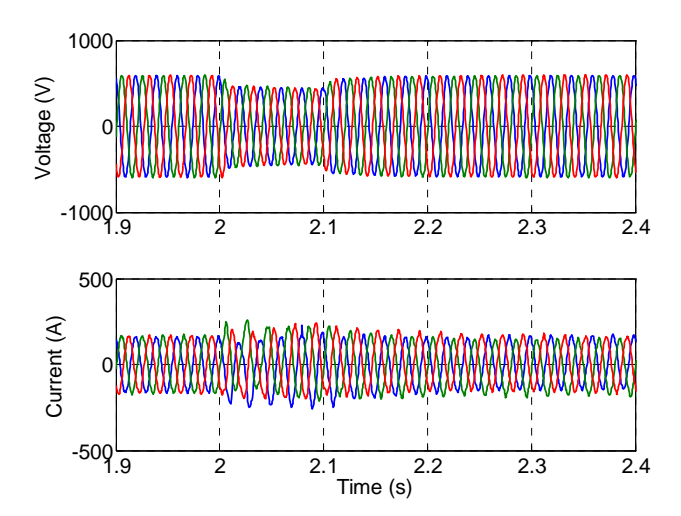


Fig. 7: Measured instantaneous three-phase voltages and currents at wind turbine terminals during a grid fault causing a voltage dip.

Analysis of the measurement data reveals that the dip is unbalanced and a significant difference is observed between positive sequence values and those calculated using eqs. (6)-(7), see Fig. 8.

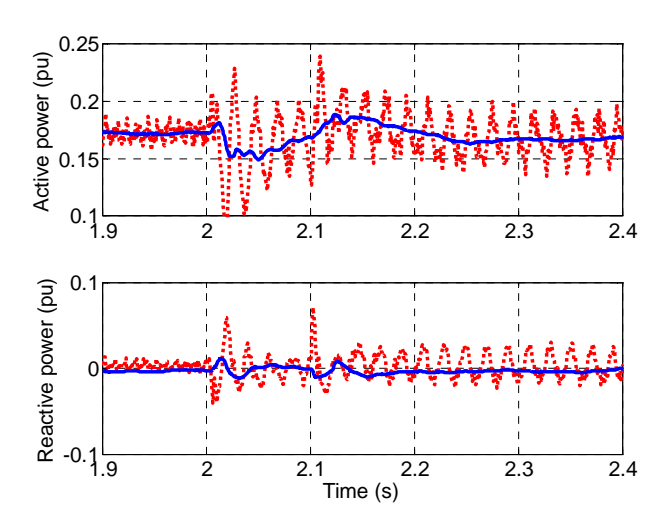


Fig. 8: Instantaneous (dotted line) and positive sequence (solid line) values of measured active and reactive power at wind turbine terminals during a voltage dip.

The measurements are compared with simulation results of user-built models in PSS/E (I) and SIMPOW (J). Both models use a third-order representation of the generator and a two-mass model of the mechanical drive train. Model J uses a piecewise linear representation of the measured (positive sequence RMS) voltage dip as input, whereas in model I a fault is simulated that roughly approximates the measured voltage dip, see Fig. 9.

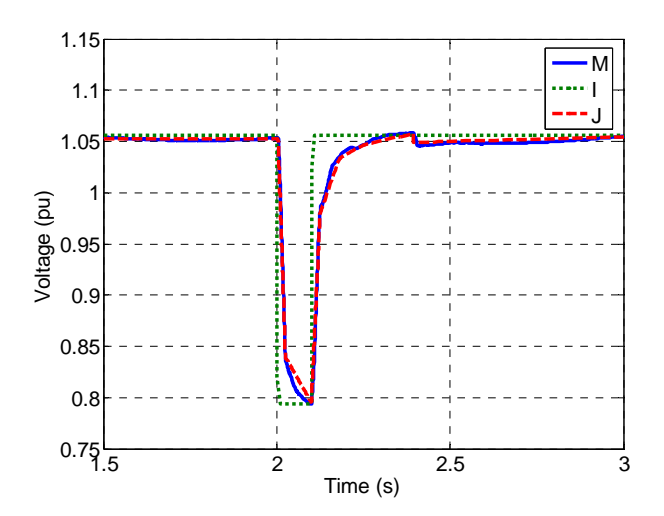


Fig. 9: Measured (M) and simulated (I and J) positive squence RMS values of voltage at wind turbine terminals.

Comparing the measured and simulated response in active and reactive power (Fig. 10), the models provide for fair results. The sharp spikes in the PSS/E simulation results are of no practical implication and are due to the applied short-circuit that gives an instantaneous drop and increase of the voltage.

It is noted that the applied wind turbine data as given in the Appendix are uncertain. This also goes for the applied control structure; the models (I and J) are of generic nature reflecting main characteristics of DFIG wind turbines and are not a one-to-one representation of manufacturer specific details.

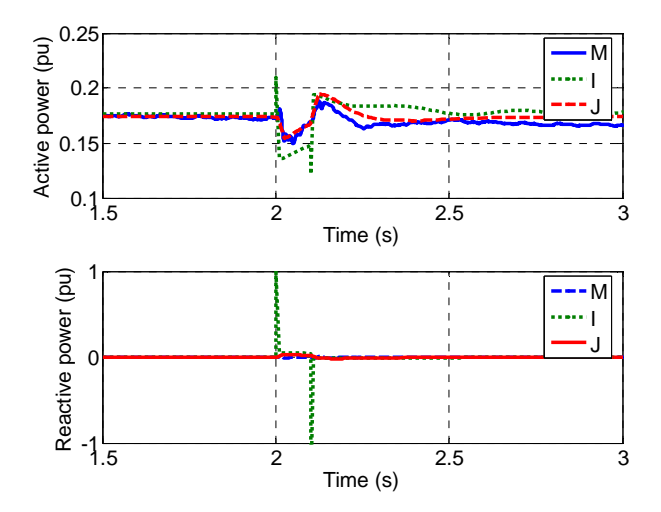


Fig. 10: Measured (M) and simulated (I and J) positive sequence values of active and reactive power at wind turbine terminals during a voltage dip.

It is suggested in [25] that the applied third-order generator model may not be well suited for accurate simulation of a DFIG wind turbine response to a voltage dip. For one, to obtain reasonable voltage dip simulation results (as shown here) it requires integration time steps in the order of 0.1 ms.

This makes the simulation slow in tools like PSS/E (that operates at fixed time-steps) and less suitable for practical use. A possible improvement may thus be to assume instant rotor current control, and then only consider the main limitations in converter voltage and current. This would allow for using a steady-state generator model and larger integration time steps.

V. CONCLUSION

This paper has presented results from studies conducted by the IEA Annex 21 on 'Dynamic models of wind turbines for power system studies'. The systematic approach developed by the Annex for model benchmark testing was described and examples were shown which compare wind generation models against measurements of wind turbine response to voltage dips. The test results were illustrated for both fixed-speed wind turbines with squirrel-cage induction generator and variable-speed wind turbines based on doubly-fed induction generators. In order to compare measured results with those from a phasor/RMS type simulation, especially in the case of voltage dips, the Annex recommends transforming the measured voltage and current to positive sequence values and from these deducting the active and reactive power.

The benchmark test results showed for the majority of the models a good agreement with the measurements. This demonstrates generally satisfactory model performance, but also that benchmark testing is important for providing confidence. It can be summarised that the results provided a clear indication of accuracy and applicability of the models tested and identified the necessity for both model development and testing.

APPENDIX

List of symbols

β	turbine blade pitch angle (rad)
ρ	air density = 1.225 kg/m^3 at 15°C , 1013.3 mbar
λ	tip speed ratio = $\omega_t R/u$
ω_l	fundamental frequency (rad/s)
\mathcal{O}_h	base angular frequency = $2\pi 50$ rad/s for a 50 Hz system
\mathcal{O}_g	generator angular speed (rad/s)
ω_t	turbine angular speed (rad/s)
θ_{t}	shaft twist (rad)
Ä	turbine rotor area = πR^2 (m ²)
C_p	turbine efficiency, function of λ and β
d_m	mutual damping (pu torque/pu speed)
f_n	nominal grid frequency (Hz)
H_g	generator inertia (s)
H_t	turbine inertia (s)
I	current (A)
I_{+}	fundamental positive sequence current (A)
I_a , i_b , i_c	instantaneous current (A)
J_g	generator inertia (kg·m²)
$oldsymbol{J}_t$	turbine inertia (kg·m²)
K	shaft stiffness (pu torque/electrical rad)
k_m	shaft stiffness (Nm/mech rad)
n_g	gearbox ratio
P	active power (W)
P	number of generator pole pairs
Q	reactive power (var)
Q_c	shunt-capacitor (var)

R	turbine rotor radius (m)
S	apparent power (VA)
S_k	short-circuit apparent power (VA)
S_n	nominal apparent power (VA)
T	fundamental period time (s)
T_g	torque at generator shaft (Nm)
T_t	torque at turbine shaft (Nm)
U	voltage (V)
$U_{\scriptscriptstyle +}$	fundamental positive sequence voltage phasor (V)
$U_{al},\ U_{bl},\ U_{cl}$	fundamental phase voltage (V)
u_a, u_b, u_c	instantaneous phase voltage (V)
$u_t(t)$	weighted average wind speed over rotor blades (m/s)
U_n	nominal voltage (V)
Z_b	base impedance (ohm)

Data conversion formulas

$$Z_b = \frac{U_n^2}{S_n} \tag{11}$$

$$\omega_b = 2\pi f_n \tag{12}$$

$$H_t = \frac{0.5J_t\omega_b^2}{S_n n_g^2 p^2} \tag{13}$$

$$H_g = \frac{0.5 J_g \omega_b^2}{S_n p^2} \tag{14}$$

$$k = \frac{k_m \omega_b}{S_n p^2 n_o^2} \tag{15}$$

Fixed speed wind turbine data

Nominal power, P_n (kW)	180
Nominal voltage, $U_n(V)$	400
Nominal apparent power, S_n (kvar)	204
Nominal frequency, f_n (Hz)	50
Number of pole pairs, p	3
Stator resistance, R_{IS} (pu)	0,012
Stator leakage reactance, X_{IS} (pu)	0,075
Rotor resistance, R_{2S} (pu)	0,008
Rotor leakage reactance, X_{2S} (pu)	0,171
Magnetizing reactance, X_M (pu)	2,684
Shunt-capacitor, Q_c (kvar)	60* / 60
Generator inertia (incl. high speed shaft), H_g (s)	0,12**
Turbine inertia, H_t (s)	2,77
Shaft stiffness, k (pu torque/electrical rad)	0,46
Gearbox ratio, n_g	23,75
Turbine rotor radius, R (m)	11,63

^{*}The shunt capacitor is rated Q_c =60 kvar, but may not have been in operation at the time of the measurements. Assuming Q_c = 16 kvar provides for a better match between simulations and measurements.

Variable speed wind turbine data

Nominal power, P_n (kW)	850
Nominal voltage, $U_n(V)$	690
Nominal apparent power, S_n (kvar)	944
Nominal frequency, f_n (Hz)	50
Number of pole pairs, p	2
Stator resistance, R_{IS} (pu)	0,006
Stator leakage reactance, X_{IS} (pu)	0,072
Rotor resistance, R_{2S} (pu)	0,009
Rotor leakage reactance, X_{2S} (pu)	0,112
Magnetizing reactance, X_M (pu)	4,238
Frequency converter rating, S_f (kvar)	300
Generator inertia (incl. high speed shaft), H_g (s)	0,54

Turbine inertia, H_t (s)	4,17
Shaft stiffness, k (pu torque/electrical rad)	1,16
Gearbox ratio, n_g	57,54
Turbine rotor radius, R (m)	26,00

ACKNOWLEDGMENT

J. O. Tande thanks Jarle Eek (NTNU, Norway) for help with simulations.

REFERENCES

- [1] Tande JO, E Muljadi, O Carlson, J Pierik, A Estanqueiro, P Sørensen, M O'Malley, A Mullane, O Anaya-Lara, B Lemstrom (2004) "Dynamic models of wind farms for power system studies status by IEA Wind R&D Annex 21", In proceedings of European Wind Energy Conference (EWEC), 22-25 November 2004, London, UK.
- 2] IEA Wind R&D Annex 21 homepage: http://www.energy.sintef.no/wind/main.htm
- Thomas Ackermann (ed) Wind Power in Power Systems, Wiley, January 2005, 742 pp, ISBN 0470855088
- [4] V. Akhmatov, Analysis of Dynamic Behaviour of Electric Power Systems with Large Amount of Wind Power, PhD- thesis, Technical University of Denmark, November 2003, available at http://www.oersted.dtu.dk/eltek/
- [5] J.G. Slootweg, Wind Power: Modelling and Impact on Power System Dynamics, PhD-thesis, Technische Universiteit Delft, December 2003, available at http://eps.et.tudelft.nl/
- [6] Petersson A. Analysis, Modeling and Control of Doubly-Fed Induction Generators for Wind Turbines, Göteborg, Sweden, Chalmers University of Technology, School of Electrical Engineering, ISBN 91-7291-600-1, 2005.
- [7] T. Thiringer, A. Petersson, T. Petru, "Grid Disturbance response of Wind Turbines Equipped with Induction generator and Doubly-Fed Induction generator" IEEE PES annual Meeting, Toronto, Canada, 2003, July 14-17
- [8] JTG Pierik, J Morren, EJ Wiggelinkhuizen, SWH de Haan, TG van Engelen, J Bozelie; Electrical and control aspects of offshore wind farms, Volume 1: Dynamic models of wind farms, ECN-C-04-050, ECN/TU Delft June 2004.
- [9] JTG Pierik, J Morren, EJ Wiggelinkhuizen, SWH de Haan, TG van Engelen, J Bozelie; Electrical and control aspects of offshore wind farms, Volume 2: Offshore wind farm case studies, ECN-C-04-050, ECN/TU Delft June 2004.
- [10] Estanqueiro, A., WIRING Project Final Report (JOR3-CT98-0245) INETI Contribution, Part A: Theoretical Basis of INETI's INPark Wind Park and Local Grid Models. Sept, 2002. pp. 57.
- [11] Estanqueiro, A., WIRING Project Final Report (JOR3-CT98-0245) INETI Contrib., Part B: Application of the Models, Sept, 2002. pp.39.
- [12] E. Muljadi, C.P. Butterfield, "Dynamic Model for Wind Farm Power Systems," Global Wind Power Conference 2004 in Chicago, IL, March 29-April 1, 2004
- [13] E. Muljadi, C.P. Butterfield, "Dynamic Simulation of a Wind Farm with Variable Speed Wind Turbines," Transactions of the ASME, Vol. 125, November 2003, Special Issue on Wind Energy, Journal of Solar Energy Engineering, pp. 410-417
- [14] Sørensen, P.; Hansen, A.D.; Christensen, P.; Mieritz, M.; Bech, J.; Bak-Jensen, B.; Nielsen, H., Simulation and verification of transient events in large wind power installations. Risø-R-1331(EN) (2003) 80 p.
- [15] Sørensen, P.; Hansen, A.D.; Janosi, L.; Bech, J.; Bak-Jensen, B., Simulation of interaction between wind farm and power system. Risø-R-1281(EN) (2001) 65 p.
- [16] Tande, JOG; Grid Integration of Wind Farms, Wind Energ. 2003; 6:281–295
- [17] Ian Norheim, K Uhlen, JOG Tande, T Toftevaag, MT Pálsson; Doubly Fed Induction Generator Model for Power System Simulation Tools, Nordic Wind Power Conference, 1-2 Marcg, 2004, Chalmers University of Technology
- [18] Palsson MT, Toftevaag T, Uhlen K, Tande JOG. Large-scale wind power integration and voltage stability limits in regional networks. Proceedings of IEEE-PES Summer Meeting, 2002; 2: 762–769.

^{**}The generator inertia $H_g = 0.12$ s does not include the high speed shaft and other high speed rotating parts. Assuming the total high speed inertia to be $H_g = 0.24$ s provides for a better match between simulations and measurements.

- [19] A Mullane; Advanced control of wind energy conversion systems, Theses (Ph.D.) NUI, 2003 at Department of Electrical and Electronic Engineering, UCC.
- [20] Anaya-Lara, O., Cartwright, P., Ekanayake, J. B., "Electrical Stability of Large Wind Farms – Grid Connections and Modelling," Proceedings of the Global Windpower Conference 2004, Chicago, Illinois, USA, 2004.
- [21] Anaya-Lara, O., Wu, X., Cartwright, P., Ekanayake, J. B., Jenkins, N., "Performance of Doubly Fed Induction Generator (DFIG) During Network Faults," Wind Engineering, Vol. 29, No. 1, pp. 49-66, 2005.
- [22] Ekanayake, J. B., Holdsworth, L., Jenkins, N., "Comparison of 5th order and 3rd order machine models for Doubly Fed Induction Generator (DFIG) Wind Turbines", Proceedings Electric Power System Research, Vol. 67, 2003, pp. 207-215.
- [23] Uski, S., Lemström, B., Kiviluoma, J., Rissanen, S. and Antikainen P. Adjoint wind turbine modeling with ADAMS, Simulink and PSCAD/EMTDC. Nordic wind power conference – NWPC'04, 1-2 March 2004 at Chalmers University of Technology, Sweden.
- [24] Jouko Niiranen, "About the active and reactive power measurements in unsymmetrical voltage dip ride through testing", In proceedings of Nordic Wind Power Conference, 22-23 May, 2006, Espoo, Finland, available at http://nwpc.vtt.fi/program_nwpc_files/frame.htm
- [25] Kjetil Uhlen, Ian Norheim, John Olav Giæver Tande "Wind farm measurements and modelling", In proceedings of European Wind Energy Conference (EWEC) Athens, Greece, 27 February - 2 March 2006, available at http://www.ewec2006proceedings.info/

John Olav Giæver Tande was born in Trondheim in 1962. He received his M.Sc. in electrical engineering from the Norwegian Institute of Science and Technology in 1988. He has worked as a research scientist at Norwegian Electric Power Research Institute (1989), Risø National Laboratory (Denmark, 1990-97) and SINTEF Energy Research (1997-). Throughout his career his research has focused on electrical engineering aspects of wind power, and he has broad experience within the field including heading EU projects and working groups of IEC and IEA.

Ian Norheim is employed by SINTEF Energy Research as a research scientist since 2002. In 2002 he achieved a PhD in electrical engineering at the Norwegian University of Science and Technology. At SINTEF Energy Research he has been heavily involved in developing dynamic models of various wind turbines for use in power system simulations. Ian Norheim has written several international papers within the area of power engineering.

Ola Carlson was born in Onsala, Sweden 1955. He received the M.Sc. and Ph.D. degree in electrical engineering from Chalmers University of Technology, Gothenburg, Sweden in 1980 and 1988, respectively. He is currently an Associate Professor at the Department of Energy and Environment at Chalmers University of Technology. He has three years of industry experience in the areas of variable-speed systems for wind turbines. His major interests are electrical systems for renewables, especial wind, and hybrid electric vehicles.

Abram Perdana (S '04) was born in 1974. He received the B.Sc degree in electrical engineering from Gadjah Mada University, Yogyakarta, Indonesia in 1998 and M.Sc degree in sustainable energy engineering from the Royal Institute of Technology, Stockholm, Sweden in 2003. Currently, he is working toward his Ph.D degree in electrical engineering at Chalmers University of Technology, Gothenburg, Sweden. His research area of interest is modelling wind turbines for power system stability studies.

Jan Pierik was born in 1954. He received his M.Sc. degree in Chemical Engineering from the Technical University Twente in 1978. Since 1980 he has been employed at the Energy Research Centre of the Netherlands ECN in Petten, presently as a Senior Research Scientist. His main technical interest is modelling and control of electrical systems for wind turbines and wind farms.

Johan Morren (S'03) received the M.Sc. degree in Electrical Engineering in 2000 from the Delft University of Technology. Currently, he is a research assistant at the Electrical Power Processing group of the Delft University of Technology. He worked on different projects regarding the grid-connection of renewable energy sources. Since 2002 he is working towards a Ph.D. on the power electronic aspects of grid integration of Distributed Generation units.

Ana Estanqueiro was born in Coimbra in 1963. She received her electrical engineer degree from the Technical University of Lisbon (TUL) in 1986 where she also did her M.Sc and PhD. in mechanical engineering, respectively in 1991 and 1997. She works as a research scientist at INETI since 1987, being currently Director of the Wind and Ocean Energy Research Unit as well as associate professor at Universidade Lusiada. Her research interests are broad within wind energy with a focus on dynamic models of wind turbine benefiting from her electrical and mechanical background. She is currently chair of the International Energy Agency-IEA Wind Agreement and President of the PT IEP/IEC CTE 88.

João Lameira was born in 1978 in Lisboa. He received his electrical engineer degree from the Technical University of Lisbon (TUL) in 2005 with a graduation thesis on doubly fed induction generator models (DFIG) models. Currently, he is working as researcher trainee at UEO, INETI, his research area of interest being the development of wind turbines models for power system studies.

Poul Sørensen (MIEEE 2004) was born in 1958. He received M.Sc. in electrical engineering from the Technical University of Denmark in 1987. Since 1987 he has been employed at Risø National Laboratory in Roskilde, presently as a Senior Scientist. His main technical interest is integration of wind power into power systems, involving power system control and stability, dynamic modelling and control of wind turbines and wind farms, and wind fluctuation statistics.

Mark O'Malley received B.E. and Ph. D. degrees from University College Dublin in 1983 and 1987, respectively. He is the professor of Electrical Engineering in University College Dublin and is director of the Electricity Research Centre with research interests in power systems, control theory and biomedical engineering. He is a senior member of the IEEE.

Alan Mullane obtained a B.E. in Electrical and Electronic Engineering in 1998 and a Ph.D. in Electrical Engineering in 2003, both from the Department of Electrical and Electronic Engineering at University College Cork. In 2004 he joined the Electricity Research Center as a postdoctoral research fellow. His research interests include non-linear modelling and control of dynamic systems, with particular interest in simulation and control of wind-turbines and their integration into electrical networks.

Olimpo Anaya-Lara (M'98) received the B.Eng. and M.Sc. degrees from Instituto Tecnológico de Morelia, Morelia, México, and the Ph.D. degree from university of Glasgow, Glasgow, U.K., in 1990, 1998 and 2003, respectively. His industrial experience includes periods with Nissan Mexicana, Toluca, México, and CSG Consultants, Coatzacoalcos, México. Currently, he is a Lecturer with the Institute for Energy and Environment at the University of Strathclyde, Glasgow, U.K. His research interests include wind generation, power electronics, stability of mixed generation power systems and bulk power transmission from intermittent energy sources.

Bettina Lemström was born in Helsinki 1966. She received her M.Sc. in electrical engineering from Helsinki University of Technology in 1992. She has worked as researcher at VTT Technical Research Centre of Finland since 1992 except during 2005 when she worked as senior adviser at the Finnish Energy Market Authority. Her main interests are power systems, wind power and energy markets.

Sanna Uski received the Master of Science degree from Lappeenranta University of Technology in 2003. Since then she has been a researcher at VTT Technical Research Centre of Finland. Her main interests are in power systems.

Eduard Muljadi received his Ph. D. (in Electrical Engineering) from the University of Wisconsin, Madison. From 1988 to 1992, he taught at California State University, Fresno, CA. In June 1992, he joined the National Renewable Energy Laboratory in Golden, Colorado. His current research interests are in the fields of electric machines, power electronics, and power systems in general with emphasis on renewable energy applications.

Development and validation	of wind farm models fo	r
power system studies: Al	svik wind farm results	

Jan Pierik, Johan Morren, Tim van Engelen, Sjoerd de Haan, Jan Bozelie.

EWEC 2006, Athene.

Development and validation of wind farm models for power system studies

Alsvik wind farm results

Jan Pierik[⋄], Johan Morren[♠],
Tim van Engelen[⋄], Sjoerd de Haan[♠]
Jan Bozelie
[⋄]Energy research Centre of the Netherlands (ECN)
[♠]Delft University of Technology (TUD)
e-mail: pierik@ecn.nl

Abstract

Dynamic models of wind farms can be used to optimise wind farm control, to investigate wind farm transient behaviour and to study the effect of the wind farm on the grid. The first part of the paper gives an overview of a model of a constant speed wind farm model. In the second part, this model is validated. A problem that can occur when validating models by closed loop measurements will be described and quantified.

Keywords - wind farm models, wind farm dynamics, model validation.

I. INTRODUCTION

In The Netherlands, offshore wind power is on the brink of implementation. Specific plans exist for two offshore wind farms of about 100 MW, located 12 and 25 km from the coast of the province of North Holland. The effect of the incorporation of 6000 MW offshore wind power in the Dutch high voltage grid is currently being investigated. Only the steady state behaviour has been considered so far, resulting in suggestions for grid reinforcement. This needs to be complemented by studies on the dynamic interaction of large amounts of wind power and the high voltage grid.

Wind turbine and wind farm control can play a role in grid control and thereby increase the value of wind power. Currently, there is relatively little experience with large wind farms and their effect on grid control. The models to evaluate these effects, locally as well as on the level of a grid control area, are now becoming available.

Dynamic models of wind farms have been developed by a number of research institutes in Europe and America. ECN and TUD have developed steady state and dynamic models of wind farms in the Erao-1 and Erao-2 project [1, 2, 3]. The dynamic models, in combination with grid models, can be used to study a number of dynamic phenomena, viz. voltage and frequency transients, small signal stability, effect of wind power on rotating reserve, grid response during a short circuit and

other extreme events. These studies will improve wind turbine, wind farm and grid control.

Before the models can be used with convidence, they should have been validated by comparing model results to measurements. In this paper the first step in the validation process is taken, viz. the validation of the constant speed stall controlled wind farm model. This will later be followed by a similar exercise for the variable speed pitch control wind farm model.

II. ROTOR EFFECTIVE WIND SPEED AND TERMINAL VOLTAGE

Before the actual validation can be executed, two critical issues have to be addressed. Both issues influence the validation method.

The first issue deals with the determination of the rotor effective wind speed. The measured instantaneous single point wind speed of a meteo mast is not a good dynamic representation of the instantaneous rotor effective wind speed at each of the turbines in a wind farm during a measurement. This is caused by the distance between the meteo mast and the turbines, the variation of the wind speed over the rotor planes, the rotational sampling by the rotors and the wakes in the farm. The rotor effective wind speed of a particular wind turbine is difficult to measure, maybe the turbine itself is the best measuring device, but a model would be required to reproduce the rotor effective wind speed. The accuracy of this model would compromise the model validation or make validation impossible by introducing a vicious circle.

Statistically, the rotor effective wind speed is well known however. This fact can be used to construct a statistically correct time series of the rotor effective wind for a given turbine type based on the average wind speed of a measurement. The method is described in [4] and in [5]. As long as only dynamic changes in voltage, current, power and other turbine variables are compared, i.e. the frequency response of a model is validated, the exact second to second value of the rotor effective wind speed during the measurement is

not needed. To validate the dynamic model, the Auto Power Spectral Density functions (APSDs) of simulation and measurement are compared. The major draw back of this method is that a high measurement sample frequency and proper signal conditioning (anti-aliasing filters) are required, in order to prepare correct APSDs with a sufficiently high cut-off frequency.

A second complication to be investiged before the validation can be executed, is which source to use for the second model input variable: the wind turbine terminal voltage. At first glance, it seems obvious to use the measured terminal voltage, if available. There is a problem with this choice however, if the frequency response of the model is compared to the frequency content of the measurement. The voltage is not an independent variable: for a constant speed turbine, it may strongly depend on the rotor effective wind speed. System identification theory shows that this makes it impossible to determine the transfer function of the turbine between voltage and current or power (see Appendix A.1). Secondly, the correlation between wind speed and voltage will lead to an error or bias in the simulatated dynamic behavour and the resulting APSDs. Appendix A describes the analytical background of this problem and quantifies it for the Alsvik wind farm. It is shown that, for the specific case of the Alsvik wind farm, the error in the frequency response caused by using the measured voltage as an input is small, because the coherence between the rotor effective wind speed and the voltage is expected to be small, due to two circumstances:

- · multiple turbines in operation;
- a substantial amount of noise on the voltage signal caused by load changes deeper in the grid.

III. ALSVIK WIND FARM MODEL

The dynamic model of the constant speed stall wind farm which is validated in this paper has been developed by ECN and TUD in the Erao-2 project. The model is programmed in Simulink, a simulation language for dynamic modelling and controller design. The preprocessor, which generates the normalised rotor effective wind speed, is written in Matlab. The model consists of two main parts:

- the Alsvik wind farm model;
- · the grid model.

The model of the Alsvik wind farm includes models of:

- four constant speed stall controlled turbines;
- four 10 kV cables connecting the turbines to a 10-150 kV transformer.

The model of the constant speed stall controlled turbine includes:

- the turbine transformer;
- the constant speed stall model for the Alsvik turbine.

The Alsvik constant speed stall model includes:

- the fourth order dq-model of an asynchronous generator;
- the rotor effective wind calculation including turbulence, wind shear and tower shadow;
- the rotor model based on tables of power and thrust coefficients;
- the mechanical model of the turbine.

The mechanical model of the turbine includes:

- a two masses-spring-damper model of the drive train:
- two single mass-spring-damper models for the tower and the nacelle (tower motion in two directions: nodding and naying).

In some of the simulations a grid model is included, which consists of models of the following components:

- a 10-150 kV transfomer;
- a 150 kV cable;
- · a 150-13.8kV transfomer;
- a 13.8 kV cable;
- two consumer loads (resistors);
- a voltage and frequency controlled synchronous generator (fifth order dynamic model).

For the mathematical description of the constant speed stall wind turbine model, the electrical component models and the grid model is referred to [2], available at the web site of ECN (www.ecn.nl).

IV. ALSVIK NORMAL OPERATION, 256 HZ SAMPLE FREQUENCY, MEASURED VOLTAGE INPUT

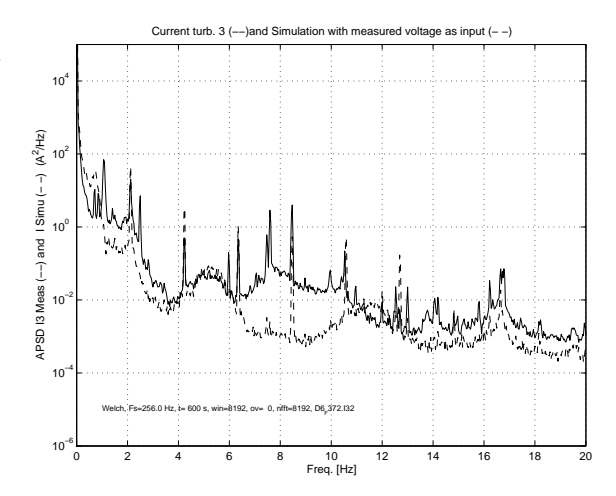


Figure 1: APSD of the measured effective current of Alsvik turbine 3 and simulated current (measured voltage as input)

Figure 1 gives the APSDs of the current of turbine 3. Level and shape of the measured and simulated APSD of the turbine 3 current are very similar, except for the range between 6-10 Hz, where the measurement is more volatile than the simulation. This indicates that there is still something missing in the model.

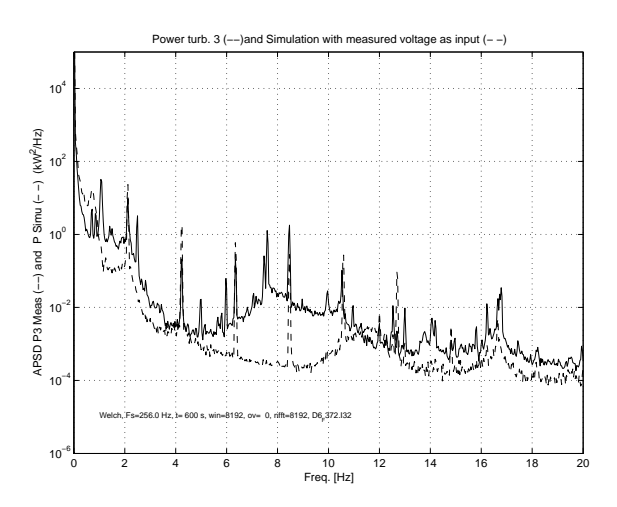


Figure 2: APSD of the measured power of Alsvik turbine 3 and simulated power (measured voltage as input)

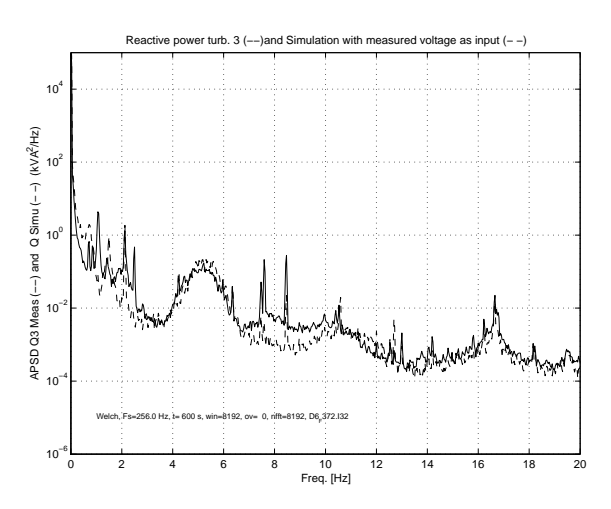


Figure 3: APSD of the measured reactive power of Alsvik turbine 3 and simulated reactive power (measured voltage as input)

Figures 2 and 3 give the APSDs of the power and the reactive power calculated from the measurements and the simulation. The APSDs of the power of turbine 3 again only differ in the 6-10 Hz range. For the reactive power the agreement is almost perfect over the complete frequency range.

V. ALSVIK TURBINE 3 VOLTAGE DIP

The second measurement available for validation is a voltage dip. For this short measurement of about 3 seconds, the exact value of the rotor effective wind is not that important and time series of measurement and simulation are compared. To simulate the dip, the measured voltage is the main model input and has to be converted to the dq0-reference frame. Since the grid frequency is not exactly know, a constant voltage phasor rotational frequency of 50 Hz is assumed. This assumption leads to a variable voltage phasor angle (the angle between ud and uq), and this is important for a good validation result for the voltage dip.

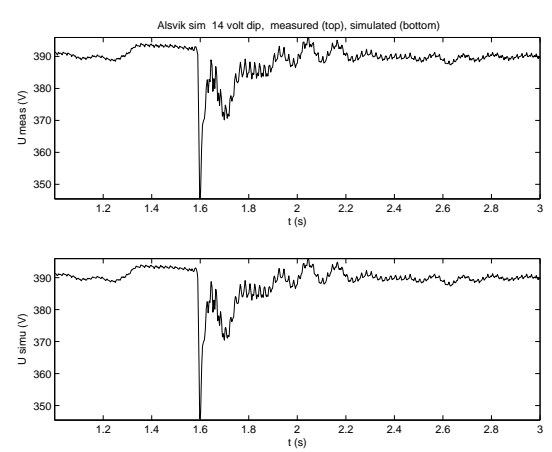


Figure 4: Alsvik voltage dip, measured and simulated effective voltage (f = 50 Hz constant)

Figure 4 compares the measured effective voltage and the effective voltage calculated from u_d and u_q , the two inputs for the model, assuming that the frequency is 50 Hz and constant.

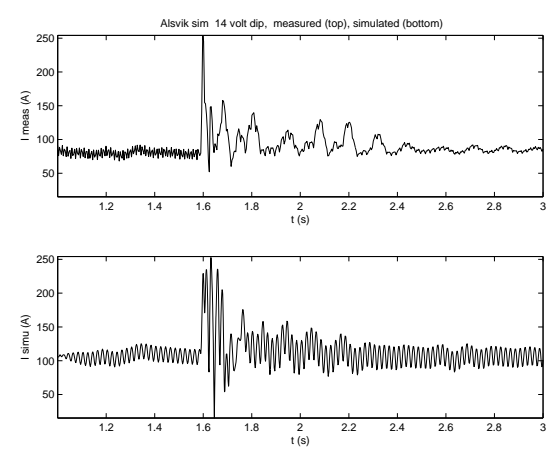


Figure 5: Alsvik voltage dip, measured and simulated effective current of turbine 3 (f = 50 Hz constant)

Figure 5 compares the measured and simulated effective current. The levels of the simulated current peaks are similar to the levels in the measurement. However, the negative excursion is larger. The two main frequencies present in the measurement are also found in the simulation, but with different levels of damping. This is an indication of inaccurate modelling of the generator

(fifth order model without saturation) or of the mechanical transmission. Underestimation of the damping may be an important consideration when the model is used in a grid stability study. Figure 6 and 7 show similar differences as for the current.

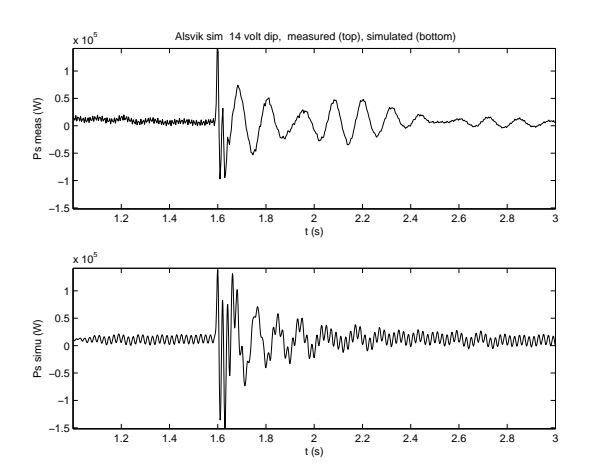


Figure 6: Alsvik voltage dip, measured and simulated power of turbine 3 (f = 50 Hz constant)

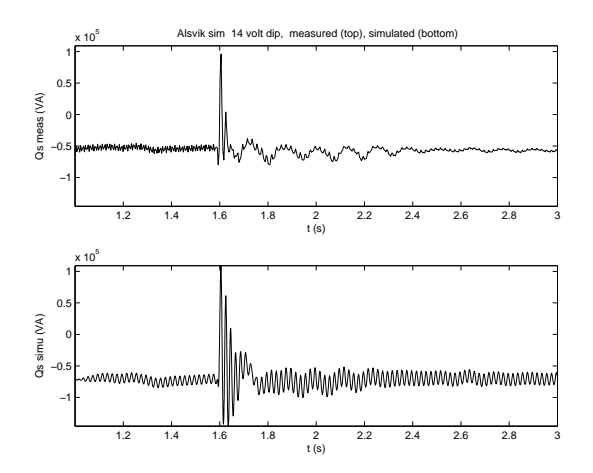


Figure 7: Alsvik voltage dip, measured and simulated reactive power of turbine 3 (f = 50 Hz constant)

VI. CONCLUSIONS

In the validation of dynamic models of wind turbines and wind farms, measurements and simulation results have been compared. The validation process was complicated by two problems:

- the time series of the rotor effective wind speed during the measurement are not known, which makes comparing time series of measured and simulated variables difficult;
- voltage and wind speed measurements are not independent. This will result in errors when the voltage is used as an input to determine the frequency response by simulation.

For the first problem a work around is found by comparing measurements and simulations in the frequency domain. Frequency domain representations are an excellent way to obtain the properties of dynamic models. The second problem requires the quantification of the coherence of voltage and wind speed. It was shown that the measured voltage is acceptabel as an input for the Alsvik wind farm validation.

In the first model validation case (normal operation), the measured voltage is used as input and the simulation results compare well to the measurements. The only major difference between measurement and simulation is a broad peak in the spectra of current and power around 8 Hz. The reactive power spectrum is almost identical.

The second measurement available for validation is a voltage dip. Oscillation frequencies are estimated with reasonable accuracy, the damping (electrical or mechanical) is different.

Summarizing, the validation of the model for the Alsvik wind farm showed that:

- the frequency response results under normal conditions are good for the electrical variables, when
 the measured voltage is used as model input instead of using a grid model;
- the transient response result for a voltage dip was reasonable, with some mismatch in the oscillation frequencies and the damping.

Frequency response results under normal conditions for the mechanical parameters (not shown in this paper) proved to be less good. This may partly be caused by the grid voltage variations, which could not be included in the validation for the mechanical parameters, because the voltage was not included in that measurement set.

REFERENCES

- [1] J.T.G. Pierik, M.E.C. Damen, P. Bauer, and S.W.H. Electrical and control aspects of offshore wind farms, Phase 1: Steady state electrical design and economic modeling, Vol. 1: Project results. Technical Report ECN-CX-01-083, ECN Wind Energy, 2001.
- [2] J.T.G. Pierik, J. Morren, E.J. Wiggelinkhuizen, S.H.W. de Haan, T.G. van Engelen, and J. Bozelie. Electrical and Control Aspects of Offshore Wind Turbines II (Erao-2). Volume 1: Dynamic models of wind farms. Technical Report ECN-CX- -04-050, ECN, 2004.
- [3] J.T.G. Pierik, J. Morren, E.J. Wiggelinkhuizen, S.H.W. de Haan, T.G. van Engelen, and J. Bozelie. Electrical and Control Aspects of Offshore Wind Turbines II (Erao-2). Volume 2: Offshore wind farm case studies. Technical Report ECN-CX--04-051, ECN, 2004.

- [4] T.G. van Engelen, E.L. van der Hooft, and P. Schaak. Ontwerpgereedschappen voor de regeling van windturbines. Technical Report –, ECN, 2004. to be published.
- [5] T.G van Engelen and E.J. Wiggelinkhuizen. ECN design tool for control development; revised points of departure; status report. Technical report, ECN, 2002.

APPENDIX

In model validation, the measured terminal voltage is often used as an input of the model. It that case, the grid impedance and the dynamic behaviour of the grid is not included in the model. This choice will be called open loop model validation. The reason for this choice is that the grid impedance is not known and the grid voltage behind the grid impedance is not measured. In this appendix will be demonstrated that the direct use of the measured terminal voltage as an input will produce an error in the model outputs. This is caused by the correlation between the wind speed and the measured voltage and the fact that the (rotor effective) wind speed during the measurement is not known. This correlation makes it impossible to determine the open loop transfer function between terminal voltage and turbine current or power. It will also have an effect on the current and power time series calculated by the open loop model, as well as on the APSDs of these signals. Prior to using a measured voltage as an input in an open loop model validation process, the error thus introduced should be quantified. This appendix will first show how closed loop measurements affect the model validation proces by determining the transfer function from terminal voltage to turbine currunt. Secondly, the correlation between wind speed and terminal voltage will be used as a criterion for the use of the measured voltage as input in the Alsvik validation.

A.1 VERIFICATION OF A TURBINE MODEL USING THE CLOSED LOOP MEASUREMENT OF TERMINAL VOLTAGE

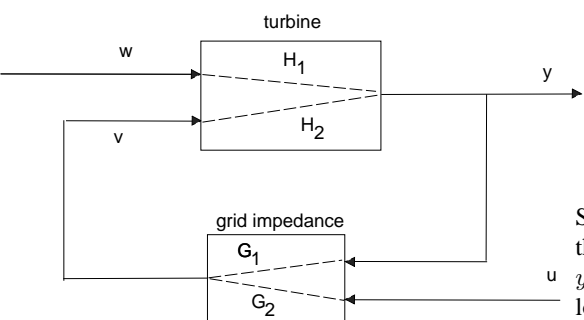


Figure 8: Schematic representation of two input-one output system with feedback and second independent input

Figure 8 gives a schematic representation of a wind turbine, connected to the grid by an impedance. The first noise source w represents the variable wind speed and enters the turbine model parallel to the voltage input v. A second noise source u represents the grid voltage and enters the system at the grid impedance. It will be shown that the architecture of the feedback system affects the model validation problem. Referring to figure 8 and rewriting to a two-input-two-output system:

$$y = H_1 w + H_2 v$$

= $(H_1 + \frac{G_1 H_1 H_2}{1 - G_1 H_2}) w + \frac{G_2 H_2}{1 - G_1 H_2} u$

Since the cross-power spectral density function $S_{wu} = S_{uw} = 0$:

$$S_{yv} = (H_1 + \frac{G_1 H_1 H_2}{1 - G_1 H_2}) (\frac{G_1 H_1}{1 - G_1 H_2})^* S_{ww} + \frac{G_2 H_2}{1 - G_1 H_2}) (\frac{G_2}{1 - G_1 H_2})^* S_{uu}$$

$$S_{vv} = (\frac{G_1 H_1}{1 - G_1 H_2}) (\frac{G_1 H_1}{1 - G_1 H_2})^* S_{ww} + \frac{G_2}{1 - G_1 H_2}) (\frac{G_2}{1 - G_1 H_2})^* S_{uu}$$

If $S_{ww} = 0$ (zero wind speed variation):

$$\frac{S_{yv}}{S_{vv}} = \frac{\frac{G_2H_2}{1-G_1H_2}(\frac{G_2}{1-G_1H_2})^*S_{uu}}{(\frac{G_2}{1-G_1H_2})(\frac{G_2}{1-G_1H_2})^*S_{uu}} = H_2$$

So, if the only independent input is the grid voltage u, which enters the closed loop at the feedback block grid impedance, then the closed loop relation between y and v is a correct representation of the open loop proces transfer function H_2 and validation is straightforward.

If $S_{uu} = 0$ (zero grid voltage variation):

$$\frac{S_{yv}}{S_{vv}} = \frac{(H_1 + \frac{G_1H_1H_2}{1 - G_1H_2})(\frac{G_1H_1}{1 - G_1H_2})^*S_{ww}}{(\frac{G_1H_1}{1 - G_1H_2})(\frac{G_1H_1}{1 - G_1H_2})^*S_{ww}}$$
$$= \frac{1}{G_1}$$

So, if a noise source enters the turbine model parallel to the feedback voltage, the closed loop relation between y and v is no longer a correct representation of the open loop proces transfer function H_2 . In the ultimate case that only this noise source exists, so $S_{uu}=0$, the value of $1/G_1$ will be estimated in stead of H_2 .

A.2 CONCLUSIONS FROM SYSTEM IDENTIFICATION THEORY

 The architecture of the closed loop system, i.e. the signal routing, determines whether a validation problem occurs. If an input signal enters the model parallel to the feedback signal, a bias term exists. If no parallel input signal exists, then there is no bias term.

- Open loop validation of a turbine model using the (closed loop) measurement of the terminal voltage as a turbine model input may lead to errors due to a bias term caused by the feedback loop.
- For the wind turbine model with grid impedance, the transfer function between terminal voltage and turbine current equals the inverse of the grid impedance if the wind speed is the only input responsible for the variation of the terminal voltage. This makes it impossible to estimate the open loop wind turbine transfer function from the voltage at the turbine terminal to the turbine current.
- The previous observations are equivalent to the observation that the wind speed and the voltage do not constitute independent variables but are correlated. The magnitude of this correlation in the relevant frequency domain should be checked before the voltage is used as an input in open loop validation.

A.3 ESTIMATION OF THE CORRELATION BETWEEN WIND SPEED AND VOLTAGE

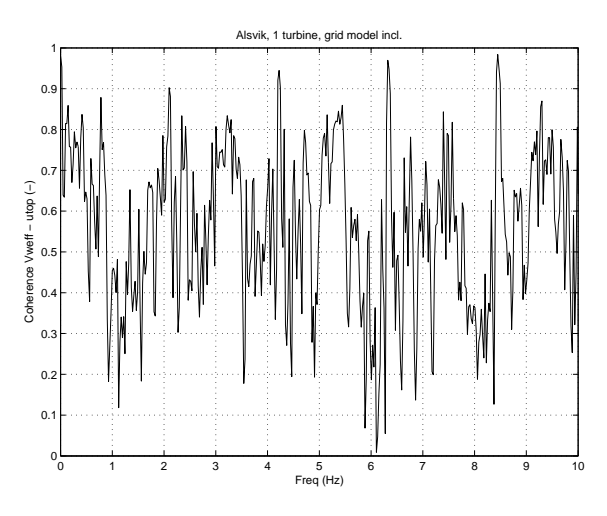


Figure 9: Coherence between rotor effective wind speed and terminal voltage for a single Alsvik turbine in operation, no grid load variations (simulation)

Simulations will be used to estimate the correlation between the wind speed and the terminal voltage for the Alsvik wind farm. Figure 9 gives the coherence between the rotor effective wind speed and the terminal voltage for a single Alsvik turbine in operation. The figure shows a high coherence (0.90-0.98) at multiples of 3P and a relatively high coherence over the full range of 1-10 Hz (0.55 on average). This is not in favour of using the voltage as a model input. The coherence should reduce if the number of turbines in operation is increased

and also if uncorrelated voltage variations caused by load changes in the grid are taken into account.

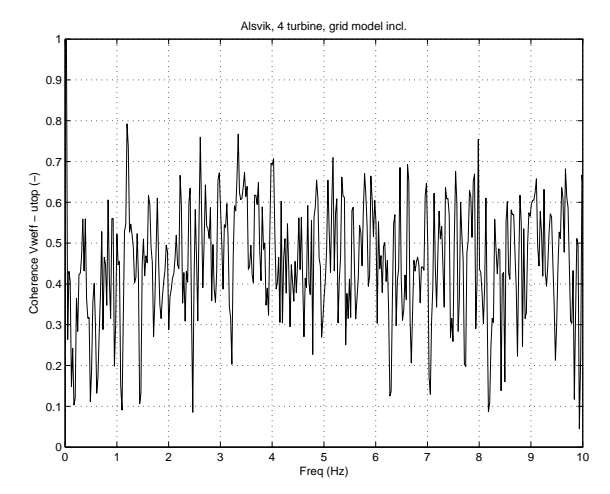


Figure 10: Coherence between rotor effective wind speed and terminal voltage for 4 Alsvik turbines in operation, no grid load variations (simulation)

Figure 10 gives the coherence between the rotor effective wind speed and the terminal voltage for a group of 4 Alsvik turbines in operation. Since the rotor positions are not synchronised, the rotationally sampled wind speeds of the different turbines are not strongly correlated and this reduces the correlation between the wind speed of a single turbine and the terminal voltage. However, the average coherence of 0.45 is still relatively high.

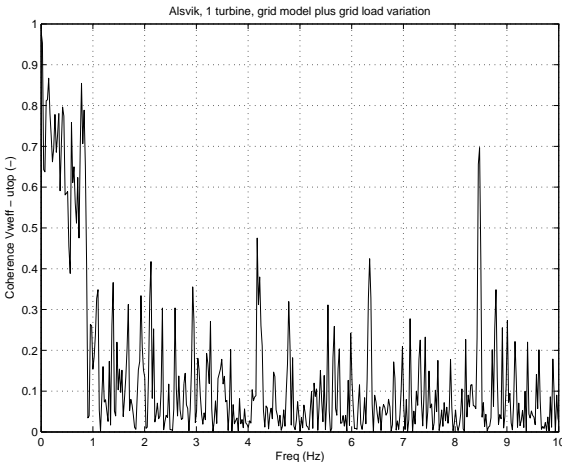


Figure 11: Coherence between rotor effective wind speed and terminal voltage for an Alsvik turbine including grid load variations causing 1 V voltage noise (simulation)

Figure 11 gives the coherence between rotor effective wind speed and terminal voltage for an Alsvik turbine including grid load variations causing 1 V random noise. These voltage variations still are significantly

smaller than the variations in the Alsvik measurements: about 3 V. The reduction at the multiples of 3P now is more substantial and the overall level is low except for the range below 1 Hz.

This shows that multiple turbines in operation and a substantial amount of noise in the terminal voltage caused by load changes in the grid sufficiently reduce the correlation between the wind speed and the terminal voltage. Therefore it is permissible to use the measured (closed loop) voltage of the Alsvik wind farm to calculate APSD functions of currents and powers in the open loop model validation. This method will still introduce an error, but since the coherence is relatively low, the error is small.

ACKNOWLEDGMENT

Erao-3 is a continuation of the Erao projects, in which steady state (load flow), economic and dynamic models of offshore wind farms have been developed. The Erao projects have been supported by the Dutch Agency for Energy and Environment (SenterNovem) in the "Programma Duurzame Energie" of the Netherlands, executed by SenterNovem by order of the Ministry of Economic Affairs.

The measurement data of the Alsvik wind farm have been supplied by Chalmers University of Technology in the framework of the IEA Annex XXI: Dynamic models of Wind Farms for Power System Studies.

Grid interaction of Offshore Wind Farms. Part 1. Models for Dynamic Simulation

Johan Morren, Jan T.G. Pierik, Sjoerd W.H. de Haan, Jan Bozelie.

Article Wind Energy 2005, 8: 265-278 (John Wiley & Sons Ltd.).



Grid Interaction of Offshore Wind Farms. Part 1. Models for Dynamic Simulation

Johan Morren*, Electrical Power Processing, Delft University of Technology, Delft, The Netherlands Jan T. G. Pierik, Energy Research Centre of the Netherlands (ECN), Petten, The Netherlands Sjoerd W. H. de Haan, Electrical Power Processing, Delft University of Technology, Delft, The Netherlands

Jan Bozelie, (former) Neg-Micon, Bunnik, The Netherlands

Key words: dynamic modelling; electrical system; Park transformation; wind energy

In this contribution, dynamic wind farm models suitable for fast simulation of power systems are presented. While deriving the models, special attention has been paid to increasing the computational speed of the simulation program. An important increase in speed is realized by the use of the well-known dq0 transformation (Park transformation) not only for the generator but also for all other electrical components. The use of the Park transformation is common practice in electrical machine models, but not in the modelling of other electrical components. For single turbines, simulations in the dq0 reference frame are 100 times faster than simulations in the abc reference frame. After a discussion of the Park transformation and its most important properties, it is explained how models in the dq0 reference frame can be obtained. The dq0 models of the most important electrical components are presented. The mechanical and aerodynamic models that are needed for dynamic simulation of wind turbines are discussed briefly. The models are applied in Part 2. Copyright © 2005 John Wiley & Sons, Ltd.

Introduction

A tendency to increase the amount of electricity generated from wind can be observed.¹ As the penetration of wind turbines in electrical power systems increases, they may begin to influence overall power system operation.² The interaction between the wind farms and the grid will be an important aspect in the planning of the farms.³ Especially the behaviour during voltage dips is important. Wind turbines supply fluctuating active and reactive power to the grid owing to the fluctuating wind. This will cause voltage fluctuations. It is essential to ensure that the grid is capable of staying within the operational limits of frequency and voltage for all foreseen combinations of wind power production and consumer loads⁴ and to ensure appropriate transient and small-signal stability of the grid.⁵

The behaviour of wind turbines with respect to their interaction with the grid is therefore studied at different places.^{5–7} In order to facilitate the investigation of the impact of a wind farm on the dynamic behaviour of the power system, adequate models of wind turbines and grid components are required. Although the speed of computers has significantly increased over the years, computational speed is still one of the limiting factors in

E-mail: J.Morren@ewi.tudelft.nl

Contract/grant sponsor: Dutch Agency for Energy and Environment (NOVEM) Contract/grant sponsor: Ministry of Economic Affairs of The Netherlands

^{*}Correspondence to: J. Morren, Electrical Power Processing, Delft University of Technology, Mekelweg 4, NL-2628 CD Delft, The Netherlands

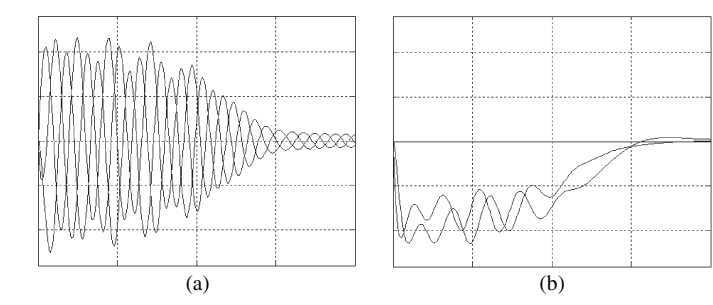


Figure 1. Inrush currents of a three-phase induction machine in the (a) abc and (b) dq0 reference systems

(dynamic) simulation of power systems. One of the problems is the complexity of the models, which limits the computational speed. When reduced models are used, simulation of complex systems such as wind farms can be done much faster, but the results may be less accurate.⁸

The Park transformation (some-times called the Blondel–Park transformation) is well known from its use in electrical machinery. The electrical signals are transformed to a stationary rotating reference frame. As this stationary frame is chosen to rotate with the grid frequency, all voltages and currents in the dq0 reference frame are constant in steady state situations. Therefore modelling in the dq0 reference frame is expected to increase the simulation speed significantly, as a variable step size simulation program can apply a large time step during quasi-steady state phenomena. An example is shown in Figure 1, where the inrush currents of a three-phase induction machine are shown in the abc and dq0 reference systems respectively. The time step that can be applied without introducing significant errors will be much larger in the case of the dq0 reference system. The drawback of modelling in a dq0 reference frame is that the models for grid components are not available and therefore have to be developed.

A research project on the grid integration of large wind farms has been initiated to develop dynamic models suited for grid impact studies. The most important for grid interaction are the models of the electrical components. Models in the dq0 reference frame have been developed for electrical wind turbine generators (induction generator, doubly-fed induction generator, permanent magnet generator), power electronic converters, transformers, cables (lines) and synchronous generators (conventional power plant). For the dynamic behaviour of wind turbines, mechanical and aerodynamical models are also needed. The following models have been developed: turbine rotor, mechanical drive train and rotor effective wind.

In this contribution a description will be given of the models that have been derived. The article starts with a discussion of the Park transformation and a description of the way in which models in the dq0 reference frame can be obtained for different electrical components, followed by a description of the electrical component models. Afterwards wind models and turbine models are given. Results obtained with these models in dynamic simulations are presented in Part 2 of this article.

Park Transformation

In the study of power systems, mathematical transformations are often used to decouple variables, to facilitate the solution of difficult equations with time-varying coefficients, or to refer all variables to a common reference frame. Probably the best known is the method of symmetrical components developed by Fortescue. This transformation is mostly used in its time-independent form and applied to phasors in electrical power system studies. Another commonly used transformation is the Park transformation, which is well known from the modelling of electrical machines. The Park transformation is instantaneous and can be applied to arbitrary three-phase time-dependent signals.

For $\theta_d = \omega_d t + \varphi$, with ω_d the angular velocity of the signals that should be transformed, t the time and φ the initial angle, the Park transformation is given by

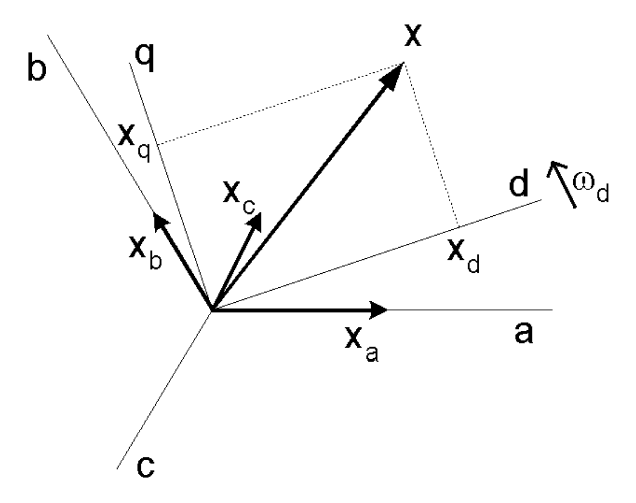


Figure 2. Relationship between abc and dq quantities

$$[\mathbf{x}_{dq0}] = [\mathbf{T}_{dq0}(\boldsymbol{\theta}_d)][\mathbf{x}_{abc}] \tag{1}$$

with

$$\begin{bmatrix} \mathbf{x}_{dq0} \end{bmatrix} = \begin{bmatrix} x_d \\ x_q \\ x_0 \end{bmatrix} \quad and \quad \begin{bmatrix} \mathbf{x}_{abc} \end{bmatrix} = \begin{bmatrix} x_a \\ x_b \\ x_c \end{bmatrix}$$
 (2)

and with the dq0 transformation matrix \mathbf{T}_{dq0} defined as

$$[T_{dq0}] = \sqrt{\frac{2}{3}} \begin{bmatrix} \cos \theta_d & \cos \left(\theta_d - \frac{2\pi}{3}\right) & \cos \left(\theta_d + \frac{2\pi}{3}\right) \\ -\sin \theta_d & -\sin \left(\theta_d - \frac{2\pi}{3}\right) & -\sin \left(\theta_d + \frac{2\pi}{3}\right) \end{bmatrix}$$

$$\frac{1}{\sqrt{2}} \qquad \frac{1}{\sqrt{2}} \qquad \frac{1}{\sqrt{2}}$$
(3)

and its inverse given by

$$[T_{dq0}]^{-1} = \sqrt{\frac{2}{3}} \begin{bmatrix} \cos\theta_d & -\sin\theta_d & \frac{1}{\sqrt{2}} \\ \cos\left(\theta_d - \frac{2\pi}{3}\right) & -\sin\left(\theta_d - \frac{2\pi}{3}\right) & \frac{1}{\sqrt{2}} \\ \cos\left(\theta_d + \frac{2\pi}{3}\right) & -\sin\left(\theta_d + \frac{2\pi}{3}\right) & \frac{1}{\sqrt{2}} \end{bmatrix}$$

$$(4)$$

The positive q-axis is defined as leading the positive d-axis by $\pi/2$, as can be seen from Figure 2.

Voltages and currents of electrical systems are often given as a set of differential equations. A short description will be given of how these differential equations can be transformed to the dq0 reference system. The derivative of a vector in the abc reference system is given by

$$\frac{\mathrm{d}}{\mathrm{d}t}[\mathbf{x}_{abc}] = \frac{\mathrm{d}}{\mathrm{d}t} \left(\left[\mathbf{T}_{dq0}(\boldsymbol{\theta}_d) \right]^{-1} / \left[\mathbf{x}_{dq0} \right] \right)$$
 (5)

With the chain rule for derivatives,

$$\frac{\mathrm{d}}{\mathrm{d}t}[\mathbf{x}_{dq0}] = [\mathbf{T}_{dq0}(\boldsymbol{\theta}_d)] \frac{\mathrm{d}}{\mathrm{d}t} [\mathbf{x}_{abc}] + \left(\frac{\mathrm{d}}{\mathrm{d}t} [\mathbf{T}_{dq0}(\boldsymbol{\theta}_d)]\right) [\mathbf{x}_{abc}]$$
(6)

$$\left[\mathbf{T}_{dq0}(\boldsymbol{\theta}_d)\right] \frac{\mathrm{d}}{\mathrm{d}t} \left[\mathbf{x}_{abc}\right] = \frac{\mathrm{d}}{\mathrm{d}t} \left[\mathbf{x}_{dq0}\right] - \left(\frac{\mathrm{d}}{\mathrm{d}t} \left[\mathbf{T}_{dq0}(\boldsymbol{\theta}_d)\right]\right) \left[\mathbf{T}_{dq0}(\boldsymbol{\theta}_d)\right]^{-1} \left[\mathbf{x}_{dq0}\right]$$
(7)

$$\left[\mathbf{T}_{dq0}(\boldsymbol{\theta}_{d})\right] \frac{\mathrm{d}}{\mathrm{d}t} \left[\mathbf{x}_{abc}\right] = \frac{\mathrm{d}}{\mathrm{d}t} \left[\mathbf{x}_{dq0}\right] - \omega_{d} \frac{1}{\omega_{d}} \left(\frac{\mathrm{d}}{\mathrm{d}t} \left[\mathbf{T}_{dq0}(\boldsymbol{\theta}_{d})\right]\right) \left[\mathbf{T}_{dq0}(\boldsymbol{\theta}_{d})\right]^{-1} \left[\mathbf{x}_{dq0}\right]$$
(8)

Knowing that, for x = x(t),

$$\frac{\mathrm{d}}{\mathrm{d}t}\sin x = \cos x \frac{\mathrm{d}x}{\mathrm{d}t} \quad \text{and} \quad \frac{\mathrm{d}}{\mathrm{d}t}\cos x = -\sin x \frac{\mathrm{d}x}{\mathrm{d}t} \tag{9}$$

and that $\omega_d = d\theta_d/dt$, the following result is obtained:

$$\left(\frac{\mathrm{d}}{\mathrm{d}t}[T_{dq0}(\theta_d)]\right)[T_{dq0}(\theta_d)]^{-1} = \omega_d \begin{bmatrix} 0 & -1 & 0 \\ 1 & 0 & 0 \\ 0 & 0 & 0 \end{bmatrix}$$
(10)

and it can be easily seen that

$$\left[\mathbf{T}_{dq0}(\boldsymbol{\theta}_d)\right] \frac{\mathrm{d}}{\mathrm{d}t} \left[\mathbf{x}_{abc}\right] = \frac{\mathrm{d}}{\mathrm{d}t} \left[\mathbf{x}_{dq0}\right] + \omega_d y \left[\mathbf{x}_{dq0}\right]$$
(11)

with y given by

$$y = \frac{1}{\omega_d} \left(\frac{d}{dt} [\mathbf{T}_{dq0}(\theta_d)] \right) [\mathbf{T}_{dq0}(\theta_d)]^{-1} = \begin{bmatrix} 0 & -1 & 0 \\ 1 & 0 & 0 \\ 0 & 0 & 0 \end{bmatrix}$$
(12)

It can be seen from (12) that differential equations will cause a cross-relation between the d- and the q-axis. Some additional properties of the Park transformation can be derived. As the transformation is orthogonal, it holds that

$$\left[\mathbf{T}_{dq0}(\boldsymbol{\theta}_d)\right]\left[\mathbf{T}_{dq0}(\boldsymbol{\theta}_d)\right]^{-1} = \left[\mathbf{T}_{dq0}(\boldsymbol{\theta}_d)\right]\left[\mathbf{T}_{dq0}(\boldsymbol{\theta}_d)\right]^{\mathrm{T}} = \left[\mathbf{I}\right]$$
(13)

The transformations of (3) and (4) are unitary. Note that, by replacing the factor $\sqrt{2/3}$ by a factor 2/3 in (3) and (4), the transformation will be amplitude-invariant, implying that the lengths of the current and voltage vectors in both the *abc* and dq0 reference frames are the same. This amplitude-invariant transformation is mostly used in the modelling of electrical machines.¹¹

The voltages and currents in the dq0 reference frame are constant in steady state situations. Be aware that also non-fundamental harmonics are correctly transformed, as x_a , x_b and x_c are time signals, including all harmonics. In the steady state a non-fundamental frequency component with frequency ω_h will appear as a sinusoidal signal with frequency $\omega_h - \omega_d$ in the dq0 domain. The highest frequency that can be represented accurately in the dq0 frame depends on the time step used.

With (13) it can be shown that the Park transformation conserves power:¹²

$$p(t) = \begin{bmatrix} \mathbf{v}_{abc} \end{bmatrix}^{\mathrm{T}} \begin{bmatrix} \mathbf{i}_{abc} \end{bmatrix}$$

$$= \begin{bmatrix} \begin{bmatrix} \mathbf{T}_{dq0}(\boldsymbol{\theta}_d) \end{bmatrix}^{-1} \begin{bmatrix} \mathbf{v}_{dq0} \end{bmatrix}^{\mathrm{T}} \begin{bmatrix} \mathbf{T}_{dq0}(\boldsymbol{\theta}_d) \end{bmatrix}^{-1} \begin{bmatrix} \mathbf{i}_{dq0} \end{bmatrix}$$

$$= \begin{bmatrix} \mathbf{v}_{dq0} \end{bmatrix}^{\mathrm{T}} \begin{bmatrix} \mathbf{T}_{dq0}(\boldsymbol{\theta}_d) \end{bmatrix}^{-1} \begin{bmatrix} \mathbf{T}_{dq0}(\boldsymbol{\theta}_d) \end{bmatrix}^{-1} \begin{bmatrix} \mathbf{i}_{dq0} \end{bmatrix}$$

$$= \begin{bmatrix} \mathbf{v}_{dq0} \end{bmatrix}^{\mathrm{T}} \begin{bmatrix} \mathbf{T}_{dq0}(\boldsymbol{\theta}_d) \end{bmatrix} \begin{bmatrix} \mathbf{T}_{dq0}(\boldsymbol{\theta}_d) \end{bmatrix}^{-1} \begin{bmatrix} \mathbf{i}_{dq0} \end{bmatrix}$$

$$= \begin{bmatrix} \mathbf{v}_{dq0} \end{bmatrix}^{\mathrm{T}} \begin{bmatrix} \mathbf{i}_{dq0} \end{bmatrix}$$

$$= \begin{bmatrix} \mathbf{v}_{dq0} \end{bmatrix}^{\mathrm{T}} \begin{bmatrix} \mathbf{i}_{dq0} \end{bmatrix}$$
(14)

The Park transformation is often used in control loops, as it offers the possibility of decoupled control between active power and reactive power. Be aware, however, that active power and reactive power cannot be directly related to the d- and q-axis components. These components are just a representation. The instantaneous active power and reactive power can be obtained directly from the voltages and currents in the dq0 reference system:¹³

$$p = v_d i_d + v_q i_q$$

$$q = v_q i_d - v_d i_q$$
(15)

Models of Electrical Components

Introduction

In this section, some of the most important electrical component models will be presented. More detailed descriptions of some specific models that have been derived can be found in References 14–19.

Electrical machine models

Mostly electrical machine models are already given in a dq0 reference frame. Therefore it is not necessary to present all these models here. They can be found in the literature, see e.g. References 5, 6, 9 and 20–22. As an example, the model for a doubly-fed induction generator (DFIG) will be given. The model of the machine is based on the fifth-order two-axis representation. A synchronously rotating dq reference frame is used with the direct d-axis oriented along the stator flux position. In this way, decoupled control between the electrical torque and the rotor excitation current is obtained. This reference frame is rotating with the same speed as the stator voltage. When modelling the DFIG, the generator convention will be used, which means that the currents are outputs and that real power and reactive power have a positive sign when they are fed into the grid. Using the generator convention, the following set of equations results:

$$v_{as} = -R_{s}i_{ds} - \omega_{s}\psi_{qs} + \frac{d\psi_{ds}}{dt}$$

$$v_{qs} = -R_{s}i_{qs} - \omega_{s}\psi_{ds} + \frac{d\psi_{qs}}{dt}$$

$$v_{dr} = -R_{r}i_{dr} - \omega_{r}\psi_{qr} + \frac{d\psi_{dr}}{dt}$$

$$v_{qr} = -R_{r}i_{qr} - \omega_{r}\psi_{dr} + \frac{d\psi_{qr}}{dt}$$

$$(16)$$

with v the voltage (V), R the resistance (Ω), i the current (A), ω_s and ω_r the stator and rotor electrical angular velocities (rad s⁻¹) respectively and ψ the flux linkage (V s). The indices d and q indicate the direct and quadrature axis components of the reference frame and 's' and 'r' indicate stator and rotor quantities respectively. All quantities are functions of time.

The generator model that has been used to model the induction machine is almost equal to the model described above in (16). The only difference is that the rotor voltages v_{dr} and v_{qr} are set to zero. The model of the permanent magnet synchronous generator can be found in References 17 and 19.

Converter Model

Modern wind turbines use a power electronic converter to connect either the rotor or the stator to the grid. In this subsection the converter model will be described. Back-to-back converters consisting of two voltage source converters with a DC-link in between are used. The DC-link separates the two converters and therefore they can be controlled independently of each other. The generator-side converter is used to control the stator (synchronous machine) or rotor (doubly-fed induction generator) currents of the electrical generator of the wind

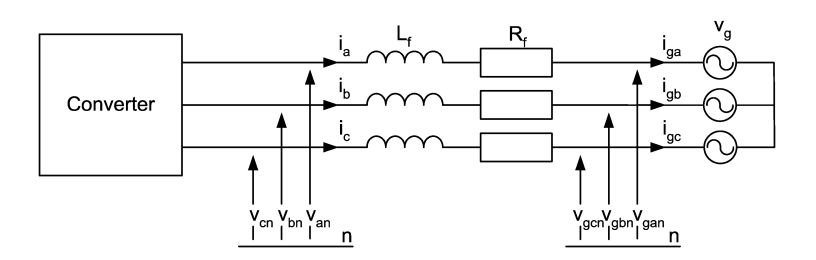


Figure 3. Three-phase full-bridge voltage source converter

turbine. By controlling these currents, active and reactive power and speed and torque of the generator can be controlled. The grid-side converter is used to pass the generator power to the grid and to control the DC-link voltage.

The voltage source converters (VSCs) are based on IGBT switches. The three-phase full-bridge grid-side IGBT-VSC is shown in Figure 3. The converter is also modelled in the dq0 reference frame. It has been modelled according to the switching function concept.²³ The switching of the IGBTs in the converter is not taken into account. It is assumed that the filters of the converter reduce the higher-frequency components.²⁴ It has been shown that good simulation results can be obtained with this model.^{25,26}

Consider the system of Figure 3. The voltage balance across the filter inductors and resistors is

$$\Delta v_{a} = v_{an} - v_{gan} = L_{f} \frac{di_{a}}{dt} + R_{f}i_{a}$$

$$\Delta v_{b} = v_{bn} - v_{gbn} = L_{f} \frac{di_{b}}{dt} + R_{f}i_{b}$$

$$\Delta v_{c} = v_{cn} - v_{gcn} = L_{f} \frac{di_{c}}{dt} + R_{f}i_{c}$$
(17)

With the Park transformation these equations can be transformed to the dq0 reference frame:²⁰

$$\Delta v_{d} = R_{f}i_{d} + L_{f}\frac{di_{d}}{dt} + \omega_{e}L_{f}i_{q}$$

$$\Delta v_{q} = R_{f}i_{q} + L_{f}\frac{di_{q}}{dt} - \omega_{e}L_{f}i_{d}$$

$$\Delta v_{0} = R_{f}i_{0} + L_{f}\frac{di_{0}}{dt}$$
(18)

The ω -terms cause a coupling of the first two equations, which makes it difficult to control both currents independently. The last terms can be considered as a disturbance on the controller output and are not taken into account for the controller. The i_d and i_q errors can be processed by a PI controller to give $v_{d,ref}$ and $v_{q,ref}$ respectively. To ensure good tracking of these currents, the cross-related flux terms are added to $v_{d,ref}$ and $v_{q,ref}$ to obtain the correct reference voltages.

Treating the cross-related terms as a disturbance, the transfer function from voltage to current (for both the d- and the q-component) of (18) can be found as

$$G(s) = \frac{1}{L_f s + R_f} \tag{19}$$

Using the internal model control principle²⁷ to design the current controllers yields

$$K(s) = k_{\rm p} + \frac{k_{\rm i}}{s} = \frac{\alpha_{\rm c}}{s} G^{-1}(s)$$
 (20)

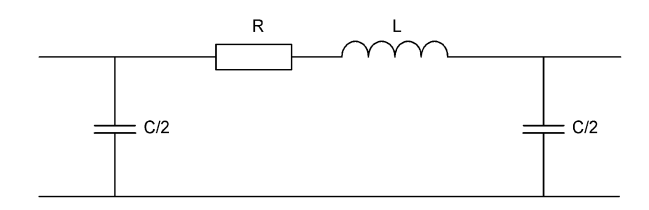


Figure 4. Single-phase equivalent circuit of a cable (transmission line)

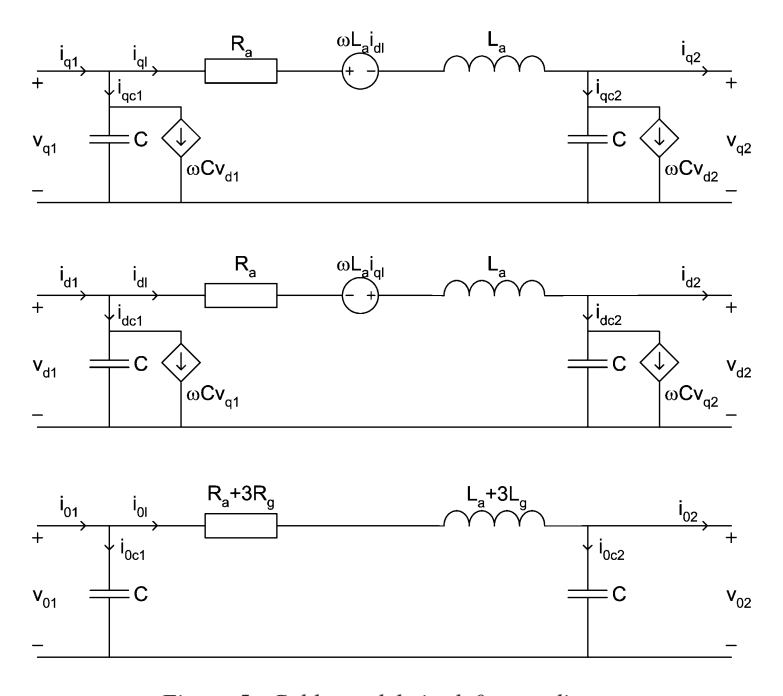


Figure 5. Cable models in dq0 co-ordinates

where α_c is the bandwidth of the current control loop and k_p is the proportional gain and k_i the integral gain of the controller. The proportional and integral gains become²⁰

$$k_{\rm p} = \alpha_{\rm c} L_{\rm f}$$

$$k_{\rm i} = \alpha_{\rm c} R_{\rm f}$$
(21)

The instantaneous active and reactive powers delivered by the converter are given by (15). With the d-axis of the reference frame oriented along the stator voltage position, v_q is zero and, as long as the supply voltage is constant, v_d is constant and the active and reactive powers are proportional to i_d and i_q respectively.

Cable (transmission line)

The general equations relating voltage and current on a transmission line or a cable recognize the fact that all impedances of a transmission line are uniformly distributed along the line. For lines of up to about 250 km, lumped parameters can be used, however.²⁸ The single-phase equivalent circuit of a lumped line (cable) is shown in Figure 4.

The dq0 models of a three-phase RL line with shunt capacitors are shown in Figure 5. The voltage and current relations are given as 18

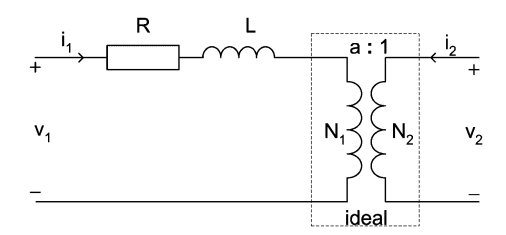


Figure 6. Transformer equivalent circuit with magnetizing current and iron loss neglected

$$\Delta v_{d} = v_{d2} - v_{d1} = R_{a}i_{d1} + L_{a}\frac{di_{d1}}{dt} - \omega L_{a}i_{q1}$$

$$\Delta v_{q} = v_{q2} - v_{q1} = R_{a}i_{q1} + L_{a}\frac{di_{q1}}{dt} - \omega L_{a}i_{d1}$$

$$\Delta v_{0} = v_{02} - v_{01} = (R_{a} + 3R_{g})i_{0} + (L_{a} + 3L_{g})\frac{di_{0}}{dt}$$
(22)

and

$$i_{dcl} = C \frac{dv_{dl}}{dt} - \omega C v_{ql}$$

$$i_{qcl} = C \frac{dv_{ql}}{dt} + \omega C v_{dl}$$

$$i_{0cl} = C \frac{dv_{0l}}{dt}$$
(23)

To obtain the models, it is assumed that the shield of the cables is grounded, which is true in most cases. The shunt capacitors in the lumped cable model represent the capacitance between cable and shield. The dq0 models obtained for the RL circuit assume that a ground return exists. As the cable shield is grounded, the ground return exists and the models of Figure 5 can be used.

Transformer

In this subsection the transformer model will be discussed. Normally the magnetizing current of a transformer is small and can be neglected. The single-phase equivalent circuit of a two-winding transformer is shown in Figure 6, where $R = R_1 + a^2R_2$ and $L = L_1 + a^2L_2$, with $a = N_1/N_2$.

The dq0 models of the transformer are shown in Figure 7. The zero-sequence model depends on the type of transformer (star-start, star-delta, etc.). The zero-sequence model represents a star-delta transformer with a ground star connection at the primary side.²⁹

Grid model

A simple grid model has been developed to simulate the interaction between a wind farm and the grid and to be able to test the voltage and frequency control capabilities of different types of wind farm. The main requirement for the grid model is a dynamic behaviour similar to a large high-voltage grid. The main component of the grid model is a synchronous machine model equipped with voltage and frequency control. The synchronous machine model is the three-winding representation in dq co-ordinates. Damper windings are not taken into account. The generator convention is adopted:

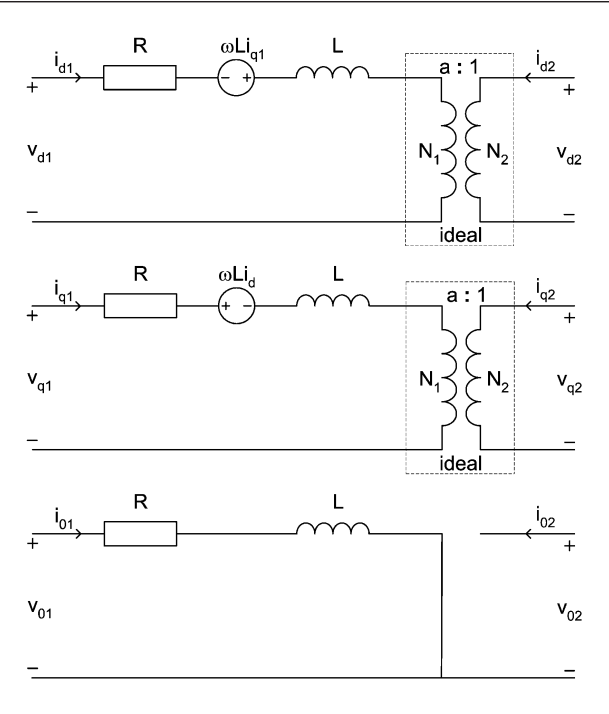


Figure 7. Equivalent transformer model for d, q and 0 sequence components

$$L_{d} \frac{di_{d}}{dt} + L_{mf} \frac{di_{fd}}{dt} = -u_{d} - R_{s}i_{d} - \omega_{s}L_{q}i$$

$$L_{md} \frac{di_{d}}{dt} + L_{f} \frac{di_{fd}}{dt} = u_{fd} - R_{fd}i_{fd}$$

$$L_{q} \frac{di_{q}}{dt} = -u_{q} - R_{s}i_{q} + \omega_{s}(L_{d}i_{d} + L_{md}i_{fd})$$
(24)

with L_d , L_q , L_{md} , L_{mf} and L_f the synchronous machine inductances and R_s and R_{fd} the stator and field winding resistances respectively.

For the voltage regulator and exciter a type 1 model is used.³⁰ The inertia and speed controller of the synchronous machine complete the model:

$$J\frac{d\omega_{s}}{dt} = T_{\text{mech}} - T_{\text{el}}$$

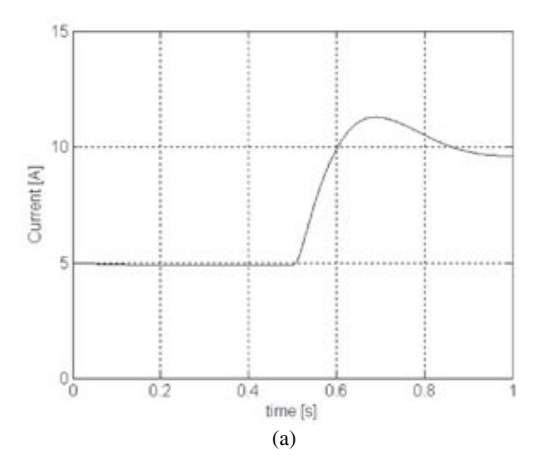
$$T_{\text{mech}} = \frac{P_{\text{mech}}}{\omega_{s}}$$

$$P_{\text{mech}} = \left(K_{\text{pw}} + \frac{K_{\text{iw}}}{s}\right)(\omega_{\text{set}} - \omega_{s})$$
(25)

The grid model further consists of some cables and loads. The parameters of the grid model have been chosen to have a fair amount of transient behaviour, not necessarily found in large-scale grids. This choice is made to demonstrate the wind farm control capabilities.

Comparison

It should be shown that the models in a dq0 reference frame give correct simulation results. The best solution would be to compare the simulation results with measurements. As this was not possible at the moment, dq0



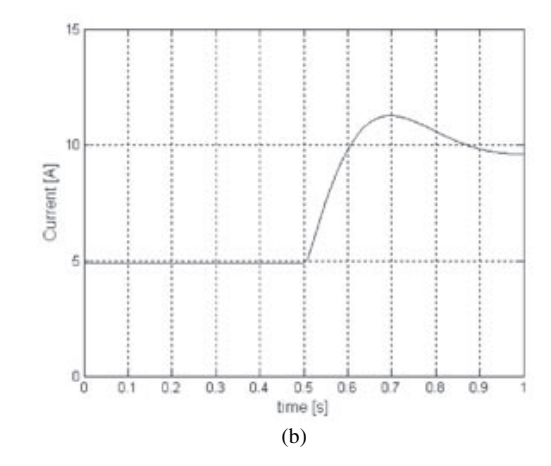
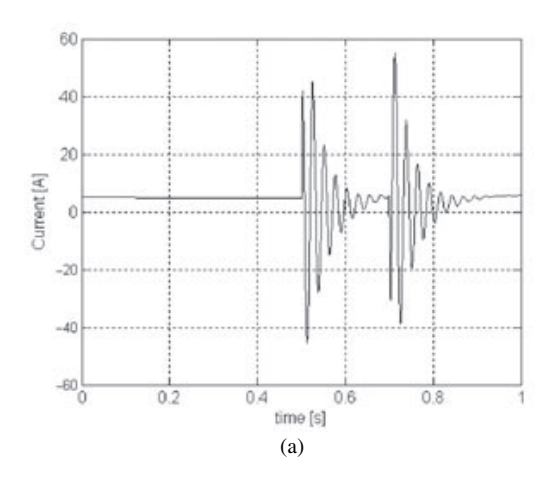


Figure 8. Response of rotor current to a step in mechanical torque for (a) abc model and (b) dq0 model



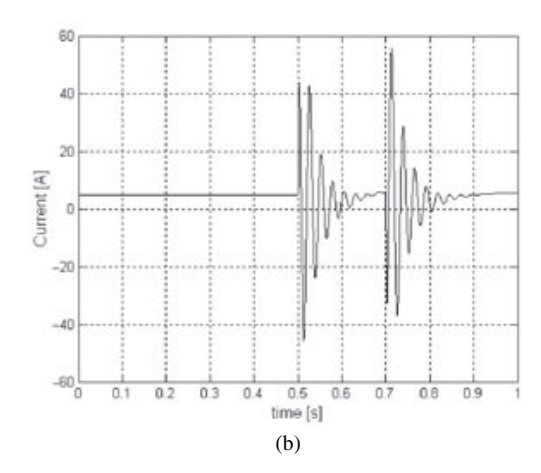


Figure 9. Response of rotor current to a dip in grid voltage for (a) abc model and (b) dq0 model

simulation results have been compared with results of simulations with well-known and accepted models in the normally used abc reference frame. The responses of a doubly-fed induction machine to a step in the mechanical torque (slow dynamics) and to a dip in the grid voltage (fast dynamics) have been considered. The response of the rotor current of the machine to a step in the mechanical torque is shown in Figure 8 and the response to a dip in the grid voltage in Figure 9. Only very small differences between the responses in the abc and the dq0 reference frame can be observed from these figures. One should be aware that the high rotor currents caused by the dip may destroy the converter if no measures are taken. The simulation time for the dq0 model is about 100 times shorter than for the abc model.

In the abc model the switching operation of the power electronic converters is not taken into consideration. A comparison has been made between the behaviour of a converter in the dq0 reference frame and a complete IGBT converter that also takes into account the switching operation of all switches. The IGBT converter that has been used is obtained from the SimPower Systems Blockset of Matlab. Again the behaviour during a dip in the grid voltage has been simulated. The d-axis current of the converter is shown for both models in Figure 10. It can be seen that, except for the high-frequency 'noise' due to the switching operation of the IGBT converter, the response to the dip is almost the same. The response is more dependent on the parameters of the converter controller than on the type of model.²⁵

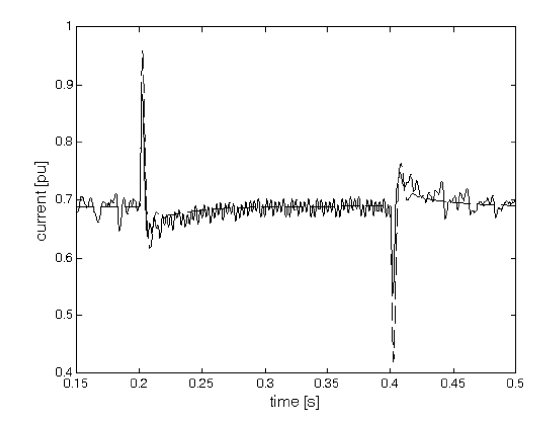


Figure 10. Response of d-axis converter current to a dip in grid voltage for reference IGBT model (full line) and dq0 model (broken line)

Other Models

Introduction

To simulate the dynamic behaviour of wind farms, not only models of the electrical system are required, but also dynamic models of the wind and the wind turbine (including the generator). The description of the wind and turbine models will be brief, as they are not the focus of this article. A more detailed description can be found in e.g. Reference 33.

Wind model

To evaluate the dynamic behaviour of wind turbines and wind farms, the short-term variation of the wind has to be known. Since wind speed variation is a statistically determined phenomenon, a wind model is needed that will calculate a realization of the stochastically changing wind speed in time. The objective of wind modelling in this type of problem is to generate a single-point wind speed realization, which gives instantaneous aerodynamic torque values that are statistically equivalent to the values experienced by the rotor of the modelled turbine. Furthermore, the wind speed averaged over the turbine rotor has to be determined, including variations caused by the passing of the blades through the inhomogeneous wind field over the rotor area. This inhomogeneous wind field is caused by turbulence, wind shear and tower shadow.³⁴ When a power measurement of a turbine is observed, the effect of the wind field inhomogeneity can most clearly be seen by regular changes in power with a frequency of the number of blades times the turbine's rotational frequency, often called *nP*. The wind model aims at a realistic representation of this effect.

The effect of wind speed variations on the aerodynamic torque is determined by the $C_p(\lambda, p)$ pitch angle) curves and for a given rotor diameter. This implies that a realization depends not only on the statistical properties of the wind but also on the size and aerodynamic properties of the turbine rotor. The method employed makes use of the auto power spectral density (APSD) of the longitudinal wind speed changes at a single point.³⁴

Turbine model

In addition to the already discussed generator and converter models, the turbine model consists of submodels for:

- aerodynamic behaviour of the rotor;
- rotating mechanical system (drive train);
- tower (i.e. motion of the tower top);
- power limitation by pitch control or stall.

The mechanical model for the turbine rotor, low- and high-speed shaft, gearbox and generator rotor is a two-mass/spring/damper model. The torque of the gearbox and generator on the nacelle is determined, since it interacts with the tower sideways motion. The simple tower model consists of a mass/spring/damper model for the translation of the tower top in two directions: front–aft (nodding) and sideways (naying). This is not sufficient if tower top rotation has to be modelled as well. In that case a lumped parameter model for rotation is used, consisting of a number of mass/spring/damper models in series.

The variable speed turbine includes two control loops: the turbine aerodynamic power is limited by pitch control and the electrical power is controlled to maximize energy production (optimal lambda control). This requires additional component models (sensor and actuator models) and the design of two controllers. How to design controllers for wind turbines can be found in Reference 34.

Conclusion

Dynamic models of offshore wind farms have been developed based on individual turbine models. The models include aerodynamic aspects and mechanical details of the turbine, the electrical system of the turbine, the cable connections inside the farm and the connection to the substation onshore. These models present a powerful tool for the investigation of wind farm dynamics and wind farm—grid interaction and for the development and optimization of wind farm controllers.

The electrical systems modelled in the wind farms are:

- the directly coupled induction generator (IG);
- the cluster-coupled induction generator (CC);
- the doubly-fed induction generator (DFIG);
- the permanent magnet generator with full converter (PM).

The turbines modelled in the wind farms are:

- the constant speed stall turbine (CSS);
- the variable speed pitch turbine (VSP).

A simplified grid model has been included to enable simulation of wind farm—grid interaction. All electrical models, including the models of cables and transformers and the grid model, are based on the Park transformation to increase computational speed in quasi-steady state conditions. For single turbines the simulation time is reduced by a factor of 100. All models have been implemented in Simulink to ensure full control over the details by the user and to have a powerful graphical interface. Simulink makes modification and extension of the wind farm models very easy and efficient.

The wind farm models can be used to develop wind farm control, to investigate dynamic interaction within the farm and between wind farm and grid and also to study wind farm response to wind gusts and grid faults. These applications are demonstrated in a number of case studies in Part 2 of this article.

Acknowledgements

The presented work is partially funded by the Dutch Agency for Energy and Environment (NOVEM) and partly by the Ministry of Economic Affairs of The Netherlands.

References

1. Slootweg JG, Polinder H, Kling WL. Dynamic modelling of a wind turbine with doubly fed induction generator. *Proceedings of 2001 IEEE Power Engineering Society Summer Meeting*, 2002;644–649.

- 2. Slootweg JG, Kling WL. Modeling of large wind farms in power system simulations. *Proceedings of 2002 IEEE Power Engineering Society Summer Meeting*, 2002; 503–508.
- 3. Jansen CPJ, de Groot RACT. Aansluiting van 6000 MW offshore windvermogen op het Nederlandse elektriciteitsnet. Deel 2: Net op land. *Technical Report 40330050-TDC 03-37074B*, Kema, 2003.
- 4. Pierik JTG, Montero Quiros JC, van Engelen TG, Winkelaar D, Sancho Chaves R. Costa Rica grid feed-in study: effect of wind power on grid frequency. *Technical Report ECN-CX-03-080*, Petten, 2003.
- 5. Slootweg JG. Wind power: modelling and impact on power system dynamics. *PhD Thesis*, TU Delft, 2003.
- Akhmatov V. Analysis of dynamic behaviour of electric power systems with large amount of wind power. PhD Thesis, Oersted, 2003.
- 7. Sorensen P, Hansen A, Janosi L, Bech J, Bak-Jensen B. Simulation of interaction between wind farm and power system. *Report Riso-R-1281 (EN)*, Riso National Laboratory, Roskilde, 2001.
- 8. Akhmatov V. Modelling of variable-speed wind turbines with doubly-fed induction generators in short-term stability investigations. *Proceedings 3rd Interactions Workshop on Transmission Networks for Offshore Wind Farms*, Stockholm, 2002; 1–23.
- 9. Ong C-H. Dynamic Simulation of Electric Machinery using Matlab/Simulink. Prentice-Hall: Upper Saddle River, NJ, 1998.
- 10. Fortescue CL, Method of symmetrical coordinates applied to the solution of polyphase networks. *Transactions of the AIEE*, 1918; **37**: 1027–1140.
- 11. Paap GC. Symmetrical components in the time domain and their application to power network calculations. *IEEE Transactions on Power Systems* 2000; **15**: 522–528.
- 12. Bachmann B, Wiesmann H. Advanced modeling of electromagnetic transients in power systems. *Proceedings of Modelica Workshop*, Lund, 2000; 93–97.
- 13. Akagi H, Kanazawa Y, Nabae A. Instantaneous reactive power compensators comprising switching devices without energy storage components. *IEEE Transactions on Industry Applications* 1984; **20**: 625–630.
- 14. Morren J, de Haan SWH, Bauer P, Pierik JTG, Bozelie J. Comparison of complete and reduced models of a wind turbine with doubly-fed induction generator. *Proceedings of 10th European Conference on Power Electronics and Applications*, Toulouse, 2003; 1–10.
- 15. Morren J, de Haan SWH, Bauer P, Pierik JTG, Bozelie J. Fast dynamic models of offshore wind farms for power system studies. *Proceedings of 4th International Workshop on Large-scale Integration of Wind Power and Transmission Networks for Offshore Wind Farms*, Billund, 2003; 1–8.
- 16. Pierik J, Morren J, de Haan S, van Engelen T, Wiggelinkhuizen E, Bozelie J. Dynamic models of wind farms for grid-integration studies. *Proceedings of Nordic Wind Power Conference* 2004, Gothenburg, 2004; 1–6.
- 17. Morren J, Pierik JTG, de Haan SWH. Fast dynamic modelling of direct-drive wind turbines. *Proceedings of PCIM Europe* 2004, Nürnberg, 2004; 1–6.
- 18. Pierik JTG, Morren J, Wiggelinkhuizen E, de Haan SWH, van Engelen TG, Bozelie J. Electrical and control aspects of offshore wind turbines II (Erao-2). Vol. 1: Dynamic models of wind farms. *Technical Report ECN-C-04-050*, ECN, Petten, 2004.
- 19. Morren J, Pierik JTG, de Haan SWH. Voltage dip ride-through of direct-drive wind turbines. *Proceedings of 39th International Universities Power Engineering Conference*, Bristol, 2004; 1–5.
- 20. Petersson A. Analysis, modelling and control of doubly-fed induction generators for wind turbines. *Technical report no. 464L*, Chalmers University, Göteborg, 2003.
- 21. Achilles S, Pöller M. Direct drive synchronous machine models for stability assessment of wind farms. *Proceedings of 4th International Workshop on Large-Scale Integration of Wind Power and Transmission Networks for Offshore Wind Farms*, Billund, 2003; 1–9.
- 22. Schiemenz I, Stiebler M. Control of a permanent magnet synchronous generator used in a variable speed wind energy system. *Proceedings of IEEE Electrical Machines and Drives Conference*, 2001; 872–877.
- 23. Ziogas PD, Wiechmann EP, Stefanović VR. A computer aided analysis and design approach for static voltage source inverters. *IEEE Transaction on Industry Applications*, 1985; **21**: 1234–1241.
- 24. Mohan N, Undeland TM, Robbins WP. Power Electronics—Converters, Applications and Design. Wiley: New York 1995.
- 25. Morren J, de Haan SWH, Ferreira JA. Model reduction and control of electronic interfaces of voltage dip proof DG units. *Proceedings of 2004 IEEE Power Engineering Society General Meeting*, Denver, CO, 2004; 2168–2173.
- 26. Morren J, de Haan SWH, Bauer P, Pierik JTG, Bozelie J. Comparison of complete and reduced models of a wind turbine with doubly-fed induction generator. *Proceedings of 10th European Conference on Power Electronics and Applications*, Toulouse, 2003; 1–10.
- 27. Harnefors L, Nee H-P. Model-based current control of AC machines using the internal model control method. *IEEE Transactions on Industry Applications* 1998; **34**: 133–141.
- 28. Grainger JJ, Stevenson WJ, Jr., Power System Analysis. McGraw-Hill: New York, 1994.
- 29. Das JC. Power System Analysis—Short Circuit Load Flow and Harmonics, Marcel Dekker: New York, 2002.
- 30. Anderson PM, Fouad AA. Power System Control and Stability. Iowa State University Press: Ames, IA, 1977.

31. Dittrich A, Stoev A. Grid voltage fault proof doubly-fed induction generator system. *Proceedings of 10th European Conference on Power Electronics and Applications*, Toulouse, 2003; 1–10.

- 32. Serban I, Blaabjerg F, Boldea I, Chen Z. A study of the doubly-fed wind power generator under power system faults. *Proceedings of 10th European conference on Power Electronics and applications*, Toulouse, 2003; 1–10.
- 33. Freris LL. Wind Energy Conversion Systems. Prentice-Hall: Upper Saddle River, NJ, 1990.
- 34. van Engelen TG, van der Hooft EL, Schaak P. Ontwerpgereedschappen voor de regeling van windturbines. *Technical Report* ECN ECN-C-03-133, ECN, Petten, December 2003.

Grid interaction of Offshore Wind Farms. Part 2. Case Study Simulations

Johan Morren, Jan T.G. Pierik, Sjoerd W.H. de Haan, Jan Bozelie.

Article Wind Energy 2005, 8: 279-293 (John Wiley & Sons Ltd.).



Grid Interaction of Offshore Wind Farms. Part 2. Case Study Simulations

Johan Morren*, Electrical Power Processing, Delft University of Technology, Delft, The Netherlands Jan T. G. Pierik, Energy Research Centre of the Netherlands (ECN), Petten, The Netherlands Sjoerd W. H. de Haan, Electrical Power Processing, Delft University of Technology, Delft, The Netherlands

Jan Bozelie, (former) Neg-Micon, Bunnik, The Netherlands

Key words: dynamic modelling; electrical system;

electrical system; grid interaction; Park transformation; wind energy Owing to an increasing penetration of wind turbines and large wind farms in electrical power systems, the wind turbines start influencing the overall power system behaviour. Dynamic wind farm models for power system studies have been presented in Part 1 of the article. In this contribution, these models are applied in a number of case studies to determine the impact of wind farms on the power grid. Four turbine concepts are evaluated with respect to their grid interaction. Case studies involving normal behaviour, voltage dip behaviour, voltage control capability and behaviour during frequency deviations will be presented. Copyright © 2005 John Wiley & Sons, Ltd.

Introduction

As the penetration of wind turbines in electrical power systems increases, they begin to influence overall power system operation.^{1,2} Two aspects are of major concern. The first is that large wind farms are a source of fluctuating active and reactive power. This fluctuating power will have its impact on the power balance and on the voltage at the connection point, while central power stations have to compensate for the fluctuating power. The second concerns the response of wind farms to voltage and frequency dips. Nowadays it is common practice that farms shut down immediately after a dip. With an increasing amount of wind energy this may worsen an already existing problem in the grid.

It is essential to ensure that the grid is capable of staying within the operational limits of frequency and voltage for all foreseen combinations of wind power production and consumer loads. The interaction between the wind farms and the grid will be an important aspect in the planning of the farms. To be able to study this interaction, models for dynamic simulation of wind farms are required. Because of the large number of components in these farms, these models should enable fast simulation. This can be achieved by using models in the dq0 reference frame. In Part 1 of this contribution a description has been given of the way in which models of different electrical components in the dq0 reference frame can be obtained. Wind and turbine models are also briefly outlined in Part 1. In this Part 2 the models are used in a number of case studies that are performed to demonstrate the effectiveness of the proposed modelling method. Four different wind farm concepts have been studied in the project that is summarized in this contribution. They are based on the following turbine concepts:

E-mail: J.Morren@ewi.tudelft.nl

Contract/grant sponsor: Dutch Agency for Energy and Environment (NOVEM). Contract/grant sponsor: Ministry of Economic Affairs of The Netherlands.

^{*}Correspondence to: J. Morren, Electrical Power Processing, Delft University of Technology, Mekelweg 4, NL-2628 CD Delft, The Netherlands

- constant speed stall turbine with directly coupled induction generator (CSS-IG, reference case);
- constant speed stall turbine with cluster-controlled induction generator operating in variable speed mode (CSS-CC);
- variable speed pitch-controlled turbine with doubly-fed induction generator (VSP-DFIG);
- variable speed pitch-controlled turbine with permanent magnet synchronous generator (VSP-PM).

For each of the park concepts, one or more 'events' are evaluated in a case study.

The contribution starts with simulation results of the normal operation of a wind farm with induction generators. It continues with an evaluation of the voltage dip behaviour of the permanent magnet generator. This is followed by the voltage control capabilities of the doubly-fed induction generator. The frequency dip response of cluster-coupled induction machines and the contribution of permanent magnet wind turbines to frequency control conclude this contribution.

Simulation Set-up

All case study simulations have been done in Simulink®, a Matlab-based platform that is widely used for dynamic simulation. The near-shore wind park (NSW park) that is planned to be built in the North Sea about 12 km from the Dutch coast will be used as a case study. The wind farm will consist of 36 turbines with a 2.75 MVA doubly-fed induction generator. The park layout is shown in Figure 1. For convenience, only one string of 12 turbines is simulated. Each of the turbines is connected to the 34 kV grid by a three-winding transformer with a nominal power of 2.5 MW. This transformer has a 960 V winding connected to the stator and a 690 V winding to the rotor via a frequency converter. The wind farm is connected to the 150 kV grid via a transformer with a nominal power of 125 MVA.

Normal Behaviour of Wind Farm with Induction Machines

The response of one string of the wind farm to a gust in the wind speed has been simulated. The gusts are important for the grid behaviour of the park, as this will lead to a gust in the output power of the park and will thus cause changes in the voltage at the connection point. The reactive power settings of the turbines are kept at zero during the simulation.

It is assumed that the gust travels through the farm with a relatively high speed. Normally the average wind speed of the gust would be taken as the gust travelling speed; in the case study simulation this was increased to increase the effect of the gust and to reduce simulation time. It is assumed that the time between affecting two turbines will be 5 s. The rotor effective wind speed at the first turbine that experiences the gust is shown in Figure 2. The wind speed before the gust is about 5 m s⁻¹. The wind speed increases to 20 m s⁻¹ during the gust.

The increasing wind speed will cause an increasing output power of the turbine. The output power of the first turbine is shown in Figure 3. The output power of the whole first string of the wind farm is shown in Figure 4. The large change in output power of the wind farm will affect the voltage of the 150 kV grid at the point of connection. The voltage at the park side of the 150 kV transformer is shown in Figure 5. Be aware that the change in output voltage of the wind farm shown in Figure 5 is only due to one string. The resulting change in output voltage due to the whole park will be significantly higher.

Voltage Dip Behaviour of Wind Turbines with Permanent Magnet Generator

Introduction

The contribution of power from wind turbines to the total energy production has so far mostly been small as compared with the power supplied by the large centralized power plants. Automatic disconnection of wind tur-

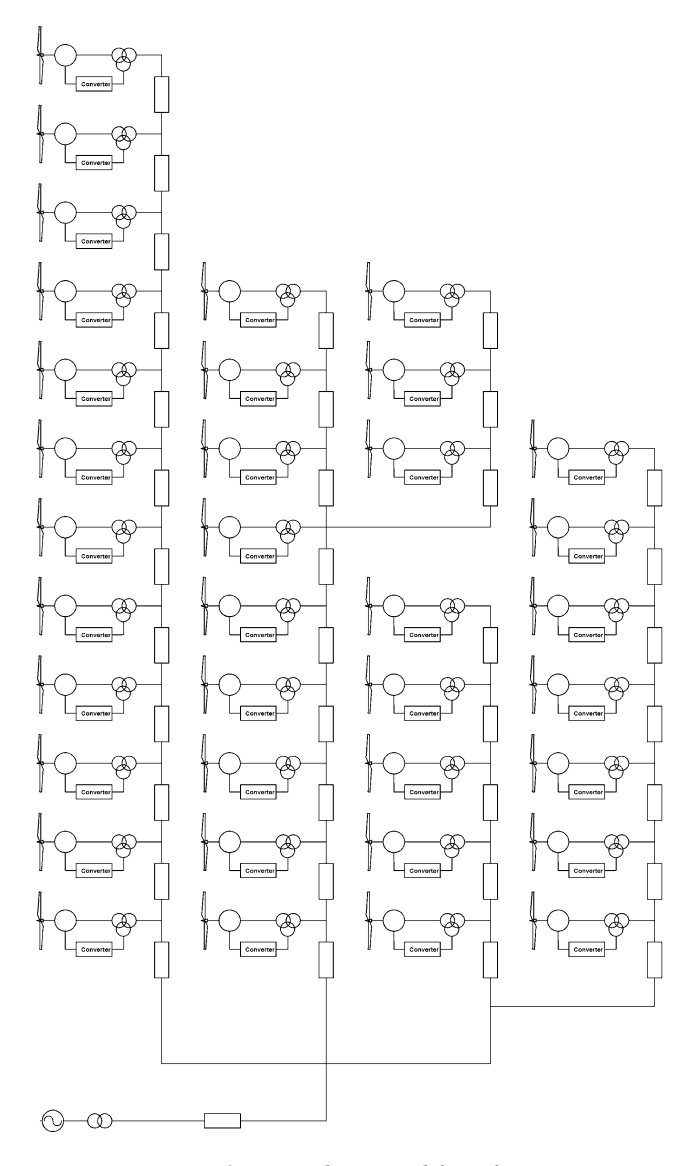


Figure 1. Near-shore wind farm layout

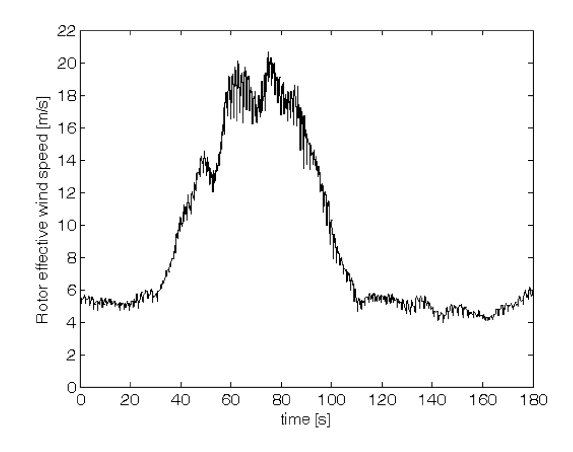


Figure 2. Gust in wind speed

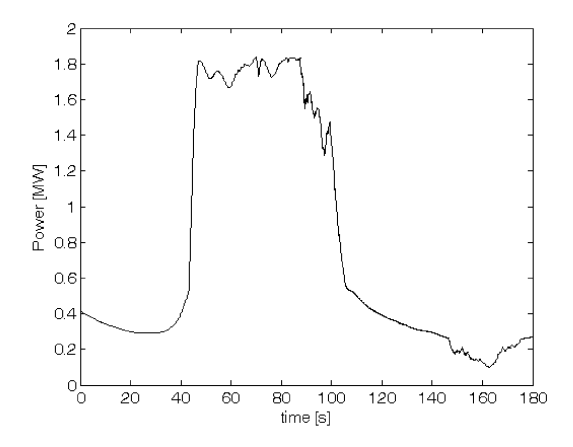


Figure 3. Output power of first wind turbine

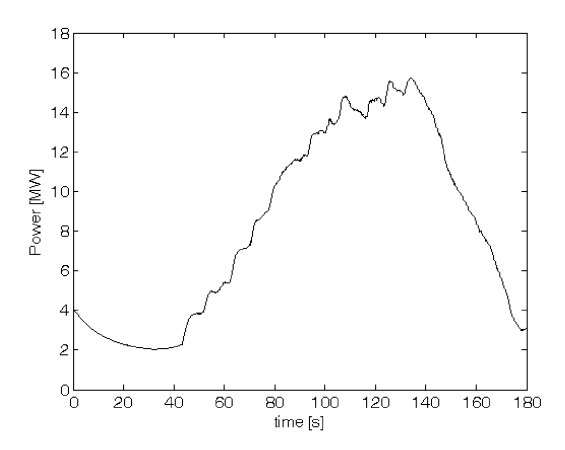


Figure 4. Output power of one string of the wind farm

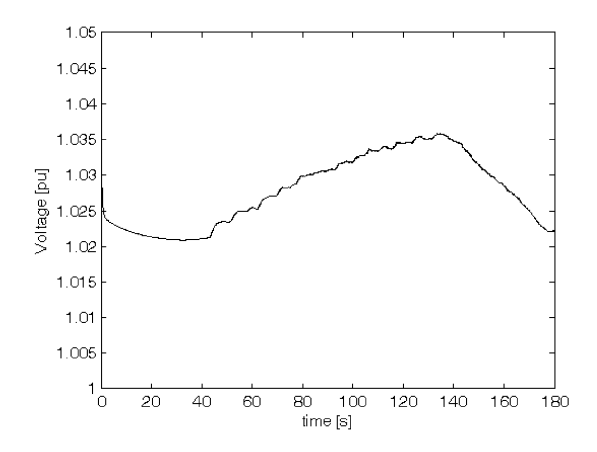


Figure 5. Output voltage of wind farm

bines in the case of a grid disturbance, as required by many grid operators, ^{5,6} is not a problem in this case. When the amount of wind energy is increasing, the disconnection of many turbines could lead to a lack of power and to instability of the local grid.⁷

To allow wind farm connection to the grid, a number of grid operators require voltage dip ride-through capability already, especially in places where wind turbines provide a significant part of the total power supply.

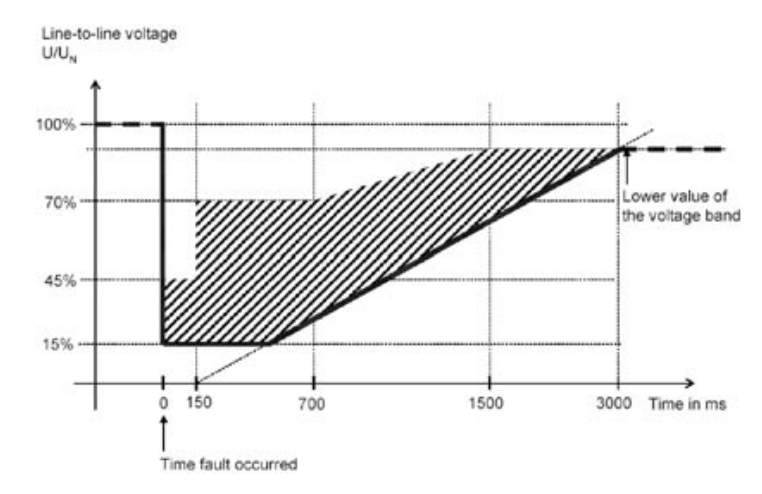


Figure 6. Voltage dips that wind turbines should be able to handle without disconnection (E.ON Netz requirements)

Examples are Denmark⁸ and parts of Northern Germany.⁹ The requirements concerning immunity to voltage dips as prescribed by E.ON Netz, a grid operator in Northern Germany, are shown in Figure 6. Only when the grid voltage drops below the curve (in duration or voltage level) is the turbine allowed to disconnect. There are large differences between the requirements in different countries. E.ON requires that wind turbines stay connected during voltage dips where the voltage drops to 15% for 300 ms, whereas in Australia 0% voltage for 175 ms is required and in Denmark 25% voltage for 100 ms.¹⁰

In this section the voltage dip behaviour of a variable speed wind turbine with permanent magnet generator will be investigated. The protection and voltage dip behaviour of a variable speed wind turbine with doubly-fed induction generator are described in Reference 11. The protection is based on a crowbar in the rotor circuit to protect the converter by providing a bypass for the rotor currents during a disturbance.

Simulation set-up

The voltage dip is assumed to occur somewhere in the 150 kV transmission grid. The dip results in a reduced voltage level at the 34/150 kV transformer. During the simulations the grid has been modelled as an ideal voltage source. Only one turbine has been used during the simulations, as during voltage dips the behaviour of the farm is primarily determined by the behaviour of the individual turbines. The output current of the turbine transformer has been multiplied by a factor 6, as the behaviour of the cables and transformer will also depend on the current level. When this current level is too low, the behaviour may be incorrect. The simulation set-up is shown in Figure 7. From left to right the turbine, the turbine transformer, the 34 kV cable, the 34/150 kV transformer and the 150 kV ideal grid are shown. The parameters represent the NSW park with only one turbine connected. All simulations have been done with the turbine operating at nominal power.

The wind turbine concept that has been used is the direct drive, variable speed turbine with permanent magnet synchronous generator. This turbine has a full back-to-back converter connected between the stator and the grid. The voltage dip behaviour of this turbine can thus mainly be considered as the voltage dip behaviour of the grid-side converter.

A detailed description of the converter model that has been used is given in Reference 12. When the grid voltage drops, the converter should increase the grid current to be able to supply the same amount of power to the grid. The current of the converter is limited, however, owing to the limited thermal capacity of the semi-conductor switches. Therefore the power that is delivered by the wind turbine to the converter should also be limited, because otherwise the DC-link voltage will increase too much. A protection scheme is implemented in the model. The converter currents and the DC-link voltage are limited. When necessary, the electrical torque setpoint of the converter that is connected to the permanent magnet generator is reduced. As a result the turbine will speed up. This increase in rotational speed is limited by the pitch controller of the turbine.

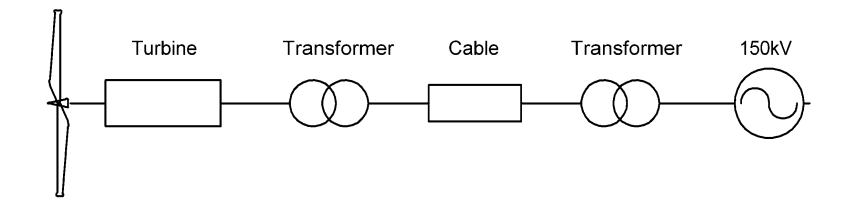


Figure 7. Simulation set-up for voltage dip simulations

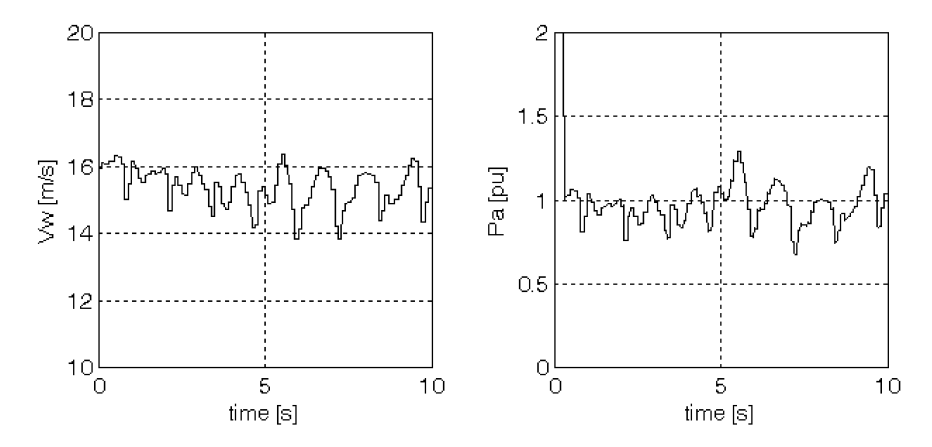


Figure 8. Rotor average wind speed and aerodynamic power of PM during 50%/0.5 s dip

Simulation results

A 50%/0.5 s dip in the voltage has been applied. The rotor average wind speed during the dip is about 15 m s⁻¹. The wind turbine then operates at nominal power. The rotor average wind speed $V_{\rm w}$ and the aerodynamic power in the wind, P_a , are shown in Figure 8. Owing to the limited thermal capacity of power electronic components, the current should not become too high for longer times. Therefore the current of the converter should be limited when the fault occurs. At the moment the fault occurs, the grid voltage drops and the current of the grid-side converter has to increase when the same power as before the fault should be supplied to the grid. The current will be limited, however, to avoid thermal breakdown of the converter. As a result the DClink voltage will increase as long as the power from the turbine is not decreased. Therefore also the generator controller will decrease its setpoint. This can be seen from the power curve in Figure 9. When the power is decreased, also the electrical torque will decrease, see again Figure 9. As a result of the decreasing electrical torque the turbine will speed up, at least as long as the aerodymical torque remains the same. The increase in rotational speed w_m is shown in Figure 9. At the moment the speed increases, the pitch angle controller has to react to limit the speed increase. In Figure 9 it can be seen that there is first a short peak in the rotational speed as the dip occurs. Afterwards the rotational speed is slightly increasing. A dip of 0.5 s is too short, however, to get a significant increase in speed. Almost no pitch controller action has been noted. When the dip persists for a longer time, the speed may increase, however, and the pitch angle controller may not be fast enough to limit the speed increase.

The DC-link voltage is shown in Figure 10. Note that the voltage is practically constant, because the switching operation of the converters has not been modelled. Otherwise there would be a high-frequency ripple on the voltage. The DC-link controller reacts fast enough to control the voltage. In reality it will not always be necessary to keep the DC-link at the pre-fault voltage. A small increase or decrease in voltage will be allowed. In Figure 11 the voltage and current of the grid-side converter are shown. It can be seen that the current is limited (after a controller overshoot) to about 1 pu. At the moment the dip is cleared, the current drops to about half the nominal current. It takes some time before the converter adjusts the current to the value before the dip occurred.

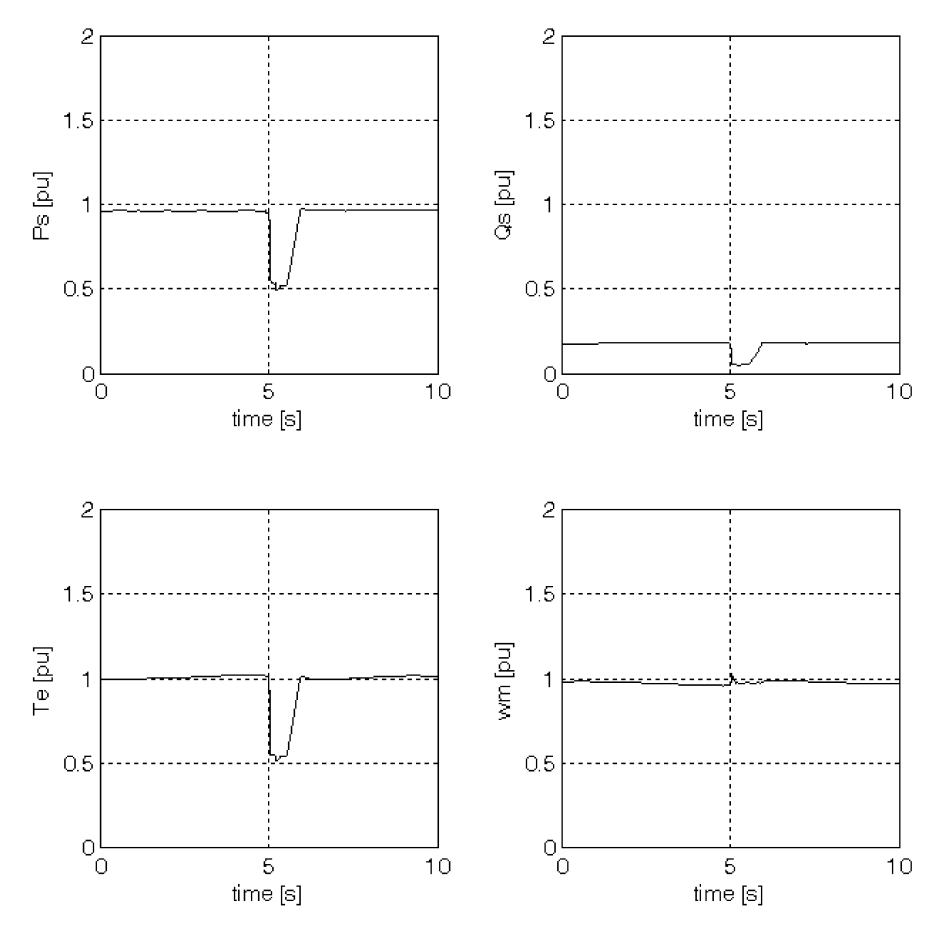


Figure 9. Active power, reactive power, electric torque and slip of PM during 50%/0.5 s dip

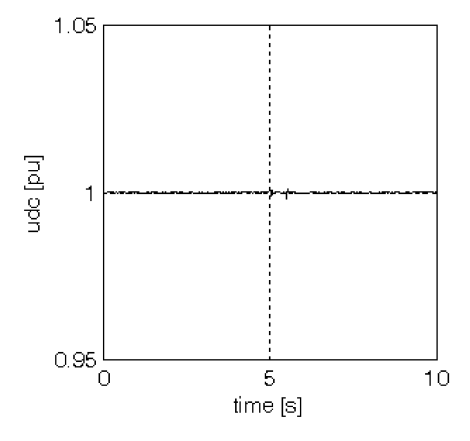


Figure 10. DC-link voltage of PM during 50%/0.5 s dip

Final remarks

In general it can be concluded that voltage dip ride-through of direct drive wind turbines with full converter connection to the grid does not present a problem. To limit the currents in the converter, the power of the permanent magnet generator should be limited when the grid voltage drops. That this is possible can be seen from Figure 9. To avoid overspeeding of the turbine, the pitch controller should limit the rotational speed of the turbine. From the figures it can be seen that the rotational speed of the turbine is limited at 1 pu.

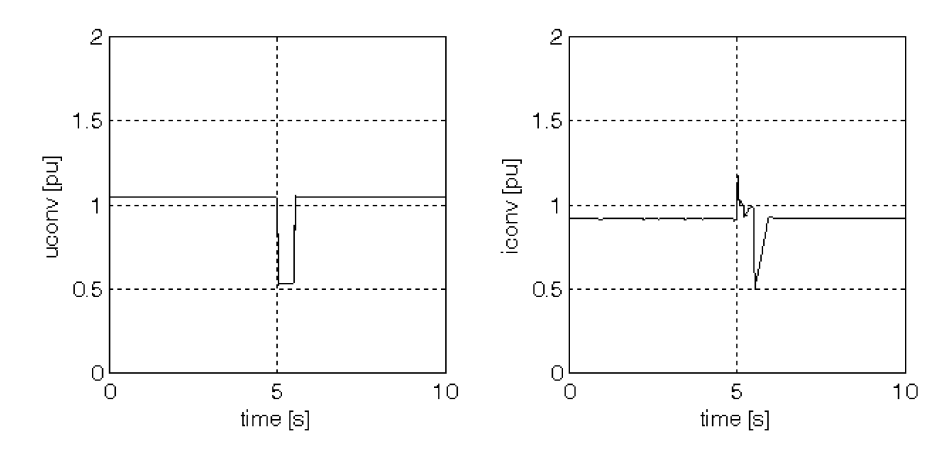


Figure 11. Voltage and current of grid-side converter of PM during 50%/0.5 s dip

At the starting point of the dip and during grid voltage recovery, small peaks can be seen in the current of the grid-side converter. They are due to the limited bandwidth of the current controller. The converter will be able to cope with these currents for a short time.

Voltage Control Contribution of Wind Farms with Doubly-fed Induction Generators *Introduction*

Nowadays the total amount of wind power that is connected to the grid is still rather small. Therefore in most cases the contribution of wind power to voltage deviations is small and node voltages remain within the allowed deviations from their nominal value. With regard to voltage deviations and voltage control, the increase in wind power capacity, especially of large offshore installations, has two important consequences. The first consequence is that, when the total power of the wind farm increases, the contribution from wind to the voltage deviations at the connection point will increase. The second is related to the way in which voltage control nowadays is implemented. The large centralized power plants take care of the voltage control in the grid. The rest of the grid is passive. Transformer taps are not adjusted dynamically but have a number of positions, so they cannot control dynamic voltage variations. When wind power increasingly replaces power from conventional generators, it will be more difficult to control the node voltages adequately with conventional power stations only, and it will become necessary that wind power also makes a contribution. In fact the synchronous generators of the centralized power stations control the voltage by supplying reactive power to the grid or consuming reactive power from the grid. Large wind farms should be operated in the same way.

Wind turbine concepts that use a power electronic converter allow independent control of the active and reactive power output of the wind turbine. As the reactive power can be controlled independently of the active power, the wind turbine can contribute to voltage control. In this section it will be investigated how a wind farm with doubly-fed induction generators can contribute to voltage control. Reactive power is supplied to the grid according to a certain droop characteristic.

Simulation set-up

One string with 12 turbines will be used to investigate the voltage control possibilities of the wind turbines. The wind turbines are connected in a string with a 34 kV cable. The total cable length between two turbines is always 660 m. The turbines are connected to the cable via a transformer. Between the coast and the turbine that is closest to the coast is a 15 km 34 kV cable. This cable is connected to the 150 kV grid via a 34/150 kV transformer. The grid is modelled as a 200 MW synchronous machine with two consumer loads, a transformer and a cable. The synchronous machine controls the voltage at its terminals in the grid. A simplified represen-

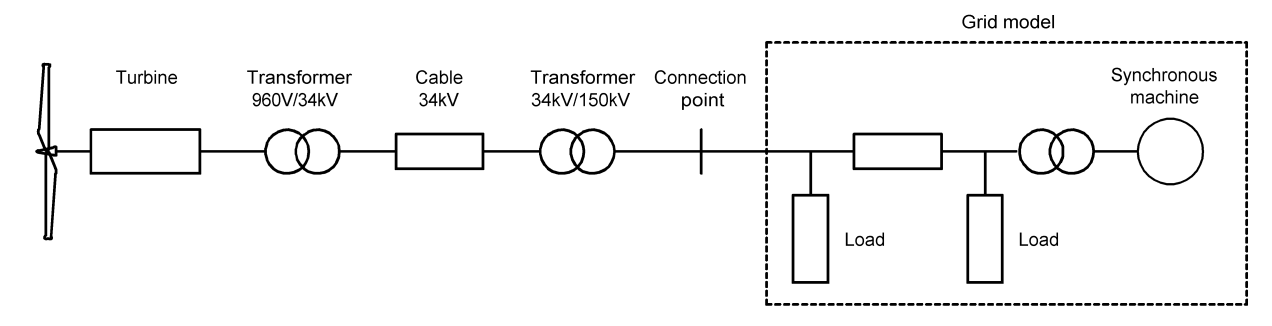


Figure 12. Simulation set-up with only one turbine shown

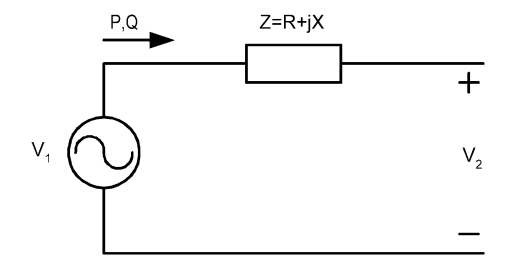


Figure 13. Source and impedance

tation of the simulation set-up is shown in Figure 12. (Only one turbine is shown, the simulations include a string of 12 turbines.)

Voltage deviations at the grid connection point (the high-voltage side of the 34/150 kV transformer) can be caused by the (varying power of the) wind farm, by load changes or by faults in the grid. Controlling the reactive power in the wind farm can compensate for these voltage deviations.

When the layout of the park is known, the voltage level and the active and reactive power at the connection point can be determined from the wind farm layout. Consider the single-line diagram in Figure 13, where a source supplying active and reactive power and an impedance are shown. As long as the angle δ between V_1 and V_2 is small, the voltage drop is approximately given by V_1

$$\Delta V \approx \frac{RP + QX}{V_1^*} \tag{1}$$

When the voltage V_1 is the voltage at the terminal of the wind turbine and Z = R + jX is the total impedance between the turbine and the connection point (transformers and cables), the controller of the wind turbine can calculate the voltage difference ΔV and thus V_2 when it knows the impedance Z and the active power P and reactive power P that are supplied by the turbine. The active and reactive power at the connection point can be calculated in a similar way based on the active and reactive power supplied by the wind turbine and on the losses in the (known) impedances.

In Figure 13, V_1 can be defined as the terminal voltage of the turbine and V_2 as the connection point voltage at the 150 kV side of the grid transformer. The impedance Z is given by the total impedance of the cable and the transformers.

It should be noted that the impedance Z is different for each turbine, as the cable length increases further into the park. However, as the impedance of the cable to the coast is much higher than for the cables in the park, the park cables can be neglected. This will introduce a small error, but the approximation will be good enough, as can be concluded from the simulations.

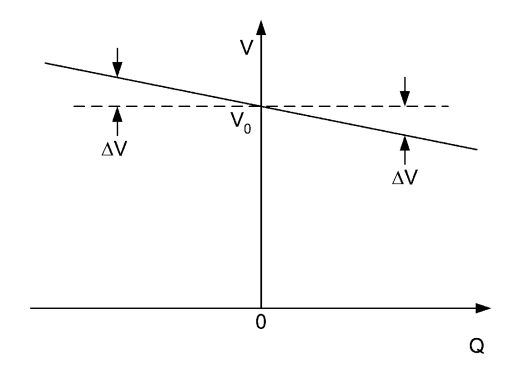


Figure 14. Droop characteristic

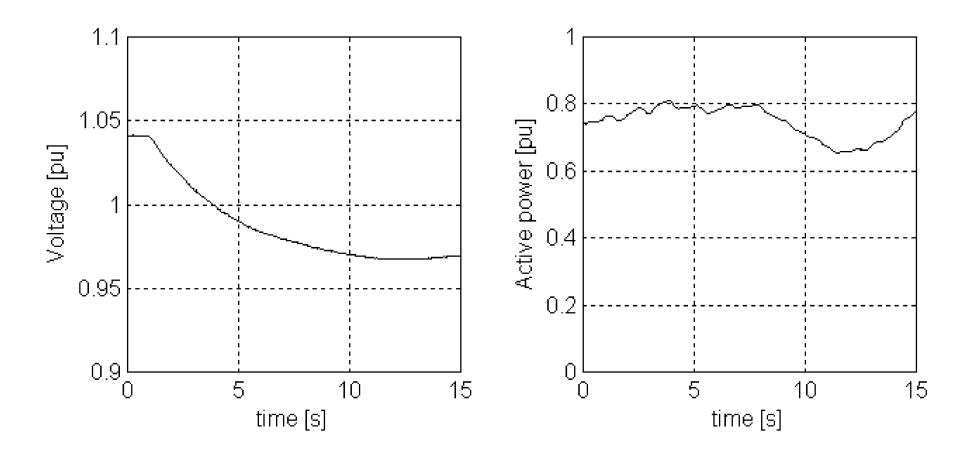


Figure 15. Voltage and active power at grid connection point

Droop characteristic control

Conventional turbines control the voltage according to a so-called droop characteristic. This droop characteristic control can be considered as a forward controller. The reactive power that is supplied to the grid depends on the voltage at the connection point. The relation between voltage and reactive power is obtained from the droop characteristic. An example of a droop characteristic is shown in Figure 14. In this section the wind farm reacts on voltage changes somewhere in the grid. Based on the grid voltage, a certain amount of reactive power is supplied to the grid or absorbed from the grid. In this way it contributes to the voltage control in the same way as is done by the large conventional power plants.

Simulation results

In the simulations that will be shown in this subsection, the droop characteristic control is implemented in the wind turbines. The voltage at the connection point is calculated, based on local parameters, as described in the previous subsection. Based on this voltage, a certain amount of reactive power is supplied to or consumed from the grid. Figure 15 shows the voltage and the active power at the grid connection point. Figure 16 shows the ratio between the voltage at the connection point and the reactive power that is supplied to the grid. In this way a wind farm behaves like a conventional power plant in its contribution to voltage control.

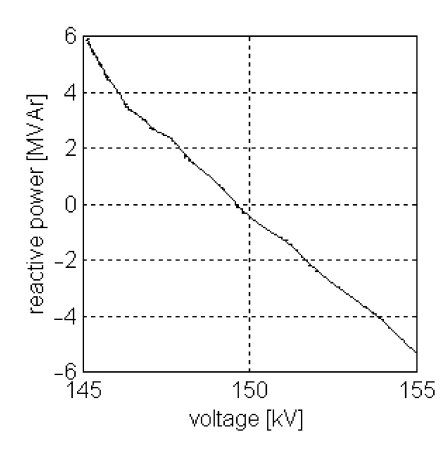


Figure 16. Voltage-reactive power characteristic

Frequency Dip Behaviour of a Variable Speed Stall Cluster-Controlled Wind Farm

Introduction

Although the grid frequency in the largest part of Western Europe can be considered to be practically constant, there are some locations with island grids in which considerable frequency deviations may occur. Wind farms connected to an island grid should be able to stay in operation during frequency dips and thereby support frequency recovery. In the following simulation the response of a cluster-controlled wind farm is determined. In this type of farm a number of stall-controlled turbines are connected to a single AC–DC–AC converter. The converter controls the common speed of these turbines based on a measured wind speed. In this way the turbines operate at near-optimal tip speed ratio as long as the wind speed differences between the turbines are not too big.

Simulation set-up and results

A cluster of three turbines is simulated. The grid frequency dip is simulated by a change in the frequency setpoint of the synchronous machine in the grid model. At t = 10 s the setpoint is decreased to 45 Hz and at 20 s it is changed to the normal value of 50 Hz (Figure 17). This dip is significantly larger than any expected dip in a large grid, in magnitude as well as rate, since grid frequency changes take time, and corrective action will be taken before this level is reached. The 5 Hz dip has been chosen as a worst-case scenario and to demonstrate the wind farm behaviour more clearly.

The total combined consumer load of P_{load1} and P_{load2} is 73 MW, which is supplied partly by the synchronous machine (of the grid model) and partly by the wind farm, see Figure 17. The frequency dip causes a voltage dip u_{grid} , which is counteracted by the synchronous machine voltage controller, dU_{fd} . The initial voltage dip is of the same magnitude as the frequency dip, about 10%.

The grid-side converter voltages v_{dcg} and v_{qcg} follow the grid voltage dip (Figure 18). The grid-side converter d-component of the current, i_{dcg} , remains almost constant, while the q-current i_{qcg} becomes more negative. The grid-side converter power P_{conv} and reactive power Q_{conv} are not affected by the frequency dip and corresponding voltage dip. The DC voltage u_{dc} shows no effect either.

The converter effectively decouples the turbines and the grid. In spite of the frequency dip, the turbine operate as if no grid dip occurs (Figure 19): aerodynamic powers P_{a1} , P_{a2} and P_{a3} , stator currents i_{s1} , i_{s2} and i_{s3} and voltages v_{s1} , v_{s2} and v_{s3} and relative turbine speeds s_1 , s_2 and s_3 follow the changes in rotor effective wind speed.

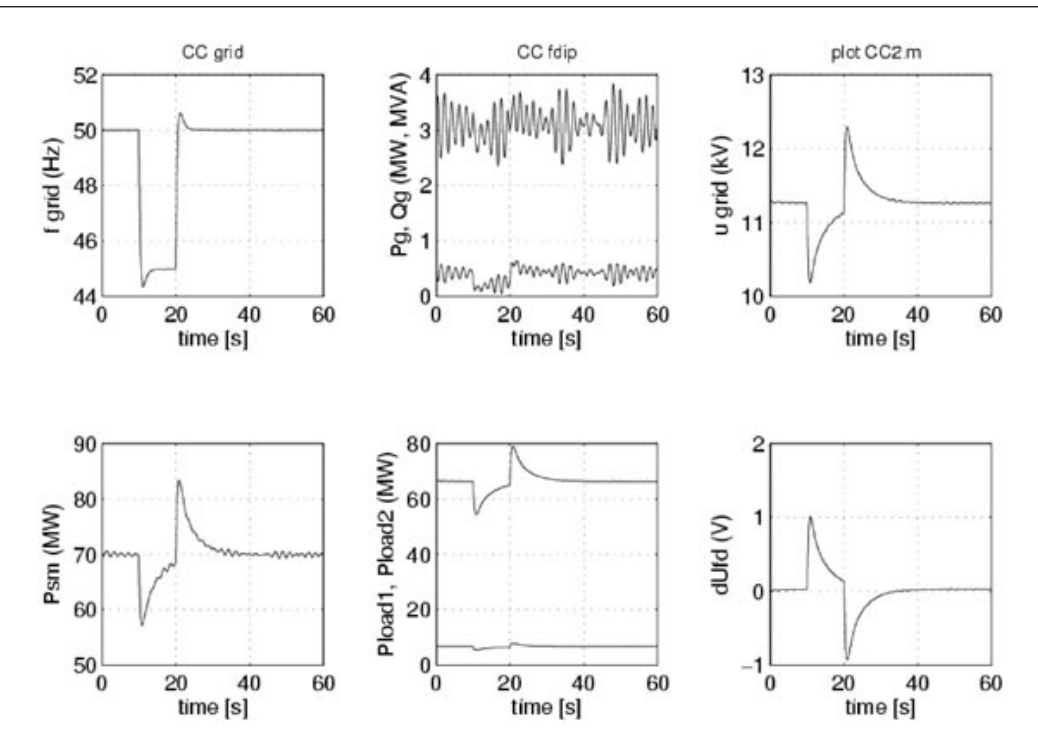


Figure 17. Response of cluster-controlled turbines to a 10% frequency dip: grid variables

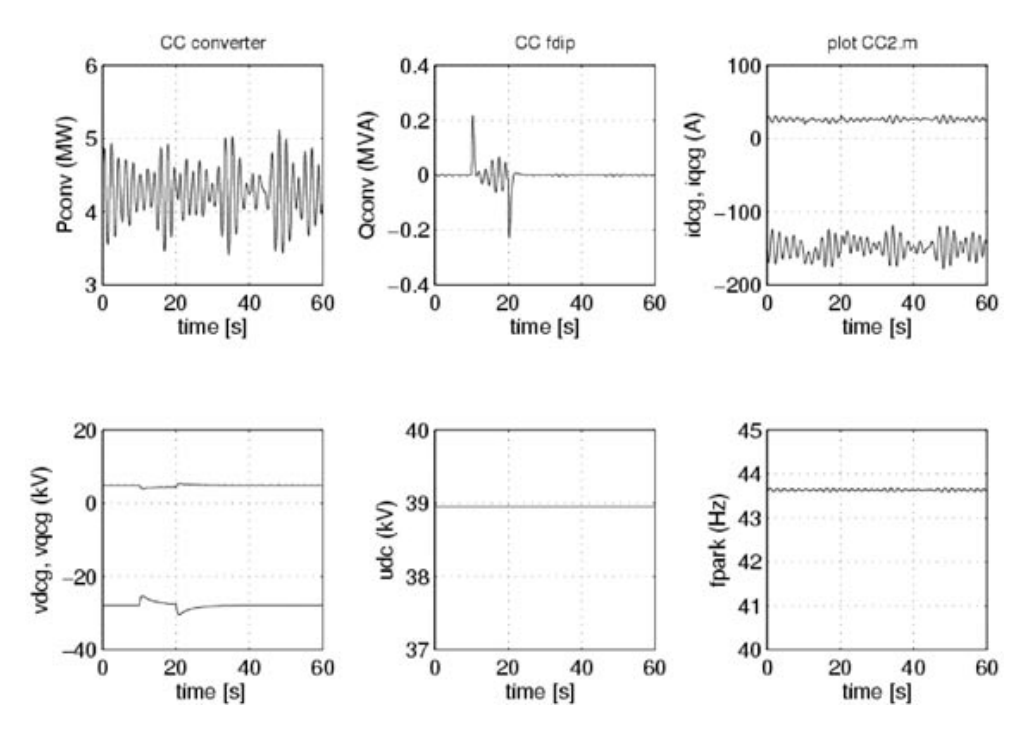


Figure 18. Response of cluster-controlled turbines to a 10% frequency dip: converter variables

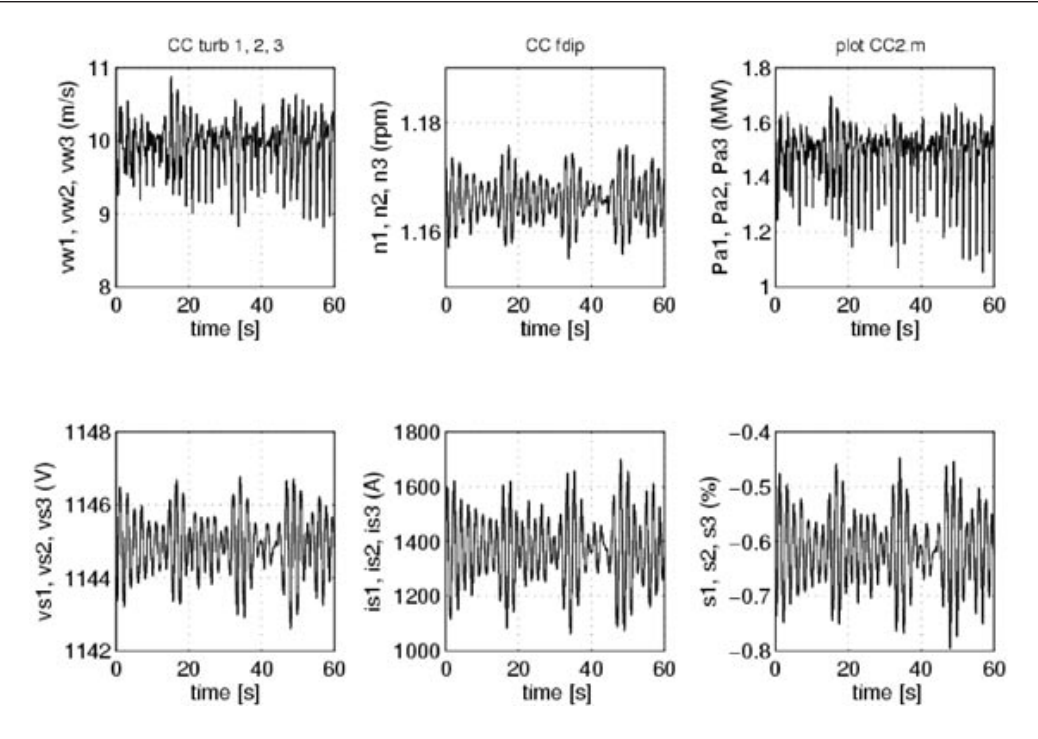


Figure 19. Response of cluster-controlled turbines to a 10% frequency dip: turbine variables

Grid Frequency Control by a Variable Speed Wind Farm with Permanent Magnet Generators

Introduction

It is not common to incorporate frequency control capability into wind farm operation. Generally, wind farm control aims at maximum power output dictated by the instantaneous wind speed. In rare cases the wind farm power is limited or a constant margin is kept to the instantaneous maximum output (sometimes called delta control). Delta control enables grid frequency support by wind power.

Simulation set-up and results

The control of a wind farm equipped with variable speed pitch-controlled turbines with a permanent magnet generator has been adapted for frequency support by implementing delta control and a control loop on frequency deviations.

In Figure 20 the power production, grid frequency and pitch angle are compared during a step in consumer power for a wind farm with and without grid frequency support. The step results in a frequency dip of about 1 Hz. The dip is corrected by the synchronous machine in the grid model, without support by the wind farm, within 4 s after the consumption increase. The recovery is faster if the wind farm supports the frequency control by reducing the pitch angle and providing a temporary increase in power. The differences are small owing to the relatively small amount of extra wind power (about 5 MW) and the relatively slow increase in the wind power. During the frequency dip the wind power initially decreases owing to the corresponding voltage dip. Compared with the reaction of the frequency controller on the synchronous generator, the wind farm needs more time to react to the dip owing to the time constant of the pitch servo. For the mechanical power supply to the synchronous machine a zero time delay was assumed. In reality the frequency recovery will be slower and the effect of assistance by the wind farm larger. The reaction can be much faster if the inertia of the rotor is used to supply more power, assuming the frequency dip is a short-time event, e.g. for starting a heavy load motor.

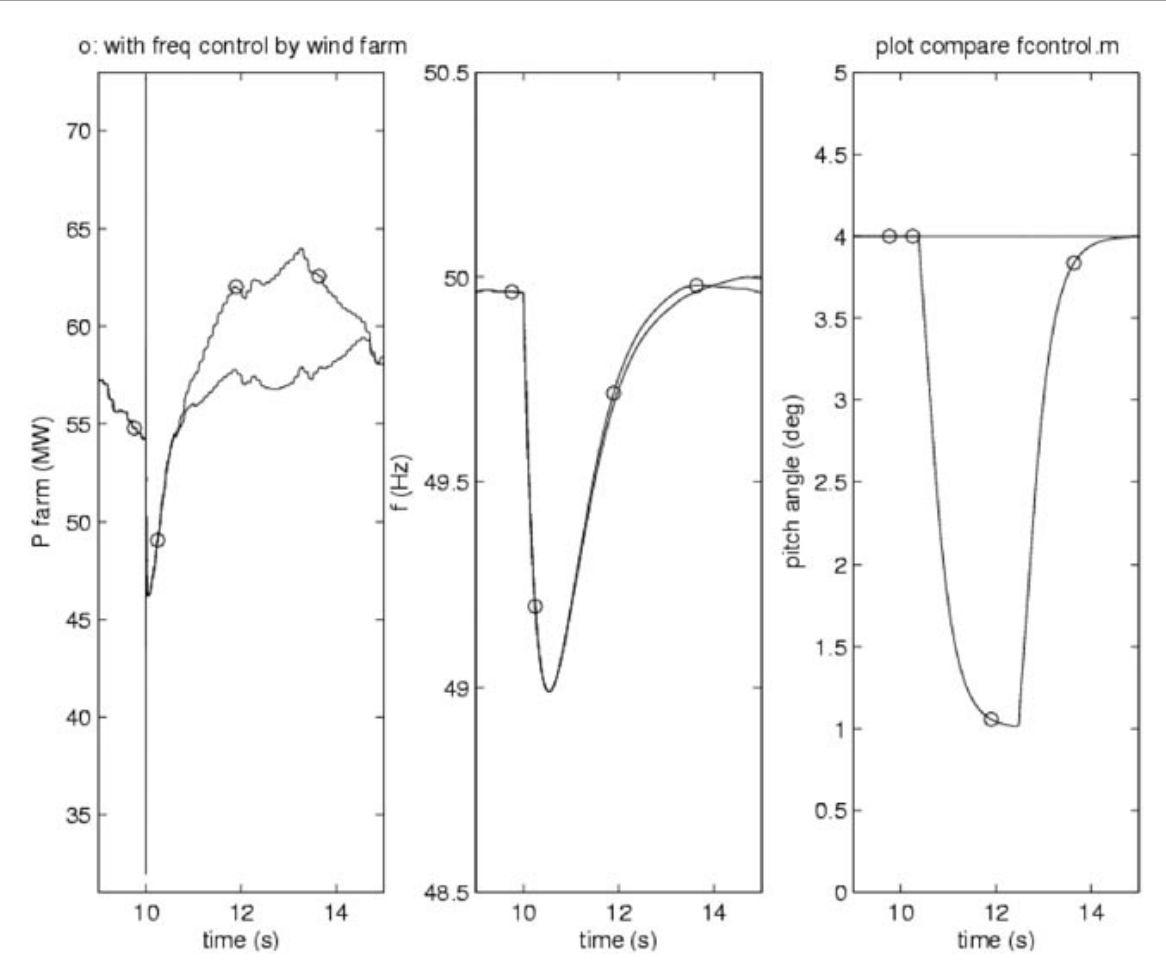


Figure 20. Variable speed pitch-controlled wind farm with PM generators and delta control with (\bigcirc) and without (\longrightarrow) frequency control support by the wind farm for a step in consumer power of about 100 MW

Conclusions

Models of wind farms, based on detailed wind turbine models as described in Part 1 of this article, have been used to investigate the dynamic behaviour and response during grid disturbances. This contribution only describes a limited number of the case studies that have been performed. More case studies can be found in Reference 15.

Gusts in the wind speed will result in large power fluctuations. The power fluctuations can cause severe voltage fluctuations in the electricity grid. This is especially true for constant speed turbines with induction machines, as they do not offer reactive power and/or voltage control possibilities.

In the variable speed pitch wind farm with permanent magnet generators (VSP-PM), all the essential parameters can be controlled. Therefore good voltage dip ride-through can be achieved. The power supplied by the generator is limited by the controllers during the dip. This is required because otherwise the current in the converter or the voltage in the DC-link becomes too high. To avoid overspeeding, the pitch controller will be activated. Owing to the short duration of the voltage dip, no significant increase in rotational speed can be noted from the simulations that have been presented.

The wind turbine concepts with converters are suitable for grid voltage control. Different voltage and reactive power control strategies are possible. In the final case, droop control has been implemented on each turbine. With this type of control the wind farm behaviour is similar to conventional power plant behaviour during voltage deviations.

The response of a wind farm to a grid frequency dip (5 Hz, 10 s) strongly depends on the presence of a converter. A full converter between wind turbine and grid decouples the turbines from the grid disturbances. The turbine itself is therefore hardly effected by a frequency dip. This has been shown for a set of cluster-coupled induction machines.

Both variable speed pitch wind farms (with doubly-fed induction generator and permanent magnet generator) can be equipped with grid frequency control support, which has been demonstrated for wind turbines with a permanent magnet generator. Since permanent frequency control capability implies maintaining a power margin, called delta control, this option may not be cost-efficient.

Acknowledgements

The presented work is partially funded by the Dutch Agency for Energy and Environment (NOVEM) and partly by the Ministry of Economic Affairs of The Netherlands.

References

- 1. Slootweg JG, Polinder H, Kling WL. Dynamic modellings of a wind turbine with doubly fed induction generator. *Proceedings of 2001 IEEE Power Engineering Society Summer Meeting*, 2001; 644–649.
- Slootweg JG, Kling WL. Modeling of large wind farms in power system simulations. Proceedings of 2002 IEEE Power Engineering Society Summer Meeting, 2002; 503–508.
- 3. Pierik JTG, Montero Quiros JC, van Engelen TG, Winkelaar D, Sancho Chaves R. Costa Rica grid feed-in study: effect of wind power on grid frequency. *Technical Report ECN-CX-03-080*, ECN, Petten, 2003.
- 4. Jansen CPJ, de Groot RACT. Aansluiting van 6000 MW offshore windvermogen op het Nederlandse elektriciteitsnet. Deel 2: Net op land. *Technical Report 40330050-TDC 03-37074B*, Kema, 2003.
- 5. Audring D, Balzer P. Operating stationary fuel cells on power systems and micro-grids. *Proceedings of 2003 IEEE Bologna Power Tech Conference*, 2003; 1–6.
- Gatta FM, Iliceto F, Lauria S, Masato P. Modelling and computer simulation of dispersed generation in distribution networks. Measures to prevent disconnection during system disturbances. *Proceedings of 2003 IEEE Bologna Power Tech Conference*, 2003; 1–10.
- 7. Slootweg JG, Kling WL. Modelling and analysing impacts of wind power on transient stability of power systems. *Wind Engineering*, 2002; **26**: 3–20. DOI: 10.1260/030952402320775254.
- 8. Rasmussen C, Jorgensen P, Havsager J. Integration of wind power in the grid in Eastern Denmark. *Proceedings of 4th International Workshop on Large-scale Integration of Wind Power and Transmission Networks for Offshore Wind Farms*, Billund, 2003; 1–6.
- 9. E.ON Netz. GmbH, Bayreuth, Germany. Ergänzede Netzanschlussregeln für Windenergieanlagen. 2001.
- 10. Bolik SM. Grid requirements challenges for wind turbines. *Proceedings of 4th International Workshop on Large-scale Integration of Wind Power and Transmission Networks for Offshore Wind Farms*, Billund, 2003; 1–5.
- 11. Morren J, de Haan SWH. Ride through of wind turbines with doubly-fed induction generator during a voltage dip. *IEEE Transactions on Energy Conversion*, 2005; **20**(2): 1–7.
- 12. Morren J, Pierik JTG, de Haan SWH. Voltage dip ride-through of direct-drive wind turbines. *Proceedings of 39th International Universities Power Engineering Conference*, Bristol, 2004; 1–5.
- 13. Slootweg JG, de Haan SWH, Polinder H, Kling WL. Voltage control methods with grid connected wind turbines: a tutorial review. *Wind Engineering* 2001; **25**: 353–365. DOI: 10.1260/030952401760217157.
- 14. Miller TJE. Reactive Power Control in Electric Systems. Wiley: New York, 1982.
- 15. Pierik JTG, Morren J. Wiggelinkhuizen E, de Haan SWH, van Engelen TG, Bozelie J. Electrical and control aspects of offshore wind turbines II (Erao-2). Vol. 2: Offshore wind farm case studies. *Technical Report ECN-C-04-051*, ECN, Petten, 2004.

Fast Dynamic Modelling of Direct-Drive Wind Turbines

J. Morren, J.T.G. Pierik, Sj. de Haan.

PCIM 2004 Conference, Nuremberg.

Fast Dynamic Modelling of Direct-Drive Wind Turbines

Johan Morren¹⁾, Jan T.G. Pierik²⁾ and Sjoerd W.H. de Haan¹⁾

¹⁾Delft University of Technology, The Netherlands ²⁾Energy Research Centre of the Netherlands (ECN) J.Morren@EWI.TUDelft.nl

Abstract--In this contribution a dynamic model of a direct-drive wind turbine with permanent magnet generator is presented. While deriving the model, special attention has been paid to increasing the computational speed of the simulations. An important increase in speed is realised by the use of the *dq0* transformation (Park transformation).

A description is given of the way in which the dq0 models can be derived. The usefulness of the model in dynamic simulations is shown by a case study.

Index Terms—Dynamic modelling, Park Transformation, Wind Energy

I. INTRODUCTION

Atendency to increase the amount of electricity generated from wind can be observed [1]. As the penetration of wind turbines in electrical power systems will increase, they may begin to influence overall power system operation [2]. The behaviour of wind turbines with respect to their interaction with the grid is therefore studied at different places [3]-[6]. In order to facilitate the investigation of the impact of a wind farm on the dynamics of the power system, an adequate model of the wind turbines is required. Although personal computers become faster and faster, computational speed is still one of the limiting factors in (dynamic) simulation of power systems. One of the problems is the complexity of the models, which limits the computational speed. When reduced models are used simulation of complex systems like wind farms can be done much faster, but the results may be less accurate [7].

The Park transformation (some-times called Blondel-Park transformation [8]) is well-known from its use in electrical machinery. The electrical signals are transformed to a stationary rotating

reference frame. As this stationary frame is chosen to rotate with the grid frequency, all voltages and currents in the dq0 reference frame are constant in steady state situations. Therefore, modelling in the dq0 reference frame is expected to increase the simulation speed significantly, as a variable step-size simulation program can apply a large time step during quasi steady-state conditions.

Nowadays, for wind turbines with a rated power above 1MW, variable speed concepts are usually applied, that are either based on doubly-fed induction machines or converter-driven synchronous machines [9]. This paper presents a *dq0* model of the direct-drive synchronous machine and its converter. With these models fast dynamic simulations can be performed.

First a short explanation will be given of the way in which models of electrical components in the dq0 reference frame can be obtained. This explanation is followed by a description of the wind turbine models in the dq0 reference frame. Case study simulations will illustrate the usefulness of the models.

II. PARK TRANSFORMATION

The Park transformation is well-known from the modelling of electrical machines. The transformation represents instantaneous values and can be applied to arbitrary three-phase time-dependent signals. For $\theta_d = \omega_d t + \varphi$, with ω_d the angular frequency of the signals that should be transformed, t the time and φ the initial angle, the Park transformation is given by [10]:

$$\left[\mathbf{x}_{dq0} \right] = \left[\mathbf{T}_{dq0} (\theta_d) \right] \left[\mathbf{x}_{abc} \right]$$
 (1)

with:

$$\begin{bmatrix} \mathbf{x}_{dq0} \end{bmatrix} = \begin{bmatrix} x_d \\ x_q \\ x_0 \end{bmatrix} \text{ and } \begin{bmatrix} \mathbf{x}_{abc} \end{bmatrix} = \begin{bmatrix} x_a \\ x_b \\ x_c \end{bmatrix}$$
 (2)

and with the dq0 transformation matrix \mathbf{T}_{dq0} defined as:

$$\left[\mathbf{T}_{dq0}\right] = \sqrt{\frac{2}{3}} \begin{bmatrix} \cos\theta_d & \cos\left(\theta_d - \frac{2\pi}{3}\right) & \cos\left(\theta_d + \frac{2\pi}{3}\right) \\ -\sin\theta_d & -\sin\left(\theta_d - \frac{2\pi}{3}\right) & -\sin\left(\theta_d + \frac{2\pi}{3}\right) \\ \frac{1}{\sqrt{2}} & \frac{1}{\sqrt{2}} & \frac{1}{\sqrt{2}} \end{bmatrix}$$
 (3)

The positive q-axis is defined as leading the positive d-axis by $\pi/2$, as can be seen in Fig. 1.

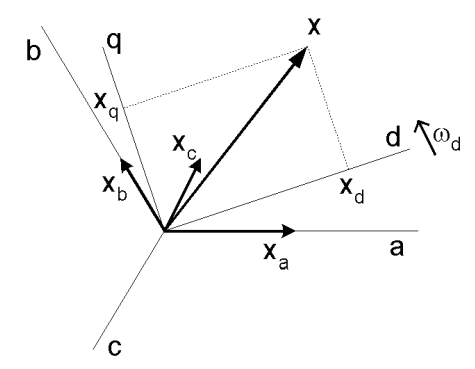


Fig. 1. Relationship between abc and dq quantities

The transformations of (3) are unitary and conserve power [11]. Note that by replacing the factor $\sqrt{2/3}$ by a factor 2/3 in (3) the transformation will be amplitude-invariant, implying that the length of the current and voltage vectors in both abc and dq0 reference frame are the same.

The voltages and currents in the dq0 reference frame are constant in steady-state situations. It should be noted that also non-fundamental harmonics are correctly transformed as x_a , x_b and x_c are time signals, including all harmonics. In steady state a non-fundamental frequency component with frequency ω_h will appear as a sinusoidal signal with frequency (ω_h - ω_p) in the dq0 domain. The highest frequency that can be represented accurately in the dq0 frame depends on the time step that is used.

Simulation software for electrical systems often has a special package in which the steady-state behaviour of a system is simulated. When the system enters a transient state however, another software package is used. The advantage of modelling in a *dq0* reference frame is that the switch between steady-state situations and transient situations is inherently incorporated in the model. In steady state situations all signals are constant just like in steady-state simulation software. When the system enters a transient

state, the signals are no longer constant, but the models are still valid.

The Park transformation is often used in control loops, as it offers the possibility of decoupled control between active and reactive power. The active and reactive power cannot directly be related to the d and the q axis component. These components are just a representation. The instantaneous active and reactive power can be obtained directly from the voltages and currents in the dq0 reference system [12]:

$$P = v_d i_d + v_q i_q$$

$$Q = v_q i_d - v_d i_q$$
(4)

III. GENERATOR MODEL

Using the generator convention, the stator voltage equations of the synchronous machine are given by:

$$v_{ds} = -R_s i_{ds} - \omega_s \psi_{qs} - \frac{d\psi_{ds}}{dt}$$

$$v_{qs} = -R_s i_{qs} + \omega_s \psi_{ds} - \frac{d\psi_{qs}}{dt}$$
(5)

with v the voltage [V], R the resistance $[\Omega]$, i the current [A], ω_s the stator electrical angular velocity [rad/s] and ψ the flux linkage [Vs]. The indices d and q indicate the direct and quadrature axis components. All quantities in (1) are functions of time.

The flux linkages in (5) are:

$$\psi_{ds} = (L_{ds} + L_m)i_{ds} + \Psi_f$$

$$\psi_{as} = (L_{as} + L_m)i_{as}$$
(6)

with Ψ_f the excitation flux of the permanent magnets linked with the stator windings, L_m the mutual inductance [H], and L_{ds} and L_{qs} the stator leakage inductances [H].

The electrical torque $T_{\rm e}$ of the permanent magnet synchronous machine is given by [13]:

$$T_{e} = 2 p i_{qs} \left[i_{ds} \left(L_{ds} - L_{qs} \right) + \Psi_{f} \right] \tag{7}$$

Here p is the number of pole pairs. For a non-salient-pole machine the stator inductances L_{ds} and L_{qs} are approximately equal. This means that the equation becomes:

$$T_e = 2 p i_{qs} \Psi_f \tag{8}$$

The stator electrical angular velocity is given by:

$$\omega_{s} = p\omega_{m}$$
 (9)

with ω_m the mechanical angular velocity [rad/s], which can be obtained from:

$$\frac{d\omega_m}{dt} = \frac{I}{J} (T_m - T_e) \tag{10}$$

with J the inertia constant of the rotor $[kg \cdot m^2]$ and

 T_m and T_e the mechanical and electrical torque [Nm] respectively.

In order to apply independent controllers for the two coordinates the influence of the q-axis on the d-axis-components and vice versa must be eliminated. This can be done by decoupling the two components, in the way shown in Fig. 2. The decoupling components should be added to the reference signals.

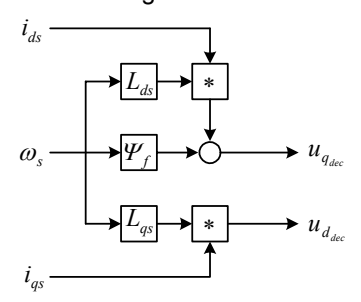


Fig. 2. Decoupling of the generator axes

With the decoupling applied, the linear transfer function of i_{ds} to u_{ds} is given by:

$$\frac{i_{ds}(s)}{u_{ds}(s)} = \frac{1}{L_s s + R_s} \tag{11}$$

The proportional and integral constants for the Plcontroller can be obtained as [14]:

$$k_p = \alpha_c L_s, \quad k_i = \alpha_c R_s \tag{12}$$

with $\alpha_{\rm c}$ is the bandwidth of the current control loop.

The torque is proportional to the current i_{qs} , as can be seen from (8). The angular velocity ω_m depends on the torque as can be seen from (10). The electrical torque is proportional to the current i_{qs} , and the controller is designed in a similar way as that of the current i_{ds} . The proportional and integral constants for the speed controller are [13]:

$$k_p = \frac{2p^2 \psi_f}{J}, \ k_i = \frac{2p^2 \psi_f R_s}{JL_s}$$
 (13)

IV. VOLTAGE SOURCE CONVERTER

The generator is connected to the grid by a back-to-back converter consisting of two voltage source converters with a dc-link in between. The Voltage Source Converters (VSC's) are based on IGBT switches. The three-phase full-bridge grid-side IGBT-VSC is shown in Fig. 3.

The converter is also modelled in the *dq0* reference frame. It has been modelled according to the switching function concept [15]. The

switching of the converter is not taken into account. It is assumed that the filters of the converter reduce the higher frequency components [16]. It has been shown in [17], [18] that good simulation results can be obtained with this model.

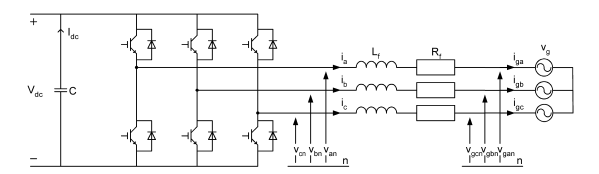


Fig. 3. Three-phase full-bridge Voltage Source Converter

Consider the system of Fig. 3. The voltage balance across the inductors and resistors is:

$$\Delta v_{a} = v_{an} - v_{agn} = L_{f} \cdot \frac{di_{a}}{dt} + R_{f} \cdot i_{a}$$

$$\Delta v_{b} = v_{bn} - v_{bgn} = L_{f} \cdot \frac{di_{b}}{dt} + R_{f} \cdot i_{b}$$

$$\Delta v_{c} = v_{cn} - v_{cgn} = L_{f} \cdot \frac{di_{c}}{dt} + R_{f} \cdot i_{c}$$
(14)

With the Park transformation this equation can be transformed to the *dq* reference frame [11]:

$$\Delta v_{d} = R_{f}i_{d} + L_{f} \cdot \frac{di_{d}}{dt} + \omega_{e}L_{f}i_{q}$$

$$\Delta v_{q} = R_{f}i_{q} + L_{f} \cdot \frac{di_{q}}{dt} - \omega_{e}L_{f}i_{d}$$
(15)

The last term in both equations causes a coupling of the two equations, which makes it difficult to control both currents independently. The last terms can be considered as a disturbance on the controller and are not taken into account for the controller. The i_d and i_q errors can be processed by a PI controller to give $v_{d,ref}$ and $v_{q,ref}$ respectively. To ensure good tracking of these currents, the cross-related flux terms are added to $v_{d,ref}$ and $v_{q,ref}$ to obtain the correct reference voltages.

Treating the cross-related terms as a disturbance, the transfer function from voltage to current (for both the d- and the q-component) of (15) can be found as:

$$G(s) = \frac{1}{L_f s + R_f} \tag{16}$$

Using the Internal Model Control principle [14] to design the current controllers yields:

$$K(s) = k_p + \frac{k_i}{s} = \frac{\alpha_c}{s} G^{-1}(s)$$
(17)

where α_c is the bandwidth of the current control loop, k_p is the proportional gain and k_i is the

integral gain of the controller. The proportional and integral gain become [14]:

$$k_p = \alpha_c L_f; \quad k_i = \alpha_c R_f \tag{18}$$

The active and reactive power delivered by the converter are given by:

$$P = v_{dg}i_{d} + v_{qg}i_{q}$$

$$Q = v_{gg}i_{d} - v_{dg}i_{g}$$
(19)

with the *d*-axis of the reference frame along the stator-voltage position, v_q is zero and as long as the supply voltage is constant, v_d is constant. The active and reactive power are proportional to i_d and i_q then.

V. WIND TURBINE MODEL

To simulate the dynamics of a wind farm, not only models of the electrical system are required, but also a dynamic model of the wind turbine excluding the generator. This part of the dynamic model of the turbine includes the following components:

- turbine rotor;
- mechanical drive train;
- tower:
- rotor effective wind;
- wind turbine pitch controller.

A description of the wind and turbine models can be found in [10] and [19].

VI. CASE STUDY SIMULATIONS

A. Introduction

Two case studies will demonstrate the effectiveness of the proposed modelling method. All simulations have been done in Simulink[®], a toolbox extension of Matlab that is widely used in dynamic simulation. The Near Shore Wind park (NSW park) that is planned to be built in the North Sea about 12 kilometres from the Dutch coast will be used as a case study. The wind farm will consist of 36 turbines with a 2.75 MVA doubly-fed induction generator. For the case study these turbines are replaced by 2.5 MW direct drive turbines. For convenience only one string of 12 turbines is simulated. The turbines are connected in series via 34kV cables. Each of the turbines is connected to the 34kV grid by a three-winding transformer with a nominal power of 2.5MW. The wind farm is connected to the 150kV grid via a transformer with a nominal power of 125MVA.

B. Fast changing wind speed

The response of one string of the wind farm to

a fast increasing wind speed has been simulated in the first case study. This situation is important for the grid behaviour of the park, as it will lead to a fast increase in the output power of the park and thus will cause fluctuations in the voltage at the grid connection point. The reactive power settings of the turbines are kept constant during the simulation.

Due to the distance between the turbines the wind speed doesn't start increasing at the same time for all turbines. It is assumed that the gust will affect first the turbine with the largest distance to shore, and it will come closer and closer to the shore, affecting each turbine. The rotor effective wind speed at the first turbine that experiences the gust is shown in Fig. 4. The increasing wind speed will cause an increasing output power of the turbine. The output power of the first turbine is shown in Fig. 5. The output power of the sixth turbine is shown in Fig. 6.

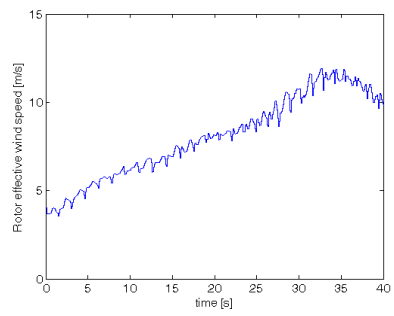


Fig. 4. Wind speed

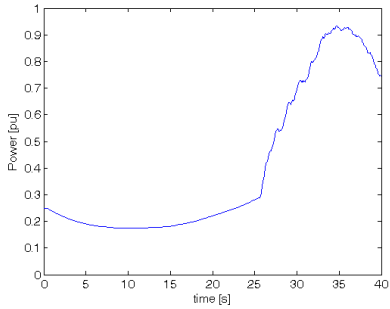


Fig. 5. Output power of first wind turbine

The output power of the whole first string of the wind farm is shown in Fig. 7. The large changes in output power of the wind farm will also affect the voltage of the 150kV grid at the point of connection. The voltage at the park side of the 150kV transformer is shown in Fig. 8. It should be noted that the change in output voltage of the wind farm shown in Fig. 8, is only due to one string. The resulting change in output voltage due to the whole park will be about 3 times higher. The turbines offer the possibility to control the

reactive power output. It should be investigated whether or not it is possible to decrease the voltage fluctuations by controlling the reactive power output of the turbines.

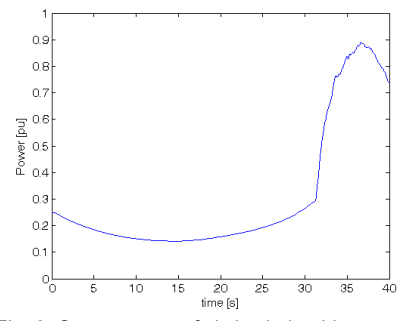


Fig. 6. Output power of sixth wind turbine

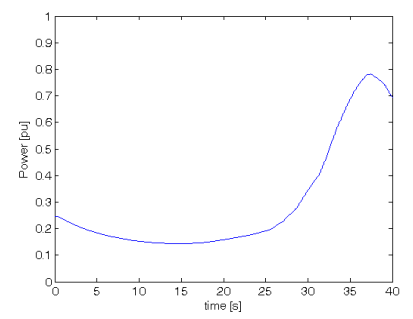


Fig. 7. Output power of one string of the wind farm

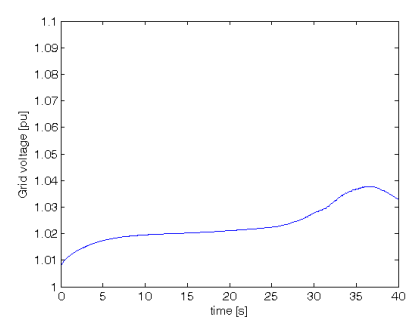


Fig. 8. Output voltage of wind farm

C. Voltage dip behaviour

In this section the voltage dip behaviour of the permanent magnet wind turbine is considered. The turbine has a full back-to-back converter connected between the stator and the grid. This converter decouples the turbine from the grid. The voltage dip behaviour of the turbine can thus mainly be considered as the voltage dip behaviour of the converter.

When the voltage drops, the converter should increase the current, in order to be able to supply the same amount of power to the grid. The current of the converter is limited however, to protect it from over-currents. Therefore the power

that is delivered by the wind turbine should be limited, because otherwise, the dc-link voltage will increase too much. A protection scheme is implemented in the model. The converter currents and the dc-link voltage are limited. When it is necessary the electrical torque set point of the converter that is connected to the permanent magnet generator is limited. As a result the turbine will speed up. The increase in rotational speed is limited by the pitch controller of the turbine.

A 30% - 10 seconds dip in the voltage has been applied. The rotor average wind speed during the dip was about 15 m/s. The wind turbine then operates at nominal power. The converter active and reactive power are shown in Fig. 9 and Fig. 10 respectively The current and voltage of the grid-side converter are shown in Fig. 11 and Fig. 12 respectively. The dc-link voltage is shown in Fig. 13.

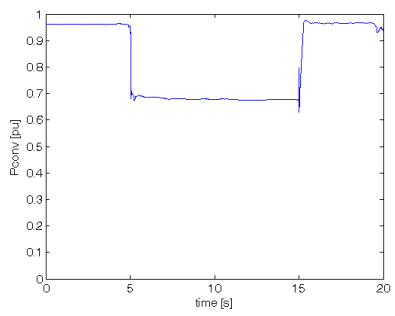


Fig. 9. Active power of converter

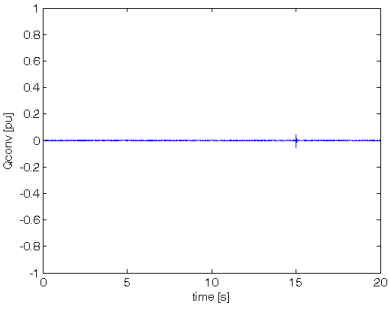


Fig. 10. Reactive power of converter

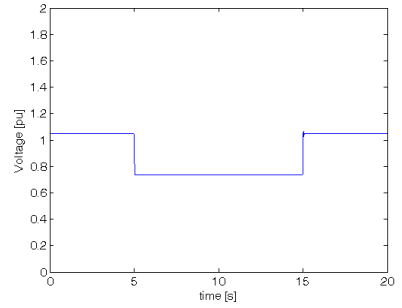


Fig. 11. Converter terminal voltage

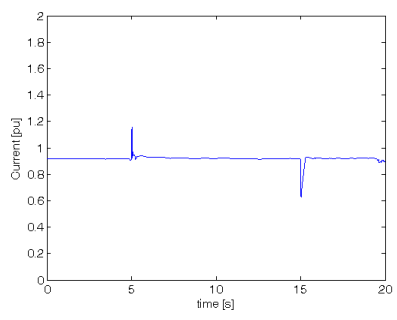


Fig. 12. Converter current

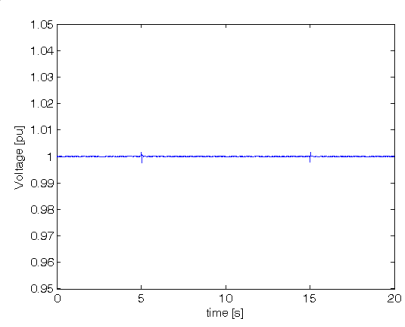


Fig. 13. DC-link voltage of converter

VII. SUMMARY

In this contribution the advantages of modelling in a dq0 reference frame has been presented. It has been shown, that the Park transformation can be used to translate wind turbine models from the abc reference frame to models in the reference frame. This has demonstrated by deriving a model permanent magnet wind turbine. Two case study simulations showed the use of the models to evaluate the impact of wind farms on the electricity grid. From these case studies it can be concluded that sudden wind speed changes can have a significant impact on the grid voltage. With an appropriate control, the turbine can withstand voltage dips.

VIII. REFERENCES

- [1] J.G. Slootweg, H. Polinder, W.L. Kling, "Dynamic Modelling of a Wind Turbine with Doubly Fed Induction Generator", in *Proc. 2001 IEEE Power Engineering* Society Summer meeting, pp. 644-649.
- [2] J.G. Slootweg, W.L. Kling, "Modeling of large wind farms in power system simulations", in *Proc. 2002 IEEE Power Engineering Society Summer meeting*, pp. 503-508.
- [3] P. Sorensen, A. Hansen, L. Janosi, J. Bech, B. Bak-Jensen, Simulation of Interaction between Wind Farm and Power System, Report Risoe-R-1281 (EN), Risoe National Laboratory, Roskilde, Denmark, December 2001.
- [4] V. Akhimatov, H. Knudsen, A. H. Nielsen, J.K. Pedersen, N.K. Poulsen, "Modelling and transient stability of large wind farms", *International Journal of Electrical Power & Energy Systems*, Vol. 25, No. 2, Feb. 2003, pp. 123-144.

- [5] J.G. Slootweg, S.W.H. de Haan, H. Polinder, and W.L. Kling, "General model for representing variable speed wind turbines in power system dynamics simulations", *IEEE Trans. Power Systems*, Vol. 18, No. 1, pp. 144-151, Feb. 2003.
- [6] Jan Pierik, Johan Morren, Sjoerd de Haan, Tim van Engelen, Edwin Wiggelinkhuizen, Jan Bozelie, "Dynamic models of wind farms for grid-integration studies", in *Proc. Nordic Wind Power Conference 2004*, Gothenburg, Sweden, 1 – 2 March 2004.
- [7] V. Akhimatov, "Modelling of variable-speed wind turbines with doubly-fed induction generators in short-term stability investigations", in: Proc. 3rd Int. Workshop on Transmission Networks for Offshore Wind Farms, April 11-12, 2002, Stockholm, Sweden.
- [8] X.Z. Liu, G.C. Verghese, J.H. Lang, M.K. Önder, "Generalizing the Blondel-Park Transformation of Electrical Machines: Necessary and Sufficient Conditions", *IEEE Trans. Circuits and Systems*, Vol. 36, No. 8, pp. 1058 –1067, 1989.
- [9] S. Achilles, M. Pöller, Direct Drive Synchronous Machine Models for Stability Assessment of Wind Farms, in Proc. 4th International Workshop on Large-Scale Integration of Wind Power and Transmission Networks for Offshore Wind Farms, 20-21 Oct. 2003 Billund, Denmark.
- [10] C.-H. Ong, Dynamic Simulation of Electric Machinery using Matlab/Simulink, Upper Saddle River: Prentice Hall. 1998.
- [11] J. Morren, S.W.H. de Haan, J.T.G. Pierik, J. Bozelie, Fast Dynamic Models of Offshore Wind Farms for Power System Studies", in Proc. 4th International Workshop on Large-scale Integration of Wind Power and Transmission Networks for Offshore Wind Farms, Billund, Denmark, 20 – 21 October 2003.
- [12] H. Akagi, Y. Kanazawa, A. Nabae, "Instantaneous Reactive Power Compensators Comprising Switching Devices Without Energy Storage Components", *IEEE Trans. Ind. Appl.*, Vol 20, pp. 625, 1984.
- [13] I. Schiemenz, M. Stiebler, Control of a permanent magnet synchronous generator used in a variable speed wind energy system, in *Proc. IEEE El. Mach. And Drives* Conf. (IEMDC), pp. 872 – 877, 2001.
- [14] A. Petersson, Analysis, Modelling and Control of Doubly-Fed Induction Generators for Wind Turbines, Licentiate thesis, Technical report no. 464L, Chalmers University, Göteborg, Sweden, 2003.
- [15] P.D. Ziogas, E.P. Wiechmann, V.R. Stefanović, "A Computer Aided Analysis and Design Approach for Static Voltage Source Inverters", *IEEE Trans. on Ind. Appl.*, Vol. 21, No. 5, pp. 1234-1241, 1985.
- [16] N. Mohan, T.M. Undeland, W.P. Robbins, Power Electronics – Converters, Applications and Design, New York: John Wiley & Sons, 1995.
- [17] J. Morren, S.W.H. de Haan, J.A. Ferreira, "Model reduction and control of electronic interfaces of voltage dip proof DG units", in *Proc. 2004 IEEE Power Engineering Society (PES) General Meeting*, Denver, 6-10 June 2004.
- [18] J. Morren, S.W.H. de Haan, P. Bauer, J.T.G. Pierik, J. Bozelie, "Comparison of complete and reduced models of a wind turbine with Doubly-Fed Induction Generator" in Proc. 10th European conference on Power Electronics and applications (EPE), Toulouse, France, 2 4 September 2003.
- [19] J.T.G. Pierik, J. Morren, E.J. Wiggelinkhuizen, S.W.H. de Haan, T,G van Engelen, J. Bozelie, Electrical and control aspects of offshore wind farms – Vol. 1: Dynamic models of wind farms, Technical report ECN-CX- -04-018, ECN, 2004.

VOLTAGE DIP PROOF CONTROL OF DIRECT-DRIVE WIND TURBINES

J. Morren, J.T.G. Pierik, S.W.H. de Haan.

UPEC 2004 Conference.

VOLTAGE DIP RIDE-THROUGH CONTROL OF DIRECT-DRIVE WIND TURBINES

Johan Morren¹⁾, Jan T.G. Pierik²⁾, Sjoerd W.H. de Haan¹⁾

ABSTRACT

With an increasing amount of wind energy installed, the behaviour of wind turbines during grid disturbances becomes more important. Grid operators require that wind turbines stay connected to the grid during voltage dips.

This contribution presents a combined control technique that can be used to keep direct-drive wind turbines with permanent magnet generator connected to the grid during voltage disturbances.

INTRODUCTION

World wide there is an ambition to install a large amount of wind power and to increase the fraction of energy that is produced by wind turbines. The interaction with the grid becomes increasingly important then. To enable large-scale application of wind energy without compromising system stability, the turbines should stay connected and contribute to the grid in case of a disturbance such as a voltage dip. They should – similar to conventional power plants – supply active and reactive power for frequency and voltage support, immediately after the fault has been cleared.

To allow wind turbine connection to the grid, a number of grid operators require voltage-dip ride-through capability already. Especially on places where wind turbines provide for a significant part of the total power supply. Examples are Denmark [1] and parts of Northern Germany [2]. The requirements concerning immunity to voltage dips as prescribed by E.ON Netz, a grid operator in Northern Germany, is shown in Fig. 1. Only when the grid voltage drops below the curve (in duration or voltage level), the turbine is allowed to disconnect.

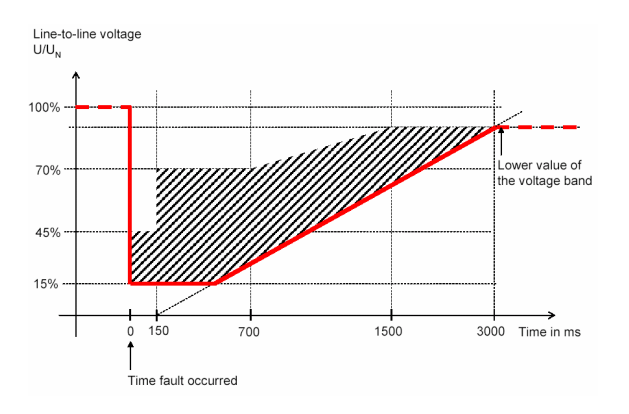


Fig. 1. Voltage dip that wind turbines should be able to handle without disconnection (E.On Netz)

Especially variable speed wind turbines, such as wind turbines with doubly-fed induction generators or direct-drive permanent magnet generators, require careful attention. These turbines use power electronic converters, which should be protected against over-currents and over-voltages during disturbances.

A number of publications have been presented on the voltage dip behaviour of doubly-fed induction generators [3] – [5], whereas only few information can be found on the voltage dip behaviour of direct-drive permanent magnet wind turbines. In this contribution we will investigate the operation of a permanent magnet wind turbine during voltage disturbances.

A combined control method has been developed to keep the wind turbine connected to the grid during voltage dips. The paper will give a description of the model of the permanent magnet generator that has been developed. A thorough description of the controllers will be presented and it will be explained how these controllers can be combined to keep the wind turbine connected during a dip. Simulations will be presented to show the behaviour of the controllers and the turbine during a voltage dip. The wind turbine model and also the grid model are based on realistic parameters.

MODEL DESCRIPTION

Most direct-drive wind turbines will use permanent magnet synchronous generators. In this section the basic equations describing the machine behaviour will be given, followed by the way in which controllers can be obtained.

Generator

The machine model that has been used is based on the following set of equations:

$$v_{ds} = -R_s i_{ds} - \omega_s \psi_{qs} - \frac{d\psi_{ds}}{dt}$$

$$v_{qs} = -R_s i_{qs} + \omega_s \psi_{ds} - \frac{d\psi_{qs}}{dt}$$
(1)

¹⁾ Electrical Power Processing, Delft University of Technology, The Netherlands

²⁾ Energy research Centre of the Netherlands (ECN), The Netherlands

with v the voltage [V], R the resistance $[\Omega]$, i the current [A], ω_s the stator electrical angular velocity [rad/s] and ψ the flux linkage [Vs]. The indices d and q indicate the direct and quadrature axis components. All quantities in (1) are functions of time.

Due to the limited space it will not be possible to give a complete description of the generator model and its control. It can be found in [6], [7].

Converter

The permanent magnet synchronous machine is connected to the grid by a three-phase back-to-back converter consisting of two Voltage Source Converters (VSCs) and a dc-link. The dc-link separates the two Voltage Source Converters, and therefore they can be controlled independent of each other and only one converter has to be considered. The controller of the converter will be based on a stationary $dq\theta$ reference frame. All signals will be constant in steady-state and therefore easily PI controllers can be used to obtain the reference signals without steady-state errors. The controller is based on two control loops. The inner loop is a current controller, which get its reference from the outer loop controller, which can be for example a reactive power or torque controller.

The switching function concept has been used to model the converter [8]. Using this concept, the power conversion circuits are modelled according to their functions, rather than to their circuit topologies. If the filter is designed well, the higher harmonics that are generated by the switching process will be attenuated. It can be shown that, with a well-designed filter, in the lower frequency range the frequency components of the reference voltage and the practical obtained voltage are equal if the switching frequency is sufficiently large [9]. The whole system can then be replaced by a system, creating sinusoidal waveforms, exactly equal to the reference waveforms. One should be aware that this is only valid for frequencies far below the resonance frequency of the filter. In case of a grid-connected converter, with a grid-frequency of 50Hz, this requirement will mostly be met.

Current control

The controllers of the VSC will be obtained with reference to the converter shown in Fig. 2. A vector-control approach is used for the supply side converter, with a reference frame oriented along the grid voltage vector. Such a reference frame enables independent control of the active and reactive power flowing between the converter and the grid.

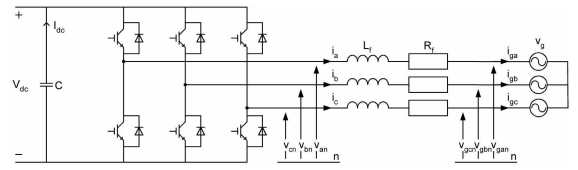


Fig. 2. Three-phase full-bridge Voltage Source Converter

Consider the system of Fig. 2. The voltage balance across the inductors and resistors is:

$$\Delta v_{a} = v_{an} - v_{agn} = L_{f} \cdot \frac{di_{a}}{dt} + R_{f} \cdot i_{a}$$

$$\Delta v_{b} = v_{bn} - v_{bgn} = L_{f} \cdot \frac{di_{b}}{dt} + R_{f} \cdot i_{b}$$

$$\Delta v_{c} = v_{cn} - v_{cgn} = L_{f} \cdot \frac{di_{c}}{dt} + R_{f} \cdot i_{c}$$
(2)

With the Park transformation this equation can be transformed to the dq reference frame:

$$\Delta v_d = R_f i_d + L_f \cdot \frac{di_d}{dt} + \omega_e L_f i_q$$

$$\Delta v_q = R_f i_q + L_f \cdot \frac{di_q}{dt} - \omega_e L_f i_d$$
(3)

The last term in both equations causes a coupling of the two equations, which makes it difficult to control both currents independently. The last terms can be considered as a disturbance on the controller. Reference voltages to obtain the desired currents can be written as:

$$\Delta v_{q}^{*} = \Delta v_{q}^{'} + \omega_{e} L_{f} i_{q}$$

$$\Delta v_{q}^{*} = \Delta v_{q}^{'} - \omega_{e} L_{f} i_{d}$$
with: (4)

$$\Delta v_{d}^{'} = R_{f}i_{d} + L_{f} \cdot \frac{di_{d}}{dt}$$

$$\Delta v_{q}^{'} = R_{f}i_{q} + L_{f} \cdot \frac{di_{q}}{dt}$$
(5)

The i_d and i_q errors can be processed by a PI controller to give v_d ' and v_q ' respectively. To ensure good tracking of these currents, the cross-related flux terms are added to v_d ' and v_q ' to obtain the reference voltages.

Treating the cross-related terms as a disturbance, the transfer function from voltage to current of (5) can be found as (for both the d- and the q-component):

$$G(s) = \frac{1}{L_f s + R_f} \tag{6}$$

A scheme of the controller is given in Fig. 3.

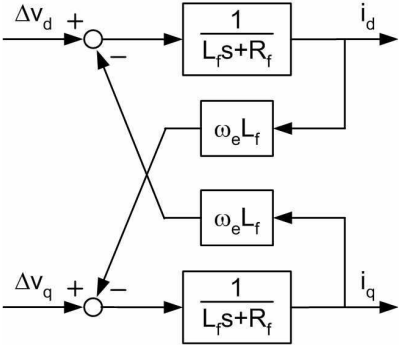


Fig. 3. Scheme of current controller

Using the Internal Model Control principle [10] to design the current controllers yields:

$$K(s) = k_p + \frac{k_i}{s} = \frac{\alpha_c}{s} G^{-1}(s)$$
 (7)

where α_c is the bandwidth of the current control loop, k_p is the proportional gain and k_i is the integral gain of the controller. The gains become [11]:

$$k_p = \alpha_c L_f; \quad k_i = \alpha_c R_f \tag{8}$$

The active and reactive power delivered by the converter are given by:

$$P = v_{dg}i_d + v_{qg}i_q$$

$$Q = v_{qg}i_d - v_{dg}i_q$$
(9)

with the d-axis of the reference frame along the statorvoltage position, v_q is zero and as long as the supply voltage is constant, v_d is constant. The active and reactive power are proportional to i_d and i_g then.

Dc-link controller

In this sub-section a description will be given of the dclink voltage controller that has been used. The dc voltage controller is designed by use of feedback linearisation [12].

The capacitor in the dc-link behaves as an energy storage device. Neglecting losses, the time derivative of the stored energy must equal the sum of the instantaneous stator power P_s and grid power P_e :

$$\frac{1}{2}C\frac{d(v_{dc}^2)}{dt} = P_s - P_g \tag{10}$$

This equation is nonlinear with respect to v_{dc} . To overcome this problem a new state-variable is introduced:

$$W = v_{dc}^2 \tag{11}$$

Substituting this in (10) gives:

$$\frac{1}{2}C\frac{dW}{dt} = P_s - P_g \tag{12}$$

which is linear with respect to W. The physical interpretation of this state-variable substitution is that the energy is chosen to represent the dc-link characteristics [12]. With the dq-reference frame of the current controller along the d-axis, (12) is be written as:

$$\frac{1}{2}C\frac{dW}{dt} = P_s - v_d i_d \tag{13}$$

and the transfer function from i_d to W is then found to be:

$$G(s) = -\frac{2v_d}{sC} \tag{14}$$

As this transfer function has a pole in the origin it will be difficult to control it. An inner feedback loop for active damping will be introduced [12]:

$$i_{d} = i_{d}^{'} + G_{a}W \tag{15}$$

With G_a the active conductance, performing the active damping, and i_a ' the reference current provided by the outer control loop, see Fig. 4. Substituting (15) into (13) gives:

$$\frac{1}{2}C\frac{dW}{dt} = P_s - v_d i_d' - v_d G_a W \tag{16}$$

Which is shown in Fig. 4. The transfer function from i_q ' to W becomes [12]:

$$G'(s) = -\frac{2v_d}{sC + 2v_d G_a} \tag{17}$$

Using the internal model control principle [11] and since (17) is a first-order system, the following controller is proposed:

$$F(s) = \frac{\alpha}{s} G^{'-1}(s) = -\frac{\alpha_d \hat{C}}{2\nu_d} - \frac{\alpha_d G_a}{s}$$
 (18)

Which is just an PI-controller. A suitable choice will be to make the inner loop as fast as the closed-loop system [12]. When the pole of G'(s) is placed at $-\alpha_d$ the following active conductance is obtained:

$$G_a = \frac{\alpha_d \hat{C}}{2\nu_d} \tag{19}$$

The PI-controller parameters are then given as [12]:

$$k_p = -\frac{\alpha_d \hat{C}}{2\nu_d}, \quad k_i = -\frac{\alpha_d^2 \hat{C}}{2\nu_d}$$
 (20)

The controller is completed by a feed-forward term from P_s to i_q . This feed-forward term is needed to improve the dynamic response of the dc-link controller.

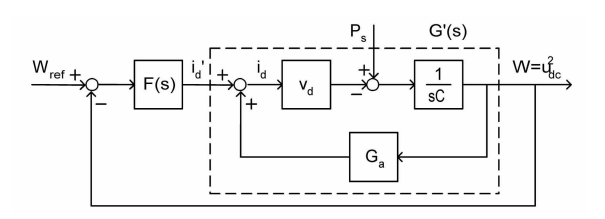


Fig. 4. dc-link controller structure

SIMULATION SETUP

The simulation set-up is shown in Fig. 5. From left to right the turbine, the turbine transformer, the 34kV cable, the 34kV/150kV transformer and the 150kV ideal grid are shown. The layout and the data have been obtained from The Near Shore Wind park (NSW park) that is planned to be built in the North Sea about 12 kilometres from the Dutch coast. One turbine is considered. In first instance the behaviour of a single turbine is most important when the voltage dip behaviour of wind turbines is investigated. All controllers and protective devices have to be developed for a single turbine. Therefore the behaviour of only one turbine will be investigated during the simulations.

In our investigation a three-phase fault will be studied. The fault is assumed to occur somewhere in the 150kV transmission grid. They result in reduced voltage levels at the 34kV/150kV transformer. During the simulations the grid has been modelled as an ideal voltage source. And the dip is modelled as a decreasing grid voltage.

All simulations have been done with the turbine operating at nominal power. The results for the simulations are presented in the following sections. Due to the limited space it will not be possible to give a description of mechanical and aerodynamical models. They can be found in [13].

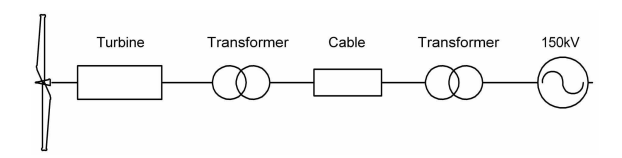


Fig. 5. Simulation set-up for voltage dip simulations

The direct-drive variable-speed turbine has a full back-to-back converter connected between the stator and the grid. The voltage dip behaviour of this turbine can thus mainly be considered as the voltage dip behaviour of the converter.

When the voltage drops, the converter should increase the current to be able to supply the same amount of power to the grid. The current of the converter is limited however. Therefore the power that is delivered by the wind turbine should be limited, because otherwise, the dc-link voltage will increase too much.

A protection scheme is implemented in the model. The converter currents and the dc-link voltage are limited. When it is necessary the electrical torque set point of the converter that is connected to the permanent magnet generator is limited. As a result the turbine will speed up. The increase in rotational speed is limited by the pitch controller of the turbine.

SIMULATION RESULTS

A 50% - 0.5 seconds dip in the voltage has been applied to the wind turbine. The rotor average wind speed during the dip was about 15 m/s. The wind turbine then operates at nominal power. The rotor average wind speed and the aerodynamic power in the wind are shown in Fig. 6. The active and reactive power supplied by the stator of the permanent magnet synchronous machine are shown in Fig. 7.

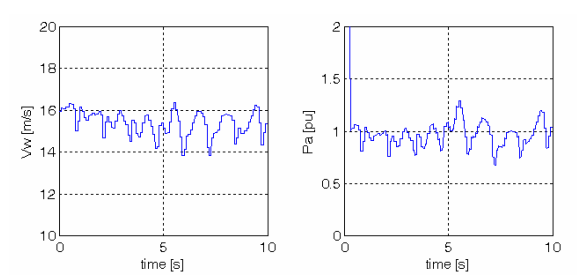


Fig. 6. Roter average wind speed and aerodynamic power

The current of the converter should be limited to 1 pu. At the moment the fault occurs the grid voltage drops and the current of the grid-side converter should increase to be able to supply the same power to the grid. The current will be limited however. As a result the DC-link voltage will increase, as long as the power from the turbine isn't decreased. Therefore also the generator controller will decrease it's setpoint. This can be seen

form the power curve in Fig. 7. When the power is decreased also the electrical torque will decrease, see again Fig. 7. As a result of the decreasing electrical torque the turbine will speed up, at least as long as the aerodymical torque remains the same. The increase in rotational speed wm is shown in Fig. 7. At the moment the speed increases the pitch angle controller reacts to limit the speed increase. When the dip will hold on for a longer time the speed may increase however, as the pitch angle controller is maybe not fast enough to limit the speed increase.

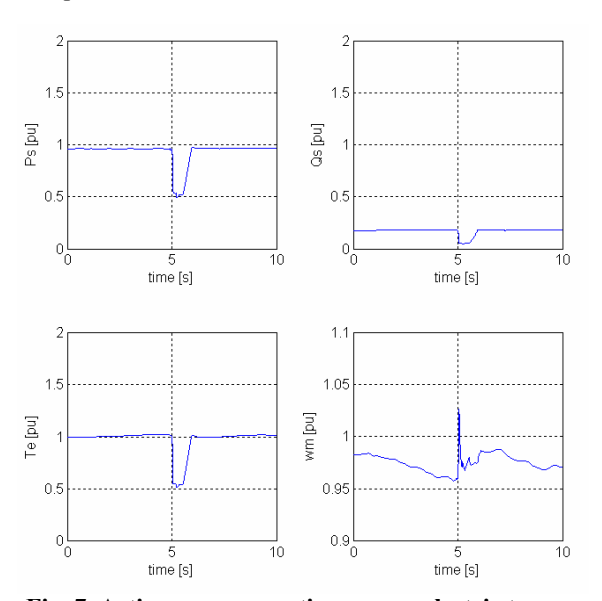


Fig. 7. Active power, reactive power, electric torque and speed

The dc-link voltage is shown in Fig. 8. Note that the voltage is so flat because the switching operation of the converters has not been modelled. When this would be done, there would be a high-frequency ripple on the voltage. The dc-link voltage remains almost the same during the voltage dip, as can be seen from the figure. This means that the dc-link controller reacts fast enough to control the voltage. In reality it will not always be necessary to keep the dc-link at the pre-fault voltage. A small increase or decrease in voltage will be allowed.

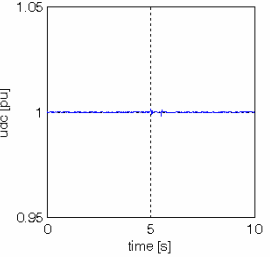


Fig. 8. DC-link voltage

In Fig. 9 the voltage and current of the grid-side converter are shown. It can be seen that the current is limited (after a controller overshoot) to about 1 pu. At the moment the dip is cleared, the current drops to about

half the nominal current. This is due to the fact that during the dip the turbine was only supplying half of its nominal power. It takes some time before it is operating at nominal power again. For that reason it also takes some time before the current is back at its nominal value.

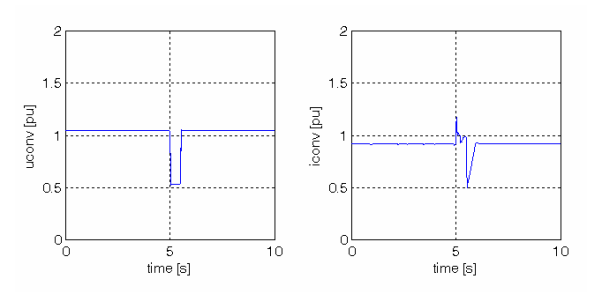


Fig. 9. Voltage and current of grid-side converter

CONCLUSION

In this paper the voltage dip behaviour of a variable speed pitch controlled wind turbine with permanent magnet generator has been considered. Models of the generator, the converter and its controllers have been presented with a special focus on those parts that are essential for the behaviour of the wind turbine during voltage dips. In the turbine all the essential parameters can be controlled. Therefore good voltage ride-through can be achieved. The power supplied by the generator is limited by the controllers during the dip. This is required because otherwise the current in the converter or the dc-link voltage becomes too high. To avoid overspeeding the pitch controller is activated.

ACKNOWLEGDMENT

This research is partially funded by Novem within the Program Renewable Energy in The Netherlands 2001, and by Senter within the Program IOP-EMVT.

REFERENCES

- 1. Rasmussen, C., Jorgensen, P., Havsager, J., "Integration of wind power in the grid in Eastern Denmark", in Proc. 4th International Workshop on Large-Scale Integration of Wind Power and Transmisson Networks for Offshore Wind Farms, 20 21 Oct. 2003, Billund, Denmark.
- 2. E.ON Netz, *Grid Code*, Bayreuth: E.ON Netz GmbH Germany, 1. Aug. 2003.
- 3. Holdsworth, L., Wu, X.G., Ekanayake, J.B., Jenkins, N., "Comparison of fixed speed and doubly-fed induction wind turbines during power system disturbances", *IEE Proc.-Communications*, Vol. 150, No. 3, pp. 343-352, May 2003.

- 4. Hudson, R.M., Stadler, F., Seehuber, M., "Latest Developments in Power Electronic Converters for Megawatt Class Windturbines Employing Doubly Fed Generators", in *Proc. Int. Conf. Power Conversion, Intelligent Motion (PCIM 2003)*, Nuremberg, June 2003
- 5. Morren, J., Haan, S.W.H. de, "Ride through of Wind Turbines with Doubly-fed Induction Generator during a voltage dip", *IEEE Trans. Energy Conv.*, accepted for publication.
- 6. Schiemenz, I., Stiebler, M., "Control of a permanent magnet synchronous generator used in a variable speed wind energy system", in *Proc. IEEE Electric Machines and Drives Conference, IEMDC 2001*, pp. 872 877
- 7. Morren, J., Pierik, J.T.G., Haan, S.W.H. de, "Fast dynamic modelling of direct-drive wind turbines", in *Proc PCIM Europe 2004*, Nürnberg, Germany 25 27 May 2004.
- 8. Ziogas, P.D., Wiechmann, E.P., Stefanović, V.R., "A Computer Aided Analysis and Design Approach for Static Voltage Source Inverters", *IEEE Trans. on Ind. Appl.*, Vol. 21, No. 5, pp. 1234-1241, 1985.
- 9. Mohan, N., Undeland, T.M., Robbins, W.P., *Power Electronics Converters, Applications and Design*, New York: John Wiley & Sons, 1995.
- 10. Harnefors, L., Nee, H.-P., "Model-Based current control of AC Machines using the Internal Model Control Method", *IEEE Trans. Ind. Appl.*, Vol. 34, No. 1, pp. 133-141, Jan./Feb. 1998.
- 11. Petersson, A., Analysis, Modelling and Control of Doubly-Fed Induction Generators for Wind Turbines, Licentiate thesis, Technical report no. 464L, Chalmers University, Göteborg, Sweden, 2003.
- 12. Ottersten, R., On control of Back-to-Back Converters and Sensorless Induction Machine Drives, Ph.D. thesis, Technical report no. 450, Chalmers University, Göteborg, Sweden, 2003.
- 13. Pierik, J.T.G., Morren, J., Wiggelinkhuizen, E.J., de Haan, S.H.W., Engelen, T.G. van, Bozelie J., *Electrical and control aspects of offshore wind turbines II, Vol. 1: Dynamic models of wind farms*, Technical Report ECN-CX--04-018, The Netherlands: ECN, 2004.

AUTHOR'S ADRESS

Johan Morren
Electrical Power Processing
Delft University of Technology
Mekelweg 4, 2628 CD Delft, The Netherlands
J.Morren@ewi.tudelft.nl

Dynamic models of wind farms for power system studies. Status by IEA Wind R&D Annex 21

J.O Tande, E. Muljadi, O. Carlson, J. Pierik, A. Estanqueiro, P. Sørensen, M. O'Malley, A. Mullane, O. Anaya-Lara and B. Lemstrom.

European Wind Energy Conference and Exhibition 2004, London.

Dynamic models of wind farms for power system studies – status by IEA Wind R&D Annex 21

John Olav G Tande¹, Eduard Muljadi², Ola Carlson³, Jan Pierik⁴, Ana Estanqueiro⁵, Poul Sørensen⁶, Mark O'Malley⁷, Alan Mullane⁷, Olimpo Anaya-Lara⁸, Bettina Lemstrom⁹

¹SINTEF Energy Research, john.o.tande@sintef.no, ²NREL, eduard_muljadi@nrel.gov,

³Chalmers, ola.carlson@elteknik.chalmers.se, ⁴ECN, pierik@ecn.nl, ⁵INETI, ana.estanqueiro@mail.ineti.pt,

⁶Risø, poul.e.soerensen@risoe.dk, ⁷UCD, mark.omalley@ee.ucd.ie, alan.mullane@ee.ucd.ie,

⁸UMIST, o.anaya-lara@manchester.ac.uk, ⁹VTT, Bettina.Lemstrom@vtt.fi

Abstract:

Dynamic models of wind farms for power system studies are at present not a standard feature of many software tools, but are being developed by research institutes, universities and commercial entities. Accurate dynamic wind farm models are critical; hence model validation is a key issue and taken up by IEA Wind R&D Annex 21. This international working group includes participants from nine countries, and has since start-up in 2002 developed a systematic approach for model benchmark testing. This paper present this methodology, including example benchmark test results, but also gives an overview of the various wind farm models now being available from both Annex partners and external entities.

Keywords: wind farms, power system, modelling.

1 Introduction

The worldwide development of wind power installations now includes planning of large-scale wind farms ranging in magnitudes of 100 MW as well as application of wind power to cover a large fraction of the demand in isolated systems. As part of the planning and design of such systems, it is well established that the stability of the electrical power system needs to be studied. The studies are commonly conducted using commercial available software packages for simulation and analysis of power systems. These packages normally facilitate a set of well-developed models of conventional components such as fossil fuel fired power stations and transmission network components, whereas models of wind turbines or wind farms are not standard features. Hence, the user is left to build his or hers own wind farm model. This is not at all trivial and certainly not efficient. Rather a coordinated effort is expected to enhance progress, and consequently Annex 21 under the IEA Wind R&D agreement was started mid 2002 with participants from nine countries.

This paper presents the status of works by the Annex, i.e. including overview of dynamic wind farm models

(section 2), measurement database (section 3) and procedure for benchmark testing of models (section 4), and finally example benchmark test results (section 5).

The overview section on dynamic wind farm models gives brief model descriptions, including a summary table of models developed by the Annex participants. The models considered are for various software tools (PSS/E, SIMPOW, DIgSILENT, Matlab/Simulink, etc) and for various wind farm technologies (fixed speed wind turbines, variable speed wind turbines with doubly feed induction generator, direct drive wind turbines with multi-pole synchronous generator, etc).

Model validation is a key issue for creating confidence. The use of invalidated models in power system studies may result in dramatically erroneous conclusions, i.e. grossly over- or under-predicting the impact of a wind farm on power system stability. The Annex consequently suggests benchmark procedures for validating model performance, i.e. validation against measurements and model-to-model comparisons. In the paper the procedure for this is explained together with example test results. The procedure considers both wind turbine / wind farm operation during normal fault free conditions and response to grid fault.

The current situation with on the one hand very varying level of confidence and knowledge about wind farm grid interaction modelling, and on the other hand ever larger wind farm projects being planned, the importance and relevance of the Annex works is highlighted. A key issue is thus dissemination of Annex results, i.e. being the goal of this paper.

Symbols used in this paper are listed in the Appendix.

2 Dynamic wind farm models

Accurate simulation of wind farms relies on detailed modelling of the applied wind turbine technology, e.g. the dynamic behaviour of a fixed speed wind turbine may differ significantly from that of a variable speed wind turbine. Figure 1 shows the main types, but there will also be manufacturer specific variations, i.e. in particular related to control system solutions. Aggregated models may be applied, i.e. letting one wind turbine model representing multiple turbines in a wind farm, but the impact of the spatial distribution and the internal wind farm grid must be reflected.

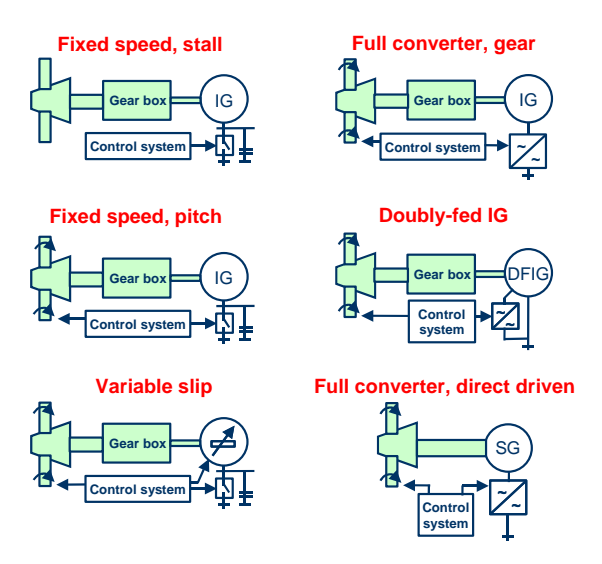


Figure 1: Main types of wind turbine technologies.

Space limitations of this paper does not allow for a detailed presentation of all the various models developed by the participants of the Annex. Hence, in the following only the common building blocks of the models are presented, whereas a brief summary of the models developed by the Annex participants is listed at the end of this section.

2.1 Wind turbine model building blocks

A detailed wind turbine model may include the following components:

- wind speed
- turbine aerodynamics
- mechanical drive-train
- generator
- capacitors or frequency converter
- control system
- other issues (relay protection, tower swings, etc)

A fair wind speed and turbine aerodynamic representation is required for simulating the aerodynamic torque fluctuations. One challenge in this relation is to include the effect of wind speed variations over the turbine area, i.e. an effect that may cause enhanced 3p power fluctuations from wind turbines. This can be done using wind field

simulations and detailed blade profile data or by application of the following relation:

$$T_t = 0.5 \rho A u_t^3 C_p(\lambda, \beta) \omega_t^{-1}$$
 (1)

Here, u_t is the weighted average wind speed over the three rotating turbine blades, i.e. determined from wind field simulations or by filtering of a single point wind speed time-series.

The mechanical drive train is commonly approximated by a two mass model, i.e. the turbine and generator inertia with a shaft and an ideal gearbox between them. Applying pu values with reference to the generator the two mass model is given by:

$$\frac{d\omega_t}{dt} = \frac{\omega_b}{2H_t} \left(T_t - d_m \left(\omega_t - \omega_g \right) - k\theta_t \right) \tag{2}$$

$$\frac{d\omega_g}{dt} = \frac{\omega_b}{2H_g} \left(d_m \left(\omega_t - \omega_g \right) + k\theta_t - T_g \right) \tag{3}$$

The generator models applied may be of varying complexity. Third order models are commonly used in tools for simulation of large power systems, whereas more detailed models may be used in tools for analyses of smaller systems. These detailed models may include stator dynamics (fifth order model), and further particulars such as full three-phase description.

The capacitors applied for reactive compensation of fixed speed wind turbines are commonly modelled as one or more shunt impedances.

In tools for simulation of large power systems the frequency converter is commonly described as an ideal component, i.e. neglecting losses and the switching dynamics. In more detailed studies these effects may be included, e.g. for assessment of harmonics.

The control system model for a fixed speed wind turbine is commonly split into two independent blocks, i.e. one for the pitching of the blades and one for switching the capacitors. The control system of variable speed wind turbines may be fairly complex, including speed control for optimising the production, but also producing a smooth output power, and further special regulation may be implemented for low-voltage ride-through and other off-normal grid situations.

Other issues such as e.g. relay protection and tower swings may be included in some models. The relevance of including such issues depends on the scope of the analysis.

2.2 Wind farm models

Wind farm models may be built to various level of detail ranging from a one-to-one modelling approach to full aggregation. The one-to-one approach is more computer demanding and in many cases not practical, hence aggregated wind farm models are often applied in power system studies. The aggregation is however not trivial, i.e. considering that a wind farm may consist of hundreds of wind turbines distributed over a large area with different impedance of line feeder from one turbine with respect to the others, different wind speeds at each turbine and different voltage drops on each bus. Aggregated models must therefore be applied with care. Possibly a cluster-by-cluster aggregation may be a fair compromise between one-to-one modelling and full aggregation.

2.3 IEA Annex 21 models

Development of dynamic wind farm / wind turbine models is ongoing amongst the participants of the Annex, see Table 1 (next page) for a brief summary.

3 Measurement database

An important activity of the Annex is the establishment of a database with technical descriptions, simulations and measurement data from wind turbines and wind farms. The data currently contained in the database is listed below.

- WT500; Sample data of fixed speed, stall controlled 500 kW wind turbine, measurement during normal operation.
- Alsvik; Data from 4x180 kW wind farm (fixed speed, stall controlled), measurement during normal operation, measurement and simulated response to voltage dip.
- Olos 5x600kW; Data from 5x600 kW wind farm (fixed speed, stall controlled), measurements during normal operation.
- Azores; Data from 4x100 + 1x150 kW wind farm (fixed speed, stall controlled), measurements during normal operation.
- Jung; Measurement of 850 kW DFIG wind turbine response to voltage dip.
- Risø benchmark; simulated response of fixed speed wind turbine on voltage dip (simulations in EMTDC and DIgSILENT).
- Data from Smøla wind farm, Norway, 20x2 MW fixed speed, active stall wind turbines (Bonus), measurements include normal operation and response to voltage dips.

The present dataset provides a fair basis for testing benchmark procedures, but should be expanded with data and measurements to constitute a better basis for model validation. Firmly planned new data to be added are from a 70 MW wind farm in Donegal, Ireland, with fixed speed, "grid code compliant" wind turbines (Bonus with thyristor switched capacitors; measurements are prepared by University College Dublin to be ongoing before end 2004). Further work is still in progress on collecting measurements from variable speed wind turbines, and during transient events, e.g. voltage dips. VTT, ECN/TUD and Chalmers are all active in pursuing such data collection.

The data in the database is for the use of the Annex partners only.

4 Benchmark test procedure

A first set of benchmark test procedures have been developed. The proposal so far is as outlined in this section.

The test should be kept simple, i.e. to start with considering only the following results:

Dynamic operation during normal conditions:

- Input:
 - Wind speed time series (and optionally voltage time series)
- Output:
 - Time series plot of active power output, reactive power, and voltage (optionally)
 - Power spectral density of active power output
 - Short-term flicker emission
 - Optionally plots of reactive power vs voltage and reactive power vs active power

Response to voltage dip:

- Input:
 - Voltage time series and constant aerodynamic torque (or optionally wind speed time series)
- Output:
 - time series plot of active and reactive power output
 - time series of voltage at wind turbine terminals

The benchmark test may include both validation against measurements and model-to-model comparisons.

Measurement data from a 180 kW fixed speed, stall controlled wind turbine and an 850 kW DFIG wind turbine are now used as a first case for testing the proposed benchmark procedure.

Partner	Tool	Model	Туре	Validated	Comment
Chalmers	Matlab	Fixed speed	Dynamic/Transient	Yes/Yes	Models and study reported, see [1] and at
		DFIG	Dynamic/Transient	Yes/Yes	http://www.elteknik.chalmers.se/
		Direct Drive	Dynamic/Transient	(Yes/Yes) ¹	¹ Converter validated in lab.
	PSSE	Fixed speed	Dynamic/Transient	Yes/Yes	
	DigSilent	Fixed speed	Dynamic/Transient	Yes/Yes	
		DFIG	Dynamic/Transient	No/No	
ECN/TUD	Matlab	Fixed speed	Dynamic/Transient	No/No	Models and study reported, see [2]-[3]
		DFIG	Dynamic/Transient	No/No	² Model include cluster control of multiple
		Direct Drive	Dynamic/Transient	No/No	induction machine wind turbines connected to
		Full Converter ²	Dynamic/Transient	No/No	one common frequency converter
INETI	INPark	Fixed speed	Dynamic/Transient ³	Yes/Yes	³ INPark model was developed by INETI for
		Direct Drive	Dynamic/(Transient)	No/No	grid integration assessment. LIB modular
	INDUSAT	WP Aggregate	Dynamic/Transient ⁴	Yes/Yes	routines available by request. Models and
	Matlab	Fixed speed	Dynamic/Transient	Yes/No	study reported, see [4]-[6].
		Direct Drive	Dynamic/(Transient)	No/No	⁴ Wind park aggregate models are developed by
					UTL – Technical University of Lisbon being
					under revision by UTL/INETI for actual
					technologies, see [7].
NREL	PSSE	Fixed speed ⁵	Dynamic/Transient	Yes/No	Models and study reported, see [8]-[9].
		DFIG ⁶	(Dynamic) ⁸ /Transient	No/No	⁵ PSSE model developed by NREL in
		Fixed-Speed ⁶	(Dynamic) ⁸ /Transient	No/No	cooperation with Southern California Edison
		Var Slip ⁶	(Dynamic) ⁸ /Transient	No/No	⁶ PSSE models (manufacturer specific)
		Full Converter ⁶	(Dynamic) ⁸ /Transient	No/No	developed for ERCOT by PTI, tested by
	RPM-Sim	Fixed speed ⁷	Dynamic/(Transient)	Yes/No	NREL
					⁷ RPM-Sim is a stand alone model for
					simulation of wind turbines and hybrid
					systems. The RPM-Sim models are available at
					wind.nrel.gov/designcodes/simulators/rpmsim/
					⁸ Wind field is modeled by aggregation.
Risø/AAU	DigSilent	Fixed speed	Dynamic/Transient	Yes/Yes	Models and study reported, see [10]-[11].
		DFIG	Dynamic/(Transient) ⁸	No/No	Matlab model library available at
	Matlab	Fixed speed	Dynamic/Transient	Yes/No	www.iet.aau.dk/Research/wts.htm
		DFIG	Dynamic/(Transient) ⁹	No/No	www.iet.aau.dk/Research/spp.htm
					^{8,9} DFIG model to be expanded with crow bar
SINTEF	PSSE	Fixed speed	Dynamic/Transient	Yes/Yes	Models and study reported, see [12]-[14].
		DFIG	Dynamic/(Transient) ¹⁰	No/No	10,11 DFIG model to be expanded with crow bar
		Direct Drive	Dynamic/Transient	No/No	¹² PSCAD is used for detailed studies of power
	Matlab	Fixed speed	Dynamic/Transient	Yes/Yes	electronics' impact on power system stability
		DFIG	Dynamic/(Transient) ¹¹	No/No	
	an mour	Direct Drive	Dynamic/Transient	No/No	
	SIMPOW	Fixed speed	Dynamic/Transient	Yes/Yes	
HCD	PSCAD ¹²	-	-	-	26.11. 11
UCD	Matlab	Fixed speed	Dynamic/(Transient)	No/No	Models and study reported, see [15].
	PSS/E	DFIG	Dynamic/(Transient)	No/No	
LIMICE	3.6.1.1	Full Converter	Dynamic/(Transient)	No/No	Mala and section
UMIST	Matlab	Fixed speed ¹³	Dynamic/Transient	No/No	Models and study reported, see [16]-[18].
	DCCAD	DFIG ¹³ DFIG ¹⁴	Dynamic/Transient	No/No	DFIG models available at
	PSCAD	DFIG	Dynamic/Transient	No/No	www.dgsee.umist.ac.uk/dfig/index.html ¹³ 3rd and 5th order models
	1				145th order models
VTT	ADAMS ¹⁵	Dinad accord	Dynamic/Transient	No/No	Models and study reported, see [19].
VTT	Matlab ¹⁵	Fixed speed	Dynamic/Transient	INO/INO	
	PSCAD ¹⁵				15 ADAMS and PSCAD-models are run jointly
	LOCAD.			1	by Matlab

Table 1: Summary of models developed by the participants of IEA Wind R&D Annex 21.

5 Example test results

5.1 Fixed speed wind turbine

In this section example test results are presented comparing measurements and simulations of a 180 kW fixed speed, stall controlled wind turbine. Results are shown for normal operation, Fig 2-3, and for the event of a voltage dip, Fig 4-5. The applied wind turbine data are given in the Appendix.

The time-series plot of active power output, Fig 2, shows fair agreement between the measurement and simulation. The time lag between the two is because the wind speed is measured at some distance upstream of the wind turbine.

The power spectral density (PSD) plot of active power output, Fig 3, indicate significant power fluctuations at 0.7 Hz (1p = turbine rotational frequency, fluctuation probably due to unbalanced blades), 1.1 Hz (fluctuation probably due to tower swing) and 2.1 Hz (3p, fluctuation due to variations in wind speed over the rotor area). The employed model makes a fair fit, but misses the 1p fluctuation as rotor blade unbalance is not included in the model.

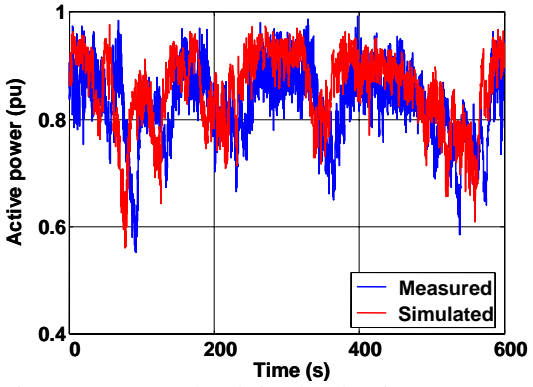


Figure 2: Measured and simulated active power output from fixed speed, stall controlled wind turbine.

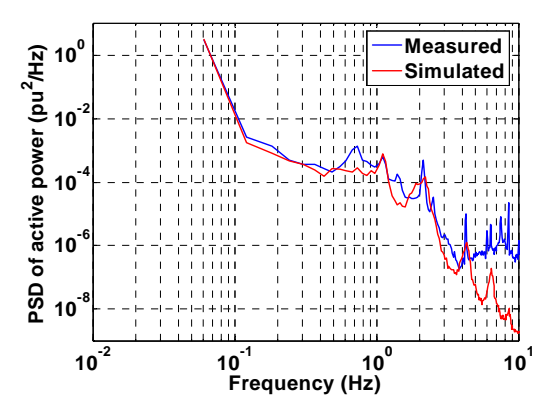


Figure 3: Power spectral density (PSD) of measured and simulated active power output from fixed speed, stall controlled wind turbine.

The wind turbine response in active power output to the voltage dip, Fig 4-5, is significant. The frequency of the simulated response matches the measured fluctuation (~10 Hz), but the measured power fluctuation amplitude is somewhat higher than the simulated. The match in frequency indicates that the model is fair, but more accurate simulation of the voltage dip and/or more detailed generator (stator) representation must be applied for better match in fluctuation amplitude.

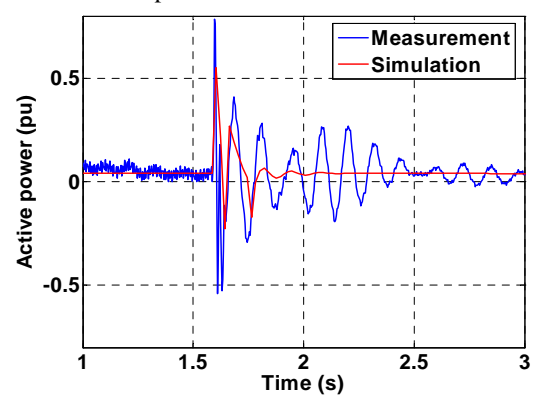


Figure 4: Time-series of measured and simulated active power output from fixed speed, stall controlled wind turbine during voltage dip.

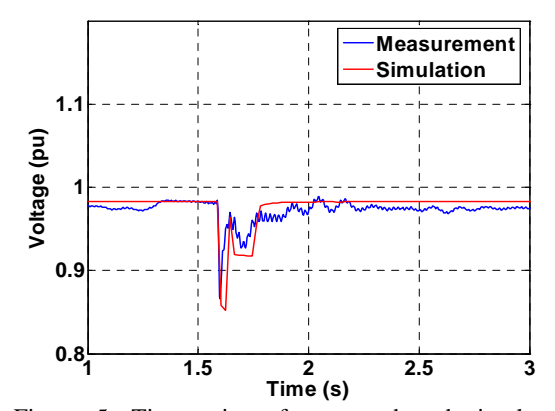


Figure 5: Time-series of measured and simulated voltage dip at wind turbine terminals.

5.2 Variable speed wind turbine

In this section example test results are presented comparing measurements and simulations of a 850 kW DFIG wind turbine. Results are shown for the event of a voltage dip, Fig 6-7. The applied wind turbine data are given in the Appendix.

The simulated response in active power output of the wind turbine to the voltage dip, Fig 6-7, reflects the measured response, but not accurately. The main challenge is that the response is to a large degree governed by the control system of the wind turbine, and that this is not known in detail.

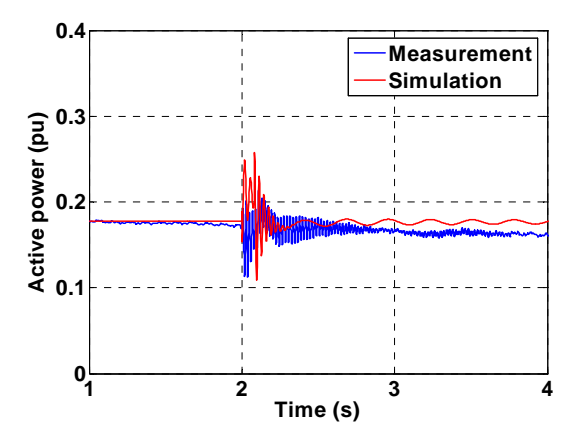


Figure 6: Time-series of measured and simulated active power output from variable speed DFIG wind turbine during voltage dip.

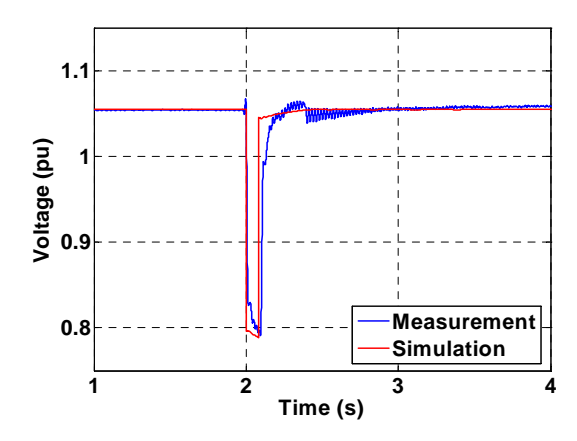


Figure 7: Time-series of measured and simulated voltage dip at wind turbine terminals.

6 Conclusion

In general the progress is good on model development. Models are available on various platforms (Matlab, PSSE etc), some are freely available, and the Annex participants take model validation seriously providing confidence.

The common major challenge is seemingly to validate the response of models on grid faults such as severe voltage dips. Relevant measurements are not easy to obtain and a further difficulty is that the response is very dependent on the detailed control of the wind turbine(s), i.e. specifications that are commonly regarded as a business secret by the manufactures. Hence, a proposal emerging as a spin-off from the Annex works is to update IEC 61400-21 to specify standardized procedures for measurements and documentation of the response of wind turbines on voltage dips, and by this lay the foundation for model validations. This work has now started aiming to

prepare a draft revision of IEC 61400-21 by June 2005.

This paper has described the status of works by IEA Wind R&D Annex 21. The work is ongoing, planned to being concluded by end 2005, and by then a more elaborate presentation of models and benchmark test results are expected.

References

- [1] T. Thiringer, A. Petersson, T. Petru, "Grid Disturbance response of Wind Turbines Equipped with Induction generator and Doubly-Fed Induction generator" IEEE PES annual Meeting, Toronto, Canada, 2003, July 14-17.
- [2] JTG Pierik, J Morren, EJ Wiggelinkhuizen, SWH de Haan, TG van Engelen, J Bozelie; Electrical and control aspects of offshore wind farms, Volume 1: Dynamic models of wind farms, ECN-C-04-050, ECN / TU Delft June 2004.
- [3] JTG Pierik, J Morren, EJ Wiggelinkhuizen, SWH de Haan, TG van Engelen, J Bozelie; Electrical and control aspects of offshore wind farms, Volume 2: Offshore wind farm case studies, ECN-C-04-050, ECN / TU Delft June 2004.
- [4] Estanqueiro, A., WIRING Project Final Report (JOR3-CT98-0245) INETI Contribution, Part A: *Theoretical Basis of INETI's INPark Wind Park and Local Grid Models*. Sept, 2002. pp. 57.
- [5] Estanqueiro, A., WIRING Project Final Report (JOR3-CT98-0245) INETI Contrib., Part B: *Application of the Models*, Sept, 2002. pp.39.
- [6] Jesus, J.; Estanqueiro, A.; Saraiva, J.; Castro, R., Modelling Machine Interaction In A Wind Park With Regard To Stability And Regulation, PO-MISTRAL NATO SFS PROGRAMME III, Final Report, Febr. 2001, pp 108.
- [7] Castro, R and J. Jesus. An Aggregated Wind Park Model, 13th Power System Computation Conference- PSCC'99; Trondheim. Jun –99
- [8] E. Muljadi, C.P. Butterfield, "Dynamic Model for Wind Farm Power Systems," Global Wind Power Conference 2004 in Chicago, IL, March 29-April 1, 2004
- [9] E. Muljadi, C.P. Butterfield, "Dynamic Simulation of a Wind Farm with Variable Speed Wind Turbines," Transactions of the ASME, Vol. 125, November 2003, Special Issue on Wind Energy, Journal of Solar Energy Engineering, pp. 410-417
- [10] Sørensen, P.; Hansen, A.D.; Christensen, P.; Mieritz, M.; Bech, J.; Bak-Jensen, B.; Nielsen, H., Simulation and verification of transient events

- in large wind power installations. Risø-R-1331(EN) (2003) 80 p.
- [11] Sørensen, P.; Hansen, A.D.; Janosi, L.; Bech, J.; Bak-Jensen, B., Simulation of interaction between wind farm and power system. Risø-R-1281(EN) (2001) 65 p.
- [12] Tande, JOG; Grid Integration of Wind Farms, Wind Energ. 2003; 6:281-295
- [13] Ian Norheim, K Uhlen, JOG Tande, T Toftevaag, MT Pálsson; Doubly Fed Induction Generator Model for Power System Simulation Tools, Nordic Wind Power Conference, 1-2 Marcg, 2004, Chalmers University of Technology
- [14] Palsson MT, Toftevaag T, Uhlen K, Tande JOG. Large-scale wind power integration and voltage stability limits in regional networks. Proceedings of IEEE-PES Summer Meeting, 2002; 2: 762-769.
- [15] A Mullane; Advanced control of wind energy conversion systems, Theses (Ph.D.) NUI, 2003 at Department of Electrical and Electronic Engineering, UCC.
- [16] Anaya-Lara, O., Cartwright, P., Ekanayake, J. B., "Electrical Stability of Large Wind Farms - Grid Connections and Modelling," Proceedings of the Global Windpower Conference 2004, Chicago, Illinois, USA, March 2004.
- [17] Anaya-Lara, O., Wu, X., Cartwright, P., Ekanayake, J. B., Jenkins, N., "Performance of Doubly Fed Induction Generator (DFIG) During Network Faults," Paper accepted for publication in the IEE Proceedings on Generation, Transmission and Distribution, April 2004.
- [18] Ekanayake, J. B., Holdsworth, L., Jenkins, N., "Comparison of 5th order and 3rd order machine models for Doubly Fed Induction Generator (DFIG) Wind Turbines", Proceedings Electric Power System Research, Vol. 67, 2003, pp. 207-215.
- [19] Uski, S., Lemström, B., Kiviluoma, J., Rissanen, S. and Antikainen P. Adjoint wind turbine modeling with ADAMS, Simulink PSCAD/EMTDC. Nordic wind power conference - NWPC'04, 1-2 March 2004 at Chalmers University of Technology, Gothenburg, Sweden.

Appendix

List of symbols

- β turbine blade pitch angle (rad)
- air density = 1.225 kg/m³ at 15°C, 1013.3 mbar ρ
- λ tip speed ratio = $\omega_t R/u$
- ω_0 Mechanical drive train eigenfreq (locked generator) (rad/s)

- base angular frequency = $2\pi 50$ rad/s for a 50 Hz system ω_b
- ω_{g} generator angular speed (rad/s)
- network impedance phase angle (rad) ψ_k
- turbine angular speed (rad/s) ω_t
- shaft twist (rad) θ_t
- Α rotor area = πR^2 (m²)
- C_p turbine efficiency, function of λ and β
- d_m mutual damping (pu torque/pu speed)
- f_0 mechanical drive train eigenfreq (locked generator) (Hz)
- f_n H_g nominal grid frequency (Hz)
- generator inertia (s)
- H_t turbine inertia (s)
- J_g generator moment of inertia (kg·m2)
- J_t turbine moment of inertia (kg·m2)
- shaft stiffness (pu torque/electrical rad)
- gearbox ratio
- number of generator pole pairs
- Q_{c} shunt-capacitor (var)
- R rotor radius (m)
- S_k short-circuit apparent power (VA)
- S_n T_g nominal apparent power (VA)
- torque at generator shaft (Nm)
- T_t torque at turbine shaft (Nm)
- $u_t(t)$ weighted average wind speed over rotor blades (m/s)
- U_n nominal voltage (V)
- Z_b base impedance (ohm)

Data conversion formulas

$$Z_b = \frac{U_n^2}{S_n} \tag{4}$$

$$\omega_b = 2\pi f_n \tag{5}$$

$$H_t = \frac{0.5 J_t \omega_b^2}{S_n n_g^2 p^2} \tag{6}$$

$$H_g = \frac{0.5 J_g \omega_b^2}{S_n p^2} \tag{7}$$

$$\omega_o = 2\pi f_o \tag{8}$$

$$k = \frac{2\omega_o^2 H_t}{\omega_h} \tag{9}$$

Fixed speed wind turbine data

Nominal power, P_n (kW)	180
Nominal voltage, $U_n(V)$	400
Nominal apparent power, S_n (kvar)	204
Nominal frequency, f_n (Hz)	50
Number of pole pairs, p	3
Stator resistance, R_{IS} (pu)	0.017
Stator leakage reactance, X_{IS} (pu)	0.105
Rotor resistance, R_{2S} (pu)	0.015
Rotor leakage reactance, X_{2S} (pu)	0.107
Magnetizing reactance, X_M (pu)	3.188
Shunt-capacitor, Q_c (kvar)	60
Generator inertia, H_g (s)	0.28
Turbine inertia, H_t (s)	3.14
Mechanical drive train eigenfreq, f_0 (Hz)	0.81
Gearbox ratio, n_g	23.75
Turbine rotor radius, R (m)	11.60

Variable speed wind turbine data

Nominal power, P_n (kW)	850
Nominal voltage, $U_n(V)$	690
Nominal apparent power, S_n (kvar)	944
Nominal frequency, f_n (Hz)	50
Number of pole pairs, p	2
Stator resistance, R_{1S} (pu)	0.004
Stator leakage reactance, X_{IS} (pu)	0.046
Rotor resistance, R_{2S} (pu)	0.006
Rotor leakage reactance, X_{2S} (pu)	0.072
Magnetizing reactance, X_M (pu)	2.724
Frequency converter rating, S_f (kvar)	300
Generator inertia, H_g (s)	-
Turbine inertia, H_t (s)	5.23
Mechanical drive train eigenfreq, f_0 (Hz)	-
Gearbox ratio, n_g	57.69
Turbine rotor radius, R (m)	26.00